STUDY ON HARD DISK DRIVE ASSEMBLY PARTS CLEANING PROCESS BY USING SNOW DRY-ICE BLASTING

[illegible] TEVOSUTAN

A THESIS SUBMITTED IN PARTIAL FULFILLMENT
OF THE REQUIREMENT FOR THE DEGREE OF
MASTER OF ENGINEERING IN CHEMICAL ENGINEERING
FACULTY OF ENGINEERING
KING MONGKUT'S INSTITUTE OF TECHNOLOGY LADKRABANG
2011

KMITL-FOLL-EN-M-220-022

STUDY ON HARD DISK DRIVE ASSEMBLY PARTS CLEANING PROCESS BY USING SNOW DRY-ICE BLASTING

SIWACH TENGSUWAN

A THESIS SUBMITTED IN PARTIAL FULFILLMENT
OF THE REQUIREMENT FOR THE DEGREE OF
MASTER OF ENGINEERING IN CHEMICAL ENGINEERING
FACULTY OF ENGINEERING
KING MONGKUT'S INSTITUTE OF TECHNOLOGY LADKRABANG
2011

KMITL-2011-EN-M-220-022

Thesis Certification

Faculty of Engineering

King Mongkut's Institute of Technology Ladkrabang

Thesis Title	Study on Hard Disk Drive Assembly Parts Cleaning Process by Using Snow Dry-Ice Blasting
Student	Mr.Siwach Tengsuwan
Student ID.	52611409
Degree	Master of Engineering
Program	Chemical Engineering
Thesis Advisor	Asst.Prof.Dr.Surat Areerat
Thesis Reference Number	KMITL-2011-EN-M-220-022

	EXAMINERS	SIGNATURES
Dr.Narisara	Thongboonchoo	
Dr.Santi	Wattananusorn	
Dr.Jintawat	Chaichanawong	
Dr.Walairat	Chandra-ambhorn	
Asst.Prof.Dr.Surat	Areerat	

Date 25th March 2011 **Time** 09.00-11.00 am.

Place Building A , 5th Floors Conference Room no.4

(Assoc.Prof.Dr.Suchatchavee Suwansawas)

Dean

25th March 2011

หัวข้อวิทยานิพนธ์	การศึกษากระบวนการทำความสะอาดชิ้นส่วนประกอบของฮาร์ดดิสก์ไดร์ฟโดยใช้การพ่นละอองน้ำแข็งแห้ง
นักศึกษา	นายสิวัช เต็งสุวรรณ
รหัสนักศึกษา	52611409
ปริญญา	วิศวกรรมศาสตรมหาบัณฑิต
สาขาวิชา	วิศวกรรมเคมี
พ.ศ.	2554
อาจารย์ที่ปรึกษาวิทยานิพนธ์	ผศ. ดร. สุรัตน์ อารีรัตน์

บทคัดย่อ

การฉีดพ่นละอองน้ำแข็งแห้ง คือการปล่อยให้คาร์บอนไดออกไซด์ความดันสูงไหลผ่านหัวฉีดออกสู่บรรยากาศ ซึ่งส่งผลให้เกิดการแพร่กระจายแบบจูล – ทอมป์สันของของไหลในระบบจนเกิดการเปลี่ยนสถานะของคาร์บอนไดออกไซด์ความดันสูงไปเป็นกระแสการไหลรวมที่มีทั้งอนุภาคของแข็งและก๊าซ หรือที่เรียกรวมกันว่า ละอองน้ำแข็งแห้ง โดยกระแสละอองน้ำแข็งแห้งจะเป็นกระแสการไหลที่มีความเร็วสูง และมีอนุภาคของน้ำแข็งแห้งที่สามารถก่อให้เกิดการส่งผ่านของโมเมนตัมได้ จึงเหมาะที่จะใช้เป็นตัวกลางในการทำความสะอาดในระดับความถี่ถ้วนสูง

จากงานวิจัยนี้ได้พบว่าคุณลักษณะของละอองน้ำแข็งแห้งที่ผลิตได้นั้น จะถูกควบคุมโดยสภาวะของคาร์บอนไดออกไซด์ที่ใช้เป็นสารป้อนเสมอ และช่วงของความหนาแน่นของคาร์บอนไดออกไซด์ที่ใช้เป็นสารป้อนควรจะอยู่ในช่วงระหว่าง 67 ถึง 213 กิโลกรัมต่อลูกบาศก์เมตร ซึ่งจะมีร้อยละของปริมาณวัฏภาคของอนุภาคน้ำแข็งแห้งภายในกระแสละอองน้ำแข็งแห้งที่ผลิตได้บริเวณปลายหัวฉีดโดยประมาณร้อยละ 41 และเมื่อความหนาแน่นของคาร์บอนไดออกไซด์ที่ใช้เป็นสารป้อนนั้นอยู่ในช่วง 78 ถึง 136 กิโลกรัมต่อลูกบาศก์เมตร อนุภาคน้ำแข็งแห้งที่ผลิตได้นั้นจะมีค่าความเค้นกระแทกอยู่ในช่วงระหว่าง 48 ถึง 54 เมกะพาสคาล (6,962-7,832 ปอนด์ต่อตารางนิ้ว) นอกจากนี้ยังพบว่าค่าเฉลี่ยของขนาดเส้นผ่านศูนย์กลางของอนุภาคน้ำแข็งแห้งจะอยู่ในช่วงระหว่าง 27 ถึง 33 ไมครอน ซึ่งเป็นค่าที่ได้จากการวัดโดยใช้แผ่นฟิล์ม Prescale นอกจากนี้เมื่อพิจารณาว่าการแพร่กระจายแบบจูล-ทอมป์สันนั้นถือเป็นกลไกสำคัญในการเกิดละอองน้ำแข็งแห้ง จึงสามารถใช้เส้นโค้งจูล-ทอมป์สันเป็นหลักในการปรับแก้กระบวนการผลิตละอองน้ำแข็งแห้งเพื่อเพิ่มประสิทธิภาพการผลิตของระบบ รวมถึงพบว่าการฉีดพ่นละอองน้ำแข็งแห้งนั้นสามารถที่จะนำไปใช้ทำความสะอาดชิ้นส่วนประกอบฮาร์ดดิสก์ไดร์ฟโดยเฉพาะชิ้นส่วนที่มีความละเอียดอ่อน ซับซ้อนต่อการทำความสะอาดด้วยวิธีการอื่นๆ

Thesis Title	Study on Hard Disk Drive Assembly Parts Cleaning Process by Using Snow Dry-Ice Blasting
Student	Mr. Siwach Tengsuwan
Student ID.	52611409
Degree	Master of Engineering
Program	Chemical Engineering
Year	2011
Thesis Advisor	Asst. Prof. Dr. Surat Areerat

Abstract

Typically, the snow dry-ice is generated by flowing high pressure CO_2 through a nozzle into the atmosphere. That is cause of the Joule-Thomson (JT) expansion for fluid flow system. This expansion drives the high pressure fluid CO_2 to change into the solid-vapor two phases flow (as so-called "snow dry-ice"). The snow dry-ice is a high velocity flowing with dry-ice particles that have an excellent ability to use as high precision cleaning agent.

The characteristic of the snow dry-ice was depended on the conditions of supplying CO_2. The range of supplying CO_2 density that available to use for the snow dry-ice generating was in the range of 67 to 213 kg/m^3, in the case of the dry-ice particle phase was still contained around 41 % at the nozzle tip. When the supplying CO_2 density was in the range of 78-136 kg/m^3. The dry-ice particles and flow characteristic was obtained from the pressure measurement by using the Prescale film. Then, the impact stress was in the range of 48-54 MPa (6,962-7,832 psi) and the average diameter dry-ice particle size was in the range of 27-33 μm. Moreover, the JT expansion is considered as a significant mechanism in the snow dry-ice generating. Thus, the JT coefficients of each supplying CO_2 experiments were evaluated. Then the JT inversion curve was used as the tuning parameters to optimize the snow dry-ice generating system. Finally, the snow dry-ice blasting has a possibility to apply for the HDD assembly parts cleaning, especially the parts which more sensitive and complicated for conventional cleaning. Nevertheless, the cleaning of sensitive parts must be concerned about the pressure effect as a prime issue. In addition, the moisture condensation, redeposition and recontamination resources cannot be disregarded. From the cleaning results, the snow dry-ice cleaning might be taken from a laboratory cleaning method to use as a solvent-free and dry cleaning process in industrial section.

Acknowledgements

This thesis would not have been possible without the assistance of many persons to whom I would like to express my appreciation.

First, I would like to express my deepest gratitude to my research advisor, Assistant Professor Dr. Surat Areerat, who has given me many helpful suggestions, useful advice, fruitful discussions during the undertaken research and constant support in helping me to conduct and complete this work.

I am grateful for the financial support from Industry/University Cooperative Research Center in Data Storage Technology and Applications, King Mongkut's Institute of Technology Ladkrabang, National Electronics and Computer Technology Center (NECTEC), National Science and Technology Development Agency (NSTDA) and Hitachi Global Storage Technology Thailand Ltd.. And I would like to thank FUJIFILM (Thailand) Ltd and Hitachi Global Storage Technology Thailand Ltd. for supporting in the equipments and samples.

My special thanks to my family and relatives who are always there for me during my life and studies. In finally, thanks to my friends and undergraduate students at School of Chemical Engineering for their help provided during I was studying at KMITL.

Siwach Tengsuwan

Contents

Contents (cont.)

Contents (cont.)

Contents (cont.)

List of Tables

List of Tables (cont.)

List of Figures

List of Figures (cont.)

List of Figures (cont.)

Nomenclature

Symbols

C_C	Cunningham correction factor
d	Cryogenic particle diameter
m	Mass of cryogenic particle
$\dot{m}$	Mass flow rate
$\bar{P}$	Momentum
r	Cryogenic particle radius
Re	Reynolds number
U_o	Nozzle velocity
U	Impact velocity
v	Kinematic viscosity
x	Distance between nozzle and substrate

Greek Symbols

μ_{JT}	Joule-Thomson coefficient
ϕ	Cross sectional area of the nozzle
ρ_{co_2}	Supplying CO_2 density
ρ_P	Dry-ice particle density
τ	Velocity relaxation time
δ	Boundary layer thickness
η	Gas viscosity
σ	Impact stress

Subscripts

c	critical
JT	Joule-Thomson
r	reduced

Chapter 1

Introduction

1.1 Rationale and Context

Nowadays, hard disk drive (HDD) and electronic device industry in Thailand has contributed greatly to the Thailand economy. Thailand is ranked to be the world's number one of HDD manufacturer. In HDD industry section, there are and more than 400,000 million Baht for exportation [1]. However, there are other concerning issues to preserve status of Thailand as the world's number one HDD production base, for example, competing with other developing countries such as, China and Malaysia to gain a larger share of HDD manufacturers. Thus, Thailand must concern about the research and development in advanced technologies in HDD production and develop the facilities for supporting the growth of HDD production section in the near future.

As a result, Thailand has to develop own technologies for HDD production as well as reducing import of the HDD production foreign technologies. If this plan has been adopted, Thailand will move to next level of electronic industry which creates more value and could generate a lot of revenue. The development of HDD industry will help to sustain Thai economy and increase our competitive advantages in HDD industry as other countries do.

During the HDD manufacturing process, there are a small percentage of the production fails in the testing process. Typically because of a problem associated with the head suspension assembly (HSA) or the disks (media) [2]. The failed HDDs can be reduced by using rework method that the defective parts can be replace. However, the rework drives pass very through and strict testing process again. It has been demonstrated that if these parts are not precision cleaned prior to reassembly. The rework yields and the long-term reliability of the HDD can be adversely affected. In actually, the relationship between contamination and performance of the HDD is well known and understood by the HDD assembly lines industry. In HDD assembly lines industry usually meet some problems with the HDD assembly parts cleaning. For examples, the motor-base assembly has an oil-filled fluid dynamic motor bearing that cannot be removed by immersion in either an aqueous or solvent cleaning system. The voice coil magnet (VCM) can be

cleaned by using an aqueous or solvent cleaning system. However, this cleaning might be have more contamination problems on other HDD components, because there are the transfer of magnet particles to other parts. From these problems it would let to spend more times for the VCM cleaning systems [2]. Thus, new methodology such as a dry cleaning system is recommended or highly desirable cleaning procedure for the HDD complex or sensitive parts. Thus, the satisfactory designed CO_2 cleaning systems could be more effective for the HDD assembly parts cleaning that cannot be cleaned by using immersion in any liquid. However, in HDD assembly line industry, production cost is always a major concerning. Thus, the cleaning system must have high reliability, high throughput and excellent cleaning performance at a reasonable cost. From the combination of the cost, reliability, and performance issues has proven to be a challenge for conventional snow cleaning processes. Thus, in this research, the new CO_2 cleaning process was focused in such a case of the replacement in the conventional processes during the manufacturing operations.

Dry-ice cleaning has been commercialized in 1980s as a process for various cleaning applications [2]. Dry-ice cleaning is widely used as an industrial technique, which is able to be applied to surface cleaning for semiconductor devices, automotive molds, food processing equipments, food refrigeration and pharmaceutical granulation. Because the dry-ice system has the specific feature of low temperature gas-solids two phase flow containing sublimation particles. The concept of dry-ice jet applied to surface cleaning was first proposed in 1980s [3]. In this study, fine particles called snow dry-ice was produced by expanding liquid carbon dioxide. Dry-ice jet can be used for the removal of fine contaminants strongly adhering to the surfaces, due to the penetration of dry-ice particles through the boundary layer. From the comparison with air jet, which is only the drag force is applied for the removal of the contaminants. The impact of dry-ice particles substantially enhances the removal efficiency. The quantitative analysis of the cleaning effect of dry-ice jet was carried out, including removal of organics as well as particulate contaminants [4-8]. The organics are dissolved in liquid carbon dioxide due to the dry-ice particles during the impact between dry-ice particles and contaminants. The particle removal mechanism based on a collision model was investigated [9,10]. The particle size of dry-ice is thought to be an important factor which greatly affects the contaminant removal efficiency.

The snow dry-ice blasting means the process of the releasing high pressure CO_2 fluid (liquid or gas) to move through a throttling device into the atmosphere. After the CO_2 has been

moving through the orifice, the expansion of CO_2 that is an ideal constant enthalpy process is going to arise (isenthalpic expansion). This expansion drives high pressure fluid CO_2 to convert to a solid-gas two phases stream (as so-called "snow dry-ice or CO_2 cryogenic aerosol"). This two phase flow is used as a cleaning media (cleaning agent) to strike and clean a surface via physical and solvent interactions [10,11]. Thus, the snow dry-ice blasting is an alternatively applied to the high precision cleaning for electronic devices especially in HDD assembly parts. The snow dry-ice is one of a dry cleaning system. The contaminants can be removed by using the momentum transfer as a major eliminating mechanism when the snow dry-ice cleaning is applied. Therefore, the snow dry-ice cleaning has typical ability to remove micron and submicron-sized particulate contaminants from the surface. Thus, the snow dry-ice cleaning can be used to clean surfaces which required cleaning within the precision cleaning level. The snow dry-ice cleaning satisfies the increasing in industrial and environmental demands together. Because when it removes the contaminants away from the surface for venting or capture, it will not leave anymore residue on parts. Thus, the snow dry-ice cleaning is using less cleaning time. Moreover, CO_2 is nontoxic, nonflammable and no ozone depletion potential (ODP). Therefore, the snow dry-ice cleaning does not damage on parts as well as its environmental friendly. From using the snow dry-ice cleaning, this cleaning is avoiding the environmental problems from an organic solvent. Thus, the snow dry-ice cleaning is a good way of relieving the greenhouse effect by recycling and utilizing the CO_2 that be generated from various industrial processes, especially natural gas separation plant [11,12].

1.2 Objectives

1. To evaluate the processing parameters, which affect to efficiency of the snow dry-ice generating and the snow dry-ice stream characteristic

2. To evaluate the suitable snow dry-ice generating conditions for applying in the HDD assembly parts cleaning

3. To design the high performance prototype of snow dry-ice generating system in laboratory scale

1.3 Scopes of the Study

1. The snow dry-ice generating was studied by using the commercial snow dry-ice machine model AFMS 100.

2. The supplying CO_2 pressure was in range of 400 – 900 psi and in range of -5 to 25°C for the supplying CO_2 temperature.

3. To evaluate the range of the supplying CO_2 conditions for using in the snow dry-ice generating system and HDD assembly parts cleaning

4. To study on the relationship between the dry-ice particle and flow characteristic and the supplying CO_2 conditions by using the pressure measurement method

5. To develop a tuning method for the snow dry-ice generating optimization by applying the Joule-Thomson expansion theory

6. To apply the snow dry-ice cleaning for using in the HDD assembly part (head gimbal assembly)

1.4 Research Methodology

1. Identify the significant problems, objectives, scopes, and limitations of the study
2. Study the theoretical background and literature review
3. Design the experiments
4. Generate the snow dry-ice stream and vary the supplying CO_2 conditions
5. Measure and analyze the characteristic of snow dry-ice stream
6. Evaluate the suitable supplying CO_2 conditions for generate snow dry-ice stream
7. Tune the snow dry-ice generating system for optimization
8. Apply the snow dry-ice blasting for the HDD assembly parts cleaning
9. Design the snow dry-ice generating prototype in laboratory scale
10. Conclude the results and write report.

1.5 Outcomes of the thesis

1. The suitable supplying CO_2 conditions for the using in the snow dry-ice generating system and applying for the HDD assembly parts cleaning

2. The tuning method for the snow dry-ice generating optimization by applying the Joule-Thomson expansion theory

3. The prototype of the snow dry-ice generating system in laboratory scale

4. The new methodology that use to evaluate the dry-ice particle and flow characteristic, which can use to obtain the impact stress, size and amount of the dry-ice particles.

Chapter 2

Literature Review and Theoretical Background

This chapter presents a literature survey on the theoretical studies and practices on snow dry-ice blasting and cleaning. It includes the backgrounds in surface contamination and cleaning, contaminant removal, introduction to snow dry-ice, snow dry-ice formation and generating, its cleaning mechanism and other cleaning parameters issues such as the nozzles, moisture control, impact stress and recontamination or redeposition issues. Moreover, this section consists of the background in the Joule-Thomson expansion and its applications.

2.1 Background in surface contamination and cleaning

Nowadays, surface contaminations are one of the most concerning topics in a broad variety of industries due to their inclination for causing the failure of some components. Normally, the contaminants might be small particles, thin films, molecular species, ionic species, or microbiological species. However, particulate contamination most often is present in the form of dust or fine airborne particles. Tiny particles of abrasive or other machining debris also can become embedded in a surface during polishing or other processing operations. On the contrary, film contamination can generate from a variety of sources, that usually include airborne pollutants (water vapor, organic materials, and cleanroom construction materials), outgassing of plastic containers holding finished components, residues from protective strip coatings, dried liquid residue following an improper cleaning operation, and fingerprints left during handling [13].

2.1.1 Effects from contaminants

In the form of contaminants, small particles can have a major impact on the performance of precision and other products. For example, the presence of impurities such as boron and phosphorous in the parts per billion (ppb) range can result in the irrecoverable loss of an entire production lot of semiconductor wafers. In a hard disk drive (HDD), a particle of dimensions similar to the nominal flying height trapped between the head and the disk can lead to catastrophic failure of the drive [14]. Similarly, the presence of low levels of hydrocarbon contaminants in the components for oxygen service can cause catastrophic damage to spacecraft

due to autoignition. Film contaminant layers on the surface of high-quality metallic mirrors or other optical components can increase scattering. Particles on a surface can act as nucleation sites and produce larger cone-shaped defects in the film with increased scattering [13].

Furthermore, contaminant layers on optical surfaces intended to be further coated with thin films, will affect the adhesion of the films. Similarly, airborne molecular contaminants (AMCs) on a silicon wafer can affect the performance of the device incorporating chips fabricated from such a contaminated wafer. Even on mechanical parts, such as precision gears or other precision metal components, that must be coated with a protective or performance coating, the presence of contaminant films or particles can lead to poor coating adhesion and subsequent failure of the critical component [15].

2.1.2 Size range of particles

In the most precision technology applications require characterization of micro-size and smaller particles. Thus, it is first necessary to separate the particles by their sizes. Separable particles can be normally classified by size as according to Table 2.1.

Table 2.1 Range of particle sizes and selected techniques for resolution of particles for characterization [13]

Particle class	Particle Size (nm)	Resolution Techniques
Macro	> 50,000	- Unaided eye
Micro	100 – 50,000	- Conventional optical microscopy
Submicrometer	0 – 100	- Near-field optical microscopy
		- Surface plasmon microscopy
Nano	1–10	- Electron and probe microscopies
Atomic	0.01 – 1	- Electron and probe microscopies
		- Holography
		- Resonance force microscopy
Subatomic	< 0.01	- Femtosecond to attosecond spectroscopy
		- Atomic force microscopy (AFM)

For a reduction of semiconductor and electronic device sizes, that affect a nano-size particle contamination will become increasingly significant to final device yield and performance. For example, to achieve a data density higher than 77.5 Gb/cm^2 (500 Gb/in^2), HDD manufacturers will have to make their magnetic bits a mere 15-20 nm across with just 25 nm between the bits. At these sizes, the overall behavior of nano-size particles (< 20 nm) is governed by the surface and binding energies of the molecules in the particle. These particles are regarded as complex structures whose behavior depends on the position of the individual molecules and the combined electronic charge distribution [2,13].

Particles smaller than around 10 μm adhere to a surface by very strong bonding interactions. These interactions can be covalent or ionic bonding, van der Waals forces, hydrogen bonding, dipole–dipole and electrostatic interactions, or a combination of these interactions [10]. The theoretical forces of adhesion are proportional to particle size, while the removal force varies as the second or third power of the particle diameter, thus requiring an increasingly larger force to overcome the adhesion force between the particle and the substrate as the particle size is reduced .

Thin films are a particularly insidious form of contamination and are very difficult to remove. Examples of such contaminant films are AMCs (airborne molecular contaminants) that are becoming increasingly significant in the semiconductor and other precision industries. The effects of AMCs are often catastrophic. As little as 1 ppb of a contaminant such as boron or phosphorous can result in a 100 percentage yield loss of the silicon wafer [15].

2.1.3 Contamination in hard disk drive

Contamination of the HDD is known to degrade the performance of the HDD. Thus, particle contamination must be controlled to increase HDD storage capacity as the flying height of a slider decreases. Particle generation in a HDD can cause serious physical and electrical damages. Therefore, precise detection and analysis of particles are the primary steps of particle control in a HDD. That is because the contamination particles in the HDD can cause serious problems including slider crash and thermal asperities [14]. mode. In magnetic HDDs, particulate contaminants can cause the thermal asperity (TA) problem, which can seriously affect the HDD reliability in near future [14]. Park et al. [17] investigated the particle generation due to slider disk interaction in a HDD during the disk drive start/stop period by using a condensation nucleus counter. They found that the most of particles were generated when the drive was started or stopped. Bhushan et al. [17] investigated particle contaminants in commercial HDDs, that were

extracted by using a wash technique, and the contaminants were analyzed by using EDX (energy-dispersive X-ray spectrometry). Aluminum is the most in the particles and the other elements that including Si, Ca, Mg, Ti, and K were also found in the particles.

D. Y. Lee et al. [14] examined the particle components in HDD by using SEM (scanning electron microscopes), AES (auger electron spectroscopy) and TOF-SIMS (time of flight-secondary ions mass spectrometry). They studied the particle generation of a commercial HDD at various disk rotational speeds. They have found that particle sizes ranged from 14 to 200 nm. Moreover, the particles were generated by slider disk interaction and came from the lubricant on the disk, the coating layer of the disk, and the slider surface. In addition, the micro-sized particles that adhered to the slider were mainly composed of F, Fe, Cr, Al and Ni. Some of the micro-sized particles came from the lubricant on the disk surface, PFPE (perfluoropolyether), which contains F.

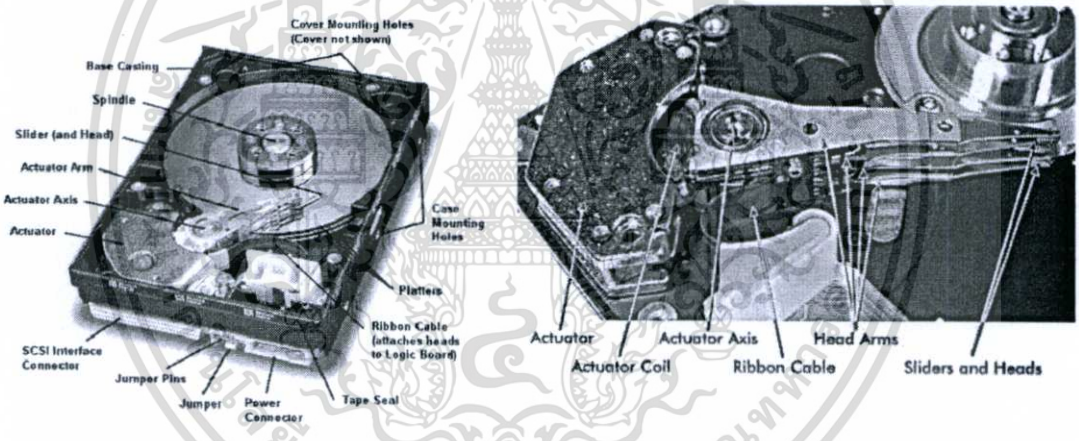

Figure 2.1 Hard disk drive components [16]

2.2 Contaminants removal

In case of critical components cleaning is necessary to ensure that the performance of the part or the system is not adversely affected. Normally, if the dust particles larger than around 10 μm often can be removed by blowing them off with air or nitrogen, or with an aerosol injection. The wet chemical and aqueous cleaning techniques are well verified for removal of contaminants around these size too [13].

From the studies of M. Free [18], that discusses the use of surfactants to enhance particle removal from surfaces. Surfactants enhance small particle removal from substrates by altering the associated interaction forces between the particle and the substrate, primarily by adsorption of the surfactant on both the particle surface as well as the substrate surface. Although Freon cleaning

has also been very effective for removal of contaminants, but it is no longer an acceptable cleaning practice due to its high ODP and potential adverse effect on the environment. A variety of alternative solvent cleaning agents have been developed to replace Freon as described in the research of J. B. Durkee [19]. However, all chemical solvents can have adverse impact on human health and the environment on exposure.

The research of P. Clark and T. Wagener [20] is devoted to particle removal by chemical solution methods, including the two most common chemistries in use today in production, SC-1 and dilute HF. As mentions earlier, aqueous cleaning techniques are well established for removal of surface contaminants; however, they are approaching the limits to remove submicrometer size particles (< 0.3 μm). In addition, in the semiconductor wafer fabrication industry, water and chemicals usage and chemical recycling and/or disposal can make up as much as 80% of the annual operating costs of a wafer cleaning tool [13]. Furthermore, there are other cleaning applications for which aqueous cleaning or wet chemical methods cannot be used, or for which a non-aqueous technique would be desirable. In response, several non-aqueous precision cleaning and processing techniques have been developed for a wide range of manufacturing applications.

One technique that is a sophisticated variation of air or nitrogen blow off is the use of a high-speed impinging air jet which can remove submicrometer size solid particle contaminants from a surface. As described in the studies of K. Gotoh [21], the efficiency of removal by the high-speed impinging air jet depends on the operating conditions, including air pressure in the jet nozzle, the distance between the nozzle tip and the substrate surface, the jet impinging angle, and the humidity of the operating environment. Other dry cleaning procedures use the basic concept of particle removal from a surface by momentum transfer from a collision source. These techniques have been developed to a very high degree of sophistication for precision cleaning. These collision sources include microabrasives and argon/nitrogen aerosols. Each of these cleaning techniques is discussed in reports by R. Kohli [22] and W. McDermott and J. Butterbaugh [23] respectively.

However, most common fluids cannot penetrate the stagnant boundary layer on the surface (1–2 mm) that traps the contaminant particles, which are smaller than the boundary layer. However, from a cleaning system innovation, such as using snow CO_2 cleaning, that employs a cleaning agent that has low surface tension as a fluid to penetrate the boundary layer and also has sufficient accelerating momentum as a solid to eliminate the particles from the surface. Thus, in

finally the particles sized as small as 30 nm have been successfully removed from a wafer surface [13], as described on the next section.

2.3 Snow dry-ice cleaning

2.3.1 Introduction

Snow dry-ice cleaning or sometimes we call it as CO_2 cryogenic aerosol or snow carbon dioxide (CO_2) cleaning is a straightforward surface cleaning process in which a stream of small dry-ice particles strike and clean a surface via physical and solvent interactions. These interactions have been shown to remove particles of all sizes, from visible to nanometer scale [11], and also to remove organic residues as well as reagent grade solvents. The combined ability of particle removal on such a wide range and also organic removal makes snow dry-ice cleaning unique in its potential. Furthermore, snow dry-ice cleaning processes satisfy the increasing stringent industrial and environmental demands together Snow dry-ice cleaning is using less cleaning time, because when it removes the contaminants away from the surface for venting or capture, it will not leave anymore residue on parts. Snow dry-ice cleaning systems do not damage on parts as well as its environmental friendly. Because CO_2 is nontoxic, nonflammable, and nonozone depleting, and the human exposure has minimal risk except for CO_2 release, but sometimes the frostbite (if used directly to the skin), or oxygen replacement might be happen. The snow dry-ice cleaning process is residue-free, nondestructive and carries away the contaminants for venting or capture.

There are four different forms of surface cleaning using CO_2. These forms is consist of using macroscopic dry-ice pellets form, liquid CO_2 form, supercritical CO_2 (SC-CO_2), and snow dry-ice cleaning. In case of using dry-ice pellet, the cleaning method has macroscopic dry-ice particles accelerated at a surface and cleaning is done via a thermo-mechanical shock. However, if we use liquid CO_2 and SC-CO_2 cleaning, we have to use as batch processes that rely upon the CO_2 solvent properties of the liquid or the supercritical state. Snow dry-ice cleaning relies upon smaller particle sizes and less dense dry-ice or snow than using dry-ice pellets, and snow dry-ice cleaning removes particulates via a momentum transfer and organics via a solvent process. In the snow dry-ice cleaning field, most applications rely upon high velocity snow streams for cleaning [3].

2.3.2 Mechanisms of snow dry-ice formation

When we would like to discuss with the thermodynamics of snow dry-ice formation, it should be start with the path of CO_2 phase changing, by using a CO_2 phase diagram. From Figure 2.2, which is shown the three of CO_2 phases (gaseous, liquid, and solid At room temperature (20-25°C) and atmospheric pressure, the gas phase is the only stable phase, regardless of the initial CO_2 phase, it can imply that the final product is always CO_2 gas,. Thus, it should also know that at atmospheric pressure, the dry-ice sublimates directly to CO_2 gas. And that is an answer of why the snow dry-ice cleaning would not let any residue on parts after cleaning. Actually, the *P-T* phase diagram tells us little regarding dry-ice formation; instead, the CO_2 pressure - enthalpy (*P-H*) diagram in Figure 2.3 provides insight into the phase changing that occurs during snow dry-ice formation. The features include the same three phases along with the region of pressure and enthalpy where these phases co-exist (the new regions were phase boundaries in Figure 2.2).

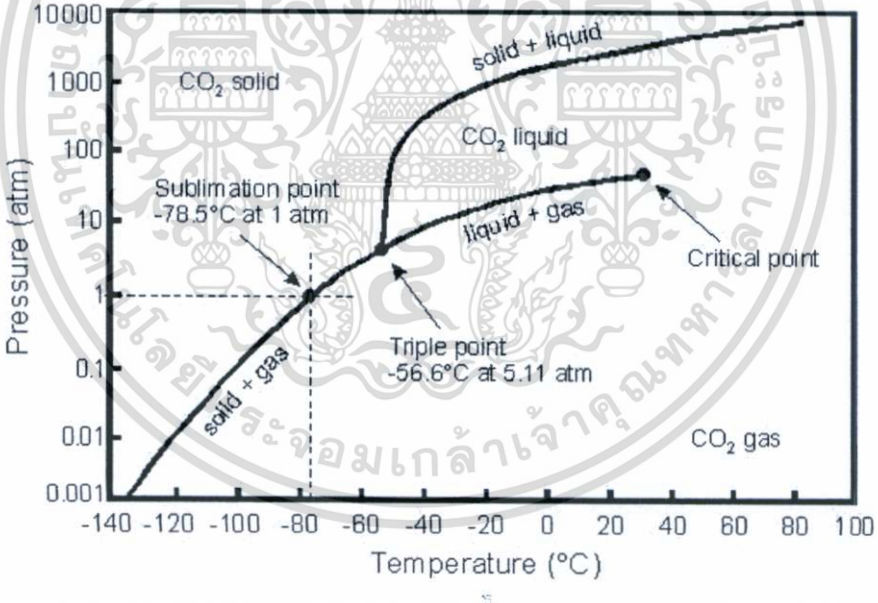

Figure 2.2 Carbon dioxide phase diagram [24]

By using the CO_2 phase diagram, the expansion is assumed as an isenthalpic expansion. Thus, when the CO_2 passes through the orifice, pressure is going to decrease along a constant enthalpy line (vertical line). It should be noted that the dry-ice formation does not go through the triple point, which is not exactly a common concept. A CO_2 cylinder at room temperature filled with liquid CO_2 has a gas pressure of about 800 psi (55 bar). Therefore, from

the enthalpy available to the cylinder contents are values in the liquid–gas two phase region at about 800 psi. Thus, for the consideration about snow dry-ice formation must be consider in two ways. The first way is starting from point A (as a gaseous supplying source) as the pressure drops when CO_2 moving through an orifice, liquid droplets nucleate and the percentage of liquid increases. When the CO_2 arrives at the interface between the liquid–gas and gas–solid regions (about 77 psi or 5.3 bar), all the liquid CO_2 converts to solid yielding about 6% dry-ice. On the contrary, if we use the supplying source as a liquid phase (that mean it starts from point B), as the same expansion and pressure drops in the orifice. Thus the gas bubbles form be replace for this case and the percentage of gas increases until the CO_2 reached the gas–solid region. After that the remaining liquid CO_2 is transformed into solid and the yielding of dry-ice in this case still around 45%. The percentage of dry-ice depends on the chosen supplying phase and is influenced by the supplying conditions (pressure and temperature). In addition, the ability of systems to maintain the constant enthalpy condition during the expansion. That mean the percentage of dry-ice will be affected by the isenthalpic expansion. For the case that dry-ice percentages are smaller and a supplying CO_2 may yield too small to not enough snow dry-ice stream and have insufficient velocity for organic removal [11].

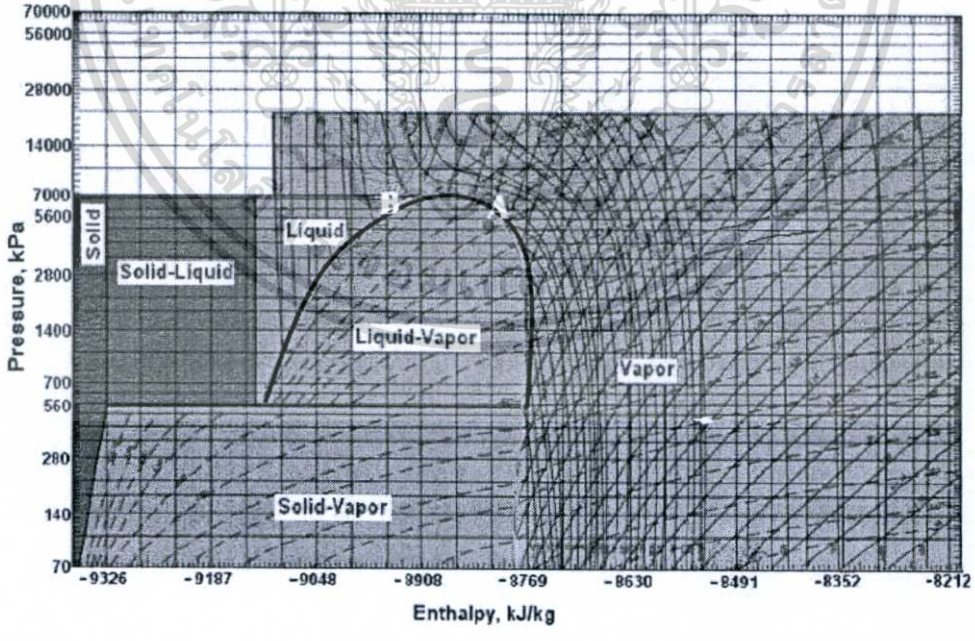

Figure 2.3 The Pressure-Enthalpy (*P-H*) phase diagram for CO_2 [11]

2.3.3 Cleaning mechanisms

Snow dry-ice cleaning is a dry surface cleaning method in which a high-velocity stream of CO_2 gas and dry-ice micro-particles are sprayed onto a substrate. The formation of snow dry-ice is based on the expansion of fluid CO_2 when being propelled through an orifice. The formation of snow dry-ice allows the snow dry-ice stream to be powerful. In normally, two different hypotheses can explain the mechanisms responsible for the removal of organic and particle residues from surfaces during snow dry-ice cleaning (as shown in Figure 2.4). One hypothesis will explain that the particle detachment involves an aerodynamic drag force of high-velocity gas flow and momentum transfer during impact (Figure 2.5). The other hypothesis will explain the organic contamination removal, based on the presence of a liquid CO_2 phase as a result of the impact (Figure 2.6) [11,25]. Removal of micron and submicron particles using only a gaseous stream is usually not effective. It is a well-known fact that the drag force is dominated by the boundary layer effect and the particle size [10]. Thus, for these small particles the adhesion force generally exceeds the drag force. With a snow dry-ice stream, small dry-ice particles at high velocity penetrate the boundary layer and provide an impact momentum transfer that is greater than the adhesion force.

Theoretically, the snow dry-ice could be clean a surface. That is because it has two primary mechanisms for cleaning. That is consist of the first is about the particle removal by momentum transfer and the second one is organic removal by the solvent action of a transient liquid CO_2 phase [11]. These two processes are well accepted, but they are not the only cleaning mechanisms.

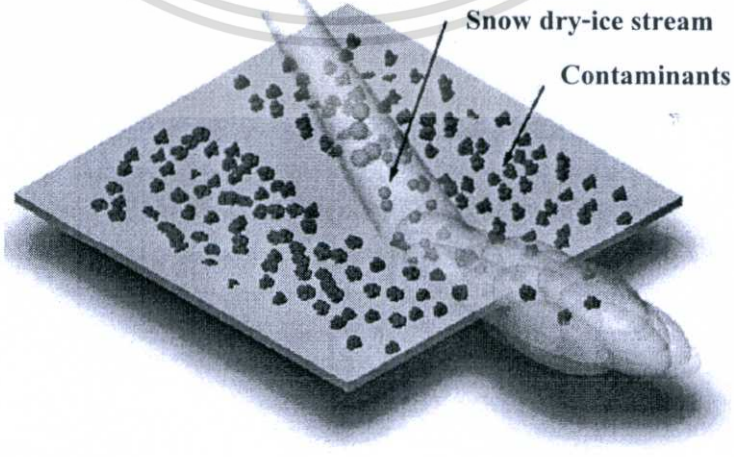

Figure 2.4 Schematic simulation of snow dry-ice cleaning mechanism [25]

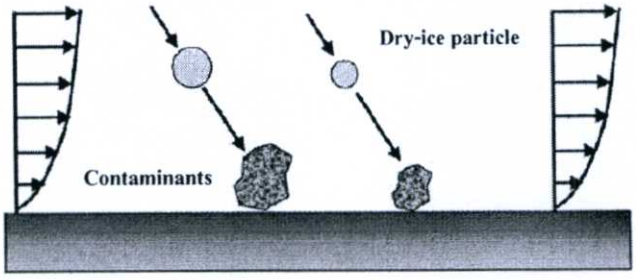

Figure 2.5 Cleaning mechanism for particle removal via the momentum transfer and the aerodynamic drag force [25].

2.3.3.1 Particle removal

The snow dry-ice cleaning could be reached the particle removal by the combination between momentum transfer and an aerodynamic drag force. A flowing gas generates an aerodynamic drag force on a particle and this force is proportional to its cross sectional area. Nevertheless, the gas flow alone cannot generate sufficient forces to remove micrometer and submicrometer-sized particles bound by physical means such as van der Waals forces, Coulombic image force, electronic double layer force, and capillary force. That is because the aerodynamic drag force at or close to a surface is zero and the boundary layer is more thicker when compare with the particles diameter. Although, the snow dry-ice cleaning that introduces mass, as dry-ice particles, into the gas stream and the combined stream strikes the particle (see in Figure 2.5). When the collision has occurred, the momentum will transfers from the dry-ice particles to the contaminant particle on the surface. Thus, if the collision potentially overcome the adhesive forces between the surface and the particulate contaminant. The liberation of the surface particulate will start. Moreover, when the particle liberated from the surface, it is easily carried the particle away with the high-velocity gas from the snow dry-ice stream.

In addition, C. Toscano and G. Ahmadi [9] found that the impact by the snow dry-ice is an effective mechanism for surface cleaning of small and moderate size particles. And the impact removal of large contaminant particles is more easier done with a cryogenic stream with larger dry-ice particles. In case removal of contaminant particles that smaller than a certain size cannot be removed with a snow dry-ice stream with dry-ice particles larger than a certain diameter. Thus, the effective removal of very small particles requires cryogenic streams with very small dry-ice particles. In addition, the effectiveness of surface cleaning by snow blasting increases as the nozzle-substrate angle (incident angle) decreases. The angle effect is

more important for larger dry-ice particles and contaminant particles. The angle effect becomes negligible for small dry-ice particles that impact with local fluid velocity. However, increasing the nozzle-substrate separation distance slightly increases the critical velocity needed for particle removal. The effect of the changes in the separation distance becomes noticeable only if it is sufficiently large to affect the level of the relaxation of particle velocity to the local flow velocity.

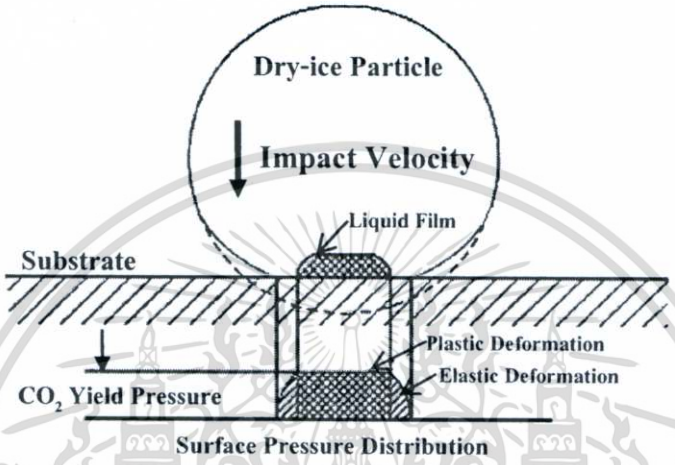

Figure 2.6 The liquid phase at the surface and dry-ice interface when the organic removal occurs. [25]

2.3.3.2 Organic removal

The mechanism for the removal of organic residues utilizes liquid CO_2 solvent properties, and liquid CO_2 is an excellent solvent for non-polar hydrocarbons. During the short time of impact, the stresses between the dry-ice particles and the substrate can exceed the triple point pressure (77 psi or 5.3 bar), and a liquid CO_2 film is formed on the dry-ice particle–surface interface. As a liquid CO_2 film is formed, the organic residues are dissolved by the liquid film, as shown in Figure 2.6. When the dry-ice particle starts to rebound off the surface, the interfacial pressures decrease and the dry-ice particle re-solidifies, carrying the contamination away [4,6,11].

Hills [8] explored the removal of various organic compounds using the snow dry-ice cleaning. In this study, the data presented of the supporting for above liquid phase mechanism and established a rule for determining which compounds are removed quickly. Generally, organics that are easily absorbed in liquid CO_2 are removed. The organics with complex or other functional nonhydrocarbon-based groups not readily soluble in liquid CO_2 are

not easily removed. Instead, an abrasive and freeze removal process was proposed for these compounds. Here, it is believed that the snow dry-ice freezes the deposit and just breaks it off from the surface.

2.3.3.3 Other mechanisms

E.A. Hill [26] studied the low-velocity snow dry-ice cleaning mechanisms in detail. E.A. Hill [26] explained that the main particle removal mechanism in the low-velocity mode was combined between a shear stress forces that generated by a sublimating of the large dry-ice particles and "thermophoresis". This phenomena occurs when the dry-ice particle does not contact the surface, but the sublimating of snow dry-ice generated a cold gas layer and it flows above the surface. Thus, particulates on surface could exposed to this cold gas flow, this will be submitted to larger shear stresses than with the a normal gas blasting. This is because the high velocity flowing caused by the sublimating of dry-ice happen so close to the surface. E.A. Hill [26] argues that this force can remove the particles for a greater rate than normal aerodynamic gas flows. The freed particle is attracted and held to the snow dry-ice flake by the thermophoretic forces. This force is arising from thermal gradients. For this case, the thermal gradient is on the particle, one side facing the cold of the snow dry-ice flake, and the other side contact with the warmer surface. The contaminant particles are pushed toward the cold side of the snow dry-ice and are carried away. Moreover, E.A. Hill [26] correctly points out that if the dry-ice particles sublimates on a clean surface, particle redepositon can occur. E.A. Hill [26] observed cleaning efficiencies increasing up to 70% for many residues. It is likely that thermophoresis may also occur with the higher velocity snow dry-ice cleaning methods but will only be one of the secondary mechanisms. In addition, the transient liquid CO_2 may also have an effect on the particle removal mechanism. When the liquid phase forms around a surface particulate, it may alter the electrostatic, van der Waals, and other binding forces. This has been speculated about in the supercritical CO_2 literature and may have relevance at these lower pressures. In any case, if a liquid forms around a particle when the snow particle starts to rebound, it can capture a surface particle and remove it. This process may play an important role in removing particles, in that the liquid phase may be critical for high efficiency micrometer and submicron particle removal.

2.3.4 Snow dry-ice cleaning applications [27]

Snow dry-ice cleaning be able to adapt for using in many cleaning applications. Cleaning applications can span from simple laboratory applications to production contamination control problems. These applications include cleaning materials, optics, vacuum components, HDD components, process tools, wafers, and systems. Several patents exist along with numerous unpublished reports of cleaning applications developed by manufacturers and users. Several of the snow dry-ice cleaning manufacturers have developed applications as part of their work and have released the data and applications to the public. As a result, the technique has gained wider acceptance and has entered many new fields.

2.4 Impact stress, σ

From the cleaning mechanism of snow dry-ice cleaning, especially in the part of particle removal that significantly shows the effect of impact stress on the cleaning efficiency. In the other meaning, the impact stress or the cleaning energy from the collision between the cryogenic particle and contaminant particulate must be overcome the adhesive energy bonding. However, the cleaning energy required to remove contaminant particles and thin films rises exponentially as the diameter of the particle or thickness of the film decreases: for example, it has to increase the energy up to several million *g*-forces for submicron particles [2]. The fluid velocities rapidly decrease from turbulent flow (high energy) to laminar flow (low energy) at microscopic distances from the surface simultaneously with the small particles and thin films run away. To overcome this energy barrier or we known as the wall or boundary layer, the high fluid velocities must be achieved to increase fluid flow characteristics from laminar to turbulent, which increases viscous drag (shear stress) upon the particle.

The snow dry-ice cleaning principles are different from the microabrasive cleaning. One difference is the low hardness of dry-ice particles (< 1 Mohs). Thus, the snow dry-ice cleaning using micro-size CO_2 particles is a nonabrasive process. From the research of G.W. Knoth et al. [2], the recent performance testing of the snow dry-ice blasting as shown in Figure 2.7. That includes the experiments by using various nozzle types, pressures, temperatures, flow rates, and capillary condenser types demonstrated that surface impact stresses (cleaning energy) can be controlled precisely from less than 1 MPa (145 psi) to as high as 60 MPa (8,702 psi), which is

more than sufficient shear stress to cause an impinging dry-ice particle to change phase to liquid at the substrate surface [2]. These tests also demonstrated that snow dry-ice cleaning energy can be sustained for relatively long distances using coarse particle streams (large capillary condenser).

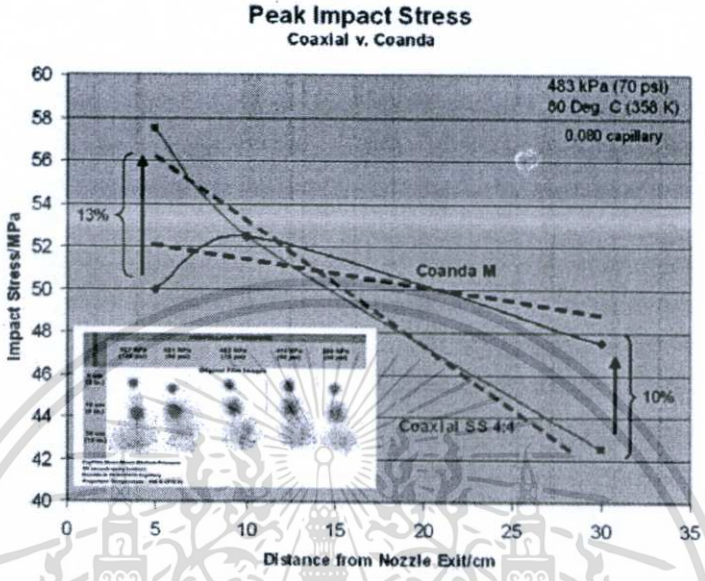

Figure 2.7 Snow dry-ice cleaning energy [2]

2.4.1 Impact stress measurement

Fuji® Prescale is one of the pressure measurement film, which can measure pressure and visualize pressure range. In addition, it can measure pressure, pressure distribution and balance. In normally, the red patches will appear on Prescale sheets when pressure is applied on the sheets. The color density changes according to pressure level. The entire Prescale functions as a sensor and can see at a glance the whole pressure distribution on it. Prescale is the material that able to measure pressure, developed by Fuji Photo Film Co., Ltd. through using the micro-encapsulated color forming material reacts with the color developing material to produce red patches on it. Thus, when pressure is applied, the microcapsules are broken and the color-forming material reacts with the color-developing material. And then the red patches will appear on the film. Prescale film has the sheets in two types (mono-sheet and two-sheet), which are different in the layer of sheets and range of the pressure measurement [29].

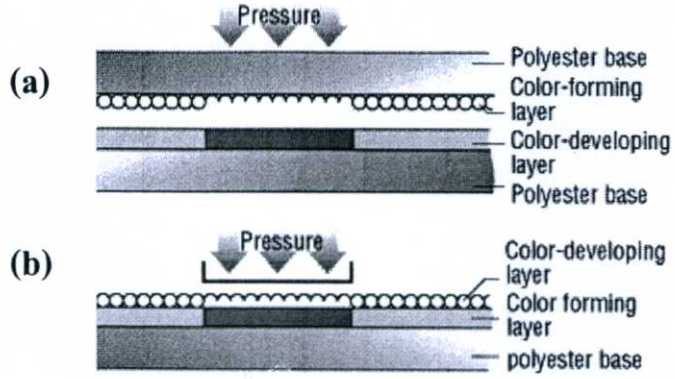

Figure 2.8 Prescale film two-sheet type (a) and mono-sheet type (b) [29]

2.5 Joule-Thomson expansion [30,32]

In thermodynamics, the Joule–Thomson effect or Joule–Kelvin effect or Kelvin–Joule effect describes the temperature change of a gas or liquid when it is forced through a valve or porous plug while kept insulated so that no heat is exchanged with the environment. This procedure is called a throttling process or Joule–Thomson process. At room temperature, all gases except hydrogen, helium and neon cool upon expansion by the Joule–Thomson process [31].

Typically, the process that high pressure fluid flow through the devices such as an orifice, a valve or a porous plug that shows in Figure 2.9 is called "throttling process". Since, there is very short residence time of the fluid flow through the device, thus it means no opportunity for heat transfer, so we can simply consider this process adiabatic. Moreover, the shaft work is zero and the kinetic energy effects are negligible. From the first law of thermodynamics at a steady state, we consider this process is an isenthalpic expansion or the Joule-Thomson expansion process. According to Figure 2.9, the pressure at the point P1 is always extremely higher than the pressure at the point P1. By the way, we need to study the effect of the Joule-Thomson expansion on the temperature of the fluid at the exit (T2). That results as the pressure decreases in the isenthalpic throttling process. In this way, if we know the derivative solution of $\left(\frac{\partial T}{\partial P}\right)_h$, one can determine the Joule - Thomson coefficient (μ_{JT}) as defined in Equation (2.1).

$$\mu_{JT} \equiv \left(\frac{\partial T}{\partial P}\right)_h \tag{2.1}$$

The value of μ_{JT} is typically expressed in °C/bar (SI units: K/Pa) and depends on the type of gas and on the temperature and pressure of the gas before expansion. Its pressure dependence is usually only a few percent for pressures up to 100 bar (1,450 psi).

Figure 2.9 Schematic of Joule - Thomson expansion through a porous plug [30]

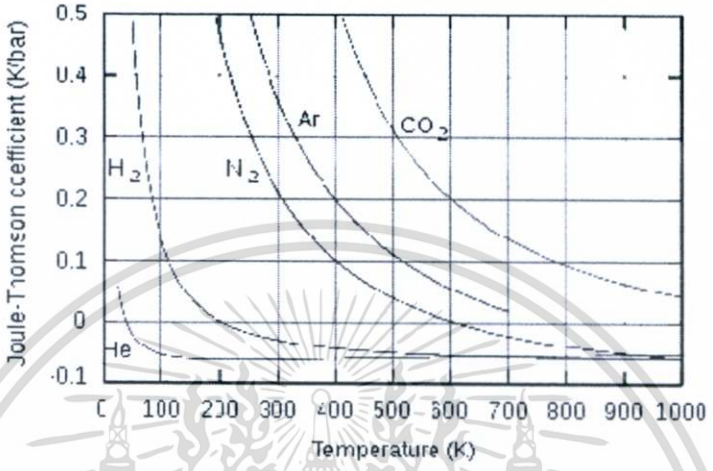

Figure 2.10 Joule-Thomson coefficients for various gases at atmospheric pressure. [31]

2.5.1 Physical mechanism of the Joule-Thomson expansion

From Figure 2.11 plots characteristic line of constant enthalpy (isenthalp line) on a temperature versus pressure diagram of CO_2 [Figure 2.11 is shown the relationship between the reduced pressure (Pr) and reduced temperature (Tr) of CO_2]. Moreover, which is seen from Figure 2.11, there are two regions. From the region inside the curve, the slope of isenthalp line is positive sign, therefore $\mu_{JT} > 0$, as defined by Equation (2.1). In this region, the temperature of the fluid will decrease as the pressure of the fluid decreases during this fluid is moving through the throttling process. Because during the expansion, the average distance between molecules grows. And because of intermolecular attractive forces, expansion causes an increase in the potential energy of the fluid. If no external work is extracted in the process and no heat is transferred, the total energy of the fluid remains the same because of the conservation of energy. The increase in potential energy thus implies a decrease in kinetic energy and therefore in temperature. Conversely, in the region outside of the curve, the slope of the isenthalp line is negative sign, which means that in this region $\mu_{JT} < 0$. Then reduction in pressure causes increasing the temperature. As a second mechanism that has the opposite effect. During fluid molecule collisions, kinetic energy is temporarily converted into potential energy. As the average intermolecular distance increases, there is a drop in the number of collisions per time unit, which

causes a decrease in average potential energy. Again, total energy is conserved, so this leads to an increase in kinetic energy or temperature.

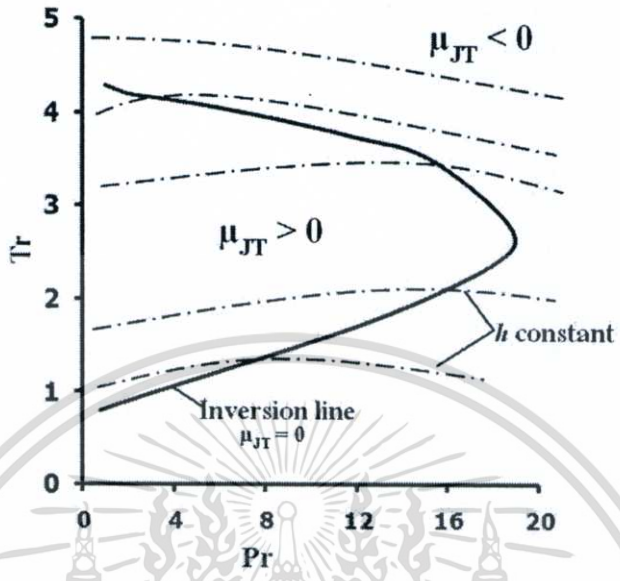

Figure 2.11 Joule-Thomson inversion curve [32]

Moreover, Figure 2.11 shows the line that separate the diagram into two region (as so-called the inversion curve or Joule-Thomson inversion curve, JTIC). The inversion line is a locus curve or the points that the Joule-Thomson coefficient equal to zero. The knowledge of the Joule-Thomson inversion curve plays an important role in optimization, designing and operation of Joule-Thomson cooling processes especially in the manufacture of fluids or petroleum industry. Including, Joule-Thomson inversion curve used to test the predictive capabilities of some recent cubic equation of state. When use the thermodynamic web to develop an expression for μ_{JT} in terms of *PvT* relationship and its heat capacities. By defining in term of differential expression for the change in enthalpy as shown in Equation (2.2).

$$h(T,P) = dh = \left(\frac{\partial h}{\partial T}\right)_P dT + \left(\frac{\partial h}{\partial P}\right)_T dP \tag{2.2}$$

From the definition of the derived thermodynamic property h given by Equation (2.3)

$$dh = Tds - vdP \tag{2.3}$$

Then Equation (2.3) was combined with the Maxwell relation, from this relationship gives

$$\left(\frac{\partial h}{\partial P}\right)_T = \left(\frac{T\partial s + v\partial P}{\partial P}\right)_T = T\left(\frac{\partial s}{\partial P}\right)_T + v \;=\; -T\left(\frac{\partial v}{\partial T}\right)_P + v \tag{2.4}$$

Applying the definition for heat capacity at constant pressure

$$\left(\frac{\partial h}{\partial T}\right)_P = c_p \tag{2.5}$$

Substitution Equation (2.4) and (2.5) into Equation (2.2) gives

$$dh = c_p dT + \left[-T\left(\frac{\partial v}{\partial T}\right)_P + v\right] dP \tag{2.6}$$

From the Joule – Thomson expansion, that mean $dh = 0$; thus, we can rewrite Equation (2.6) into the μ_{JT} form as shown in Equation (2.7).

$$\mu_{JT} = \left(\frac{\partial T}{\partial P}\right)_h = \frac{\left[T\left(\frac{\partial v}{\partial T}\right)_P - v\right]}{c_P} \tag{2.7}$$

Moreover, when the chain rule was used. The differential change in heat capacity at any given pressure is therefore given by:

$$dc_P = \left[T\left(\frac{\partial^2 v}{\partial T^2}\right)_P\right] dP \tag{2.8}$$

Integrating both sides of Equation (2.8) gives

$$\int_{ideal\ gas}^{real} dc_P = \int_{P_{ideal\ gas}}^{P} \left[T\left(\frac{\partial^2 v}{\partial T^2}\right)_P\right] dP \tag{2.9}$$

Solving for c_P^{real}, we get:

$$c_P^{real} = \int_{P_{ideal\ gas}}^{P_{real}} \left[T\left(\frac{\partial^2 v}{\partial T^2}\right)_P\right] dP \tag{2.10}$$

Alternatively, the real heat capacity at constant pressure could be calculated, since intermolecular interactions are important and if an equation of state or other appropriate PvT data and heat capacity of a fluid could be obtained, the μ_{JT} can be calculated from Equation (2.6).

$$\mu_{JT} = \frac{\left[T\left(\frac{\partial v}{\partial T}\right)_P - v\right]}{c_P^{ideal\ gas} - \int_{P_{ideal\ gas}}^{P_{real}} \left[T\left(\frac{\partial^2 v}{\partial T^2}\right)_P\right] dP} \tag{2.11}$$

2.5.2 Applications of the Joule-Thomson expansion

The Joule-Thomson effect is of considerable importance in refrigeration and gas liquefaction processes. Under appropriate conditions, adiabatic throttling of gas will cause to lower its temperature, an endothermic effect that may be strong enough even to induce condensation. Moreover, the snow dry-ice generating system prefers to operate in association with low temperature CO_2. Thus, the modified Peng - Robinson equation of state [MPR EOS; as shown in Equation (2.12)] can use to evaluate the μ_{JT} and Joule-Thomson inversion curve in this research. Because the calculation method of MPR EOS is not complicated. Other than, B. Haghighi et al. [33] has proposed that the inversion curve predicted by MPR EOS shown good predictions at low temperature range (see in Figure 2.12). The low-temperature region of the inversion curve is well matched by MPR EOS for CO_2. The deviation of MPR EOS predictions from the experimental data occurs at reduced pressure above 9 for CO_2. In addition, Peng-

Robinson EOS was recently used for CO_2 freezing prediction of hydrocarbon mixtures at cryogenic conditions of gas plants [31,34].

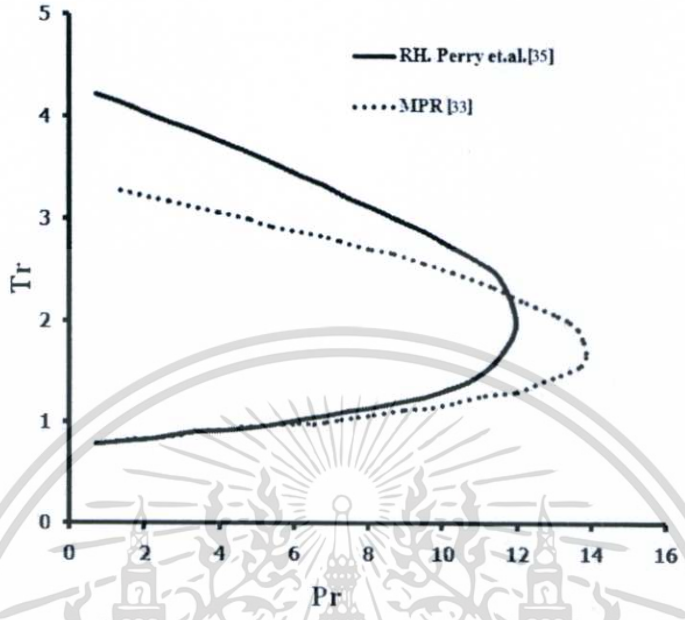

Figure 2.12 Joule-Thomson inversion curves for CO_2 [33,35].

2.6 Related equations

2.6.1 The modified Peng - Robinson equation of state (MPR EOS) [32,36]

The MPR EOS that was used for the μ_{JT} calculation in this studies as shown in Equation (2.12) and its related parameters that were shown by Equation (2.13) to (2.17)

$$P = \frac{RT}{V-b} - \frac{a_c\alpha(T_r)}{V^2+2Vb-b^2} \tag{2.12}$$

$$a_c = 0.45724\frac{R^2T_C^2}{P_C} \tag{2.13}$$

$$b = 0.0778\frac{RT_C}{P_C} \tag{2.14}$$

$$\alpha = \left[1 + \acute{m}\left(1 - \sqrt{T_r}\right)\right]^2 \tag{2.15}$$

$$\acute{m} = 1.21m \tag{2.16}$$

$$m = 0.3796 + 1.485\omega - 0.1644\omega^2 + 0.01667\omega^3 \tag{2.17}$$

2.6.2 Nozzle Velocity of the CO_2 stream, U_0

$$U_0 = \frac{\dot{m}}{\rho_{CO_2}\cdot\emptyset} \tag{2.18}$$

by U_0 is the CO_2 nozzle velocity (m/s).

$\dot{m}$ is the supplying CO_2 mass flow rate (kg/s).

ρ_{CO_2} is the supplying CO_2 density (kg/m^3).

$\emptyset$ is the nozzle cross sectional area (m^2).

2.6.3 Impact velocity(U) [10]

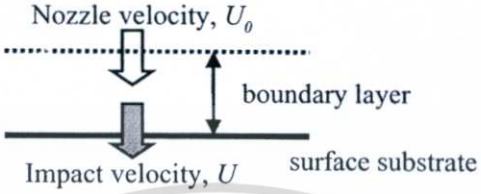

Figure 2.13 The dry-ice particle velocity when it moved through the boundary layer

When the snow dry-ice stream is injected into the cleaning substrate, the boundary layer is generated from the CO_2 gas stream in the combination flow. Therefore, the dry-ice particles must travel through the boundary layer before the dry-ice particles could reach the contaminant and the impact has occurred. This boundary layer will affect to decrease the velocity of the dry-ice particles, thus the impact velocity of the dry-ice particles might be changed from the dry-ice particles velocity at the nozzle tip. Because the effect of the drag force in the boundary layer. Finally, the particle impact velocity could be estimated by using Equation (2.19).

$$U = U_0\left(1 - \frac{\delta}{U_0\tau}\right) \tag{2.19}$$

When U is the impact velocity (m/s).

U_0 is the nozzle velocity (m/s).

τ is the velocity relaxation time (μs) by using Equation (2.20).

$$\tau = \frac{2r^2\rho_P C_C}{9\eta} \tag{2.20}$$

by r is the dry-ice particle radius (m).

ρ_p is the dry-ice particle density (kg/m^3).

η is the CO_2 gas viscosity (Pa·s).

C_c is the Cunningham correction factor that obtains from Equation (2.21).

$$C_c = 1 + \frac{2}{Pd}[6.32 + 2.01exp(-0.1095Pd)] \tag{2.21}$$

where:

P is the absolute pressure (kPa).

d is the dry-ice particle diameter (μm).

δ is the boundary layer thickness (m) that is calculated from Equation (2.22) as:

$$\delta = 0.16 \times \frac{x}{(Re)^{1/7}} \tag{2.22}$$

Then, *Re* is the Reynolds number given as follows:

$$Re = \frac{U_0 x}{\nu} \tag{2.23}$$

where

ν is the kinematic viscosity of the CO_2 gas calculated at plume temperature of –73 °C (m^2/s).

U_o is the nozzle velocity (m/s).

x is the distance between the nozzle and substrate (m).

2.6.4 Momentum of the dry-ice particle, $\bar{P}$

When the dry-ice particle shape is assumed as a spherical particle. The dry-ice particle diameter could be obtained. The mass of the dry-ice particle is evaluated by using Equation (2.24). Then, the momentum of dry-ice particle before the impact with surface could be estimated by using Equation (2.25).

$$m = \frac{4\rho_P \pi r^3}{3} \tag{2.24}$$

where

ρ_p is the dry-ice particle density (kg/m^3).

r is the dry-ice particle radius (m).

and

$$\bar{P} = m \cdot U \tag{2.25}$$

where

$\bar{P}$ is the momentum of dry-ice particle (kg·m/s).

m is the dry-ice particle mass(kg).

U is the impact velocity (m/s) from Equation (2.19).

2.7 Literature Review

2.7.1 Snow dry-ice cleaning process parameters

The key aspects for performing snow dry-ice cleaning are paying attention to processing parameters and methods to insure proper cleaning. Snow dry-ice cleaning must be done in a proper environment to insure proper results. As in any cleaning process, the process cannot allow for redeposition of existing contamination or for any new contamination sources. The redeposition must also be avoided, which means that once a particle or organic contaminant is removed from the surface, it cannot be allowed to deposit on that surface again. The user must also make sure there are no new sources of contamination from the cleaning equipment, or from the environment, or from the process. Therefore, for critical cleaning applications, the system, procedures, and equipment must not allow for recontamination [27].

2.7.1.1 Redeposition

After a particle or organic contaminant is removed from the surface, it must not redeposit on the cleaned areas. This can happen from improper work space and also from poorly chosen cleaning techniques. The first major risk here is that the cleaning environment is a small space or limited volume. Cleaning should not be performed in small or crowded areas. The stream should be allowed to escape from the cleaned surface and no walls or other equipment should be present near the sample to obstruct the contaminated stream [27]. In addition, the turbulence of the stream can remove particles from the obstructions [8], or allow for flow back to the cleaned sample. Therefore, the snow cleaning user must ensure there is enough space around the sample. This can help to make sure that the stream after cleaning the surface is going to escape into a vent region without contacting other objects.

Moreover, the cleaning procedure is also important too. In normally, cleaning is from one side to another to ensure that the stream cannot flow back to the cleaned surface. Cleaning must proceed from a cleaned area into a dirty area. For precision cleaning, it is essential that the cleaned stream be removed from cleaning area, before venting or filtering [27].

2.7.1.2 Recontamination sources

Contamination sources can come from the equipment, the supplying CO_2, and the cleaning systems. The equipment can generate particles, and these particles can enter the supplying CO_2 stream. Therefore, in the choosing material for the snow dry-ice

generating systems such as the valves, tube and fittings must be concerned in precisely. For precision or critical cleaning applications, electropolished stainless steel valves are best suited along with parts cleaned to industry standards. Point-of-use filtration is strongly recommended. This means placing a high quality filter just before the nozzle; generally, filter specifications should be the best possible for the process. It is common to see all metal filters rated at 0.003 mm selected for use [27].

1) CO_2 impurities

In many research has investigated the sources and effects of impurities in supplying CO_2 [7,8,27]. Whitlock [27] identified potential heavy hydrocarbons, possibly as remains from purification process, as a source of submicrometer particulate residue.

Under best conditions, this residue was less than one particle per square centimeter. Hill [8] identified polymeric residues on a surface after snow dry-ice cleaning and traced them back to hose materials. Sherman et al. [7] compared the ability of different CO_2 purity sources to clean a ''clean'' wafer surface. They identified the SFC grades as the best CO_2 source for this application and determined that the added contamination was hydrocarbon-based for lower quality CO_2 grades.

The liquid fed welding source led to greater contamination than the gas fed welding source suggesting that cleaning with a liquid fed cylinder can lead to a greater recontamination on a surface than a gas fed cylinder. Since liquid CO_2 is an excellent solvent, it is expected that the hydrocarbon contamination in a cylinder is concentrated in the liquid and can cause greater recontamination. Onsite purifiers can reduce the heavy hydrocarbon contamination by a factor of 10–100 or more [27].

2) Moisture condensation

When the snow dry-ice stream strikes the surface always decreases the surface temperature and the moisture can be condense later. In normally, moisture condensation does not concern in the ordinary cleaning in most applications, until the moisture is going to freeze or stay on the surface for long time. That mean the cleaning procedure usually have a method to minimize moisture condensation. The easiest method is to use a hot plate as part of the sample support. For samples with poor thermal conductivity, an external heat source (hot air gun or heat lamp) or nitrogen purges are needed. Other choices for moisture control are dry boxes, enclosed hoods or environmental chambers that are purged or heated, or a combination of

these. In critical cleaning applications, such as submicrometer particle removal from wafers or precision cleaning, moisture condensation must not occur, otherwise removal of these small particles will be hindered, or submicrometer moisture particles can remain on the surface. Cleaning should be done in dry, particle-free environmental chambers [11].

2.7.1.3 Cleaning surface damage

In almost every case of cleaning applications by using snow dry-ice, it usually do not seem about the problem of surface damage. However, sometimes there are limitations within the process, mostly related to severe thermal shock, mechanical strength, phase transitions etc. In the fact of most applications, it is the rare sample that has problems. If a sample is suitably supported, it can be cleaned. Patterned wafers can be cleaned, while MEMS (microelectromechanical systems) devices pose challenges and can only withstand lower snow dry-ice velocities. In fact, for the vast majority of samples, no damage or changes can be found unless unique thermal stress issues are present. Methods have been developed to clean CMOS (complementary metal oxide semiconductor) chips that have delicate wires bonds attached. Atomic force microscopy (AFM) [27] has shown the extent of expected surface changes. On materials where atomic scale imaging is possible, it may be possible to see atomic rearrangements on soft materials such as gold.

2.7.1.4 Incident angle and cleaning distance

From the studies of S.C. Yang et al. [25] by using Taguchi method to optimize a pulsed snow CO_2 stream for cleaning CMOS image sensors. That shows the quality characteristics response graphs of the cleaning factors. It is evident that the effect of incident angle is low. The effectiveness of snow dry-ice spraying increases as the incident angle decreases. This agrees with the result of Toscano and Ahmadi [9] in removal section. However, the cleaning distance and orifice size have the greater effect on particle removal. Finally, the parameters of the snow dry-ice cleaning system, which can have an influence on the residue rate of particles, were optimized, resulting in optimal values of 15° incident angle and 40 mm cleaning distance with above 95% confidence.

2.7.2 Other concerning issues in snow dry-ice cleaning

2.7.2.1 Nozzles

Conventional cryogenic spray cleaning processes have traditionally employed supersonic De Laval-type (convergent-divergent) spray nozzles. These nozzles can be described as convergent (narrowing down from a wide diameter to a smaller diameter in the direction of the flow) or divergent (expanding from a smaller diameter to a larger one). A De Laval nozzle has a convergent section followed by a divergent section and is often called a convergent-divergent nozzle ("con-di nozzle"). The convergent nozzles accelerate subsonic fluids. If the nozzle pressure ratio is high enough the flow will reach sonic velocity at the narrowest point [28]. However, the main disadvantage of De Laval cryogenic spray nozzles is an unbalancing effect at the nozzle exit of the fluid stream. As shown in Figure 2.14, the surrounding fluid (ambient atmosphere) tends to drag the nozzle fluid stream, causing the flow stream to diverge rapidly upon discharge from the nozzle exit. This action causes the liquid droplets or sublimable solid particles to expand quickly, resulting in a significant loss of cleaning agent (dry-ice particles) through plume expansion or the production of numerous small dry-ice particles, which generally requires the spray nozzle to be placed in close proximity to a substrate surface to be effective. De Laval spray nozzles produce a two-phase aerosol (gas-liquid) or snow dry-ice through a rapid Joule-Thompson expansion process that wastes liquid CO_2, and spray cleaning energy is mainly controlled only by changing the distance between the nozzle exit and the surface. However, this practice is counterproductive because the CO_2 aerosol particles, already microscopic, are shrinking in size, quantity, and velocity, all of which adversely affects spray cleaning energy control and efficiency [2].

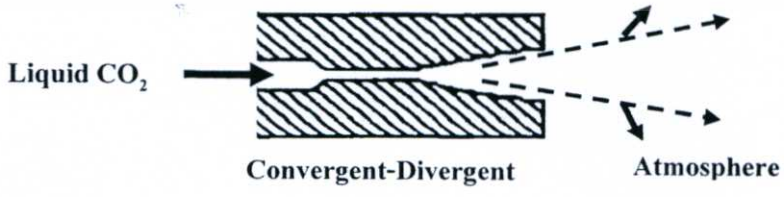

Figure 2.14 De Laval-type (convergent-divergent) spray nozzles [2]

Another failing common to conventional cryogenic spray techniques using De Laval nozzle designs is the intrusion and entrainment of atmospheric contaminants into

the cryogenic particle flow. The most important aspect of these contaminants is atmospheric moisture condensation in the spray stream. Wet atmosphere entrained within the cold spray stream boundary is delivered to the surface along with cleaning spray particles, which complicates the cleaning process. Wetness is caused by the lack of effective shielding of the sublimating particle stream from the ambient atmosphere and insufficient heat capacity within the spray boundary to prevent condensation.

Thus, in case to use conventional snow dry-ice generating designs, some decreasing methods must be installed to remove the humidity of the ambient atmosphere in the cleaning section. These methods may including an inert gas-purged environmental chamber or tunnel, hot plates, infrared heat lamp, hot gas purging streams, or a combination of these methods. However, all of these methods add complexity and cost to the final cleaning system.

Recently, snow dry-ice cleaning improvement that replaces many of the failing of conventional snow dry-ice generating systems in general, and the De Laval nozzle design in particular. That is changed into the advanced CO_2 composite spray nozzle (as shown in Figure 2.15). Advanced CO_2 composite sprays use coaxial or coaxial-Coanda two-phase composite spray nozzle designs with capillary condensation. Coaxial composite sprays produce cleaning plume or stream containing dry-ice particles of controllable size, density, concentration, heat capacity, and kinetic energy. To make dry-ice particles, a capillary condenser assembly with an elongated segment of thermally insulated, so a polyetheretherketone (PEEK) capillary tubing is used. The capillary condenser assembly provides a means for subcooling (boiling) and condensing small amounts of liquid CO_2 into a low-velocity but dense mass of dry-ice particles. Varying the length and internal diameters of the capillary condenser, including stepping, produces particles having different particle size distribution ranges and density. Once formed, dry-ice particles are injected and vortically mixed into a heated propellant gas such as nitrogen or clean-dry air (air zero), which flows coaxially with the capillary condenser assembly [2].

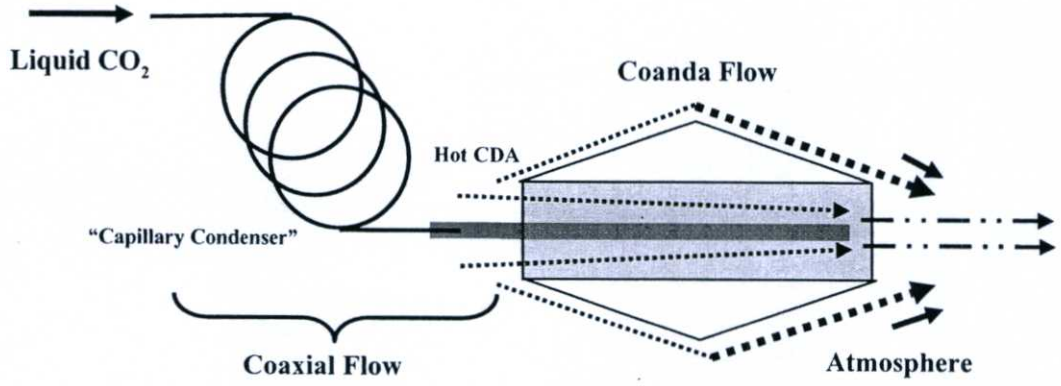

Figure 2.15 Advanced CO_2 composite spray nozzle [2]

2.7.2.2 Moisture control

Moisture condensation can potentially interfere with cleaning or lead to new contamination; therefore, the user must minimize or eliminate moisture condensation. Simple methods include using nitrogen purges, heating with a hot plate, infrared lamps, or even a hot air gun. Other users have used dry boxes. The cleaning environment is enclosed and has a low due point so that moisture condensation does not occur. The best dry boxes for snow dry-ice cleaning operate in the range of 253 to 223 K (-20 to -50 °C) as dew point range. HEPA filters have been introduced to capture the released particles and proper material selections and chamber sizes have made it possible for snow dry-ice cleaning in dry ISO Class 4 (Federal Standard 209 Class 10) conditions or better environment [13]. Sneed et al. [27] discussed a method of heating nitrogen and having the nitrogen warm the surface either before, during, or after CO_2 cleaning. In obvious extension of studies used room temperature nitrogen for a blanketing purge [3,27]. In also the using of heated nitrogen as a blanketing gas [27].

1) Effects of the pulsed injection

Since this very low temperature (below -25 °C) on the surface causes an accumulation of snow, in practice a thermal compensation needs to be introduced to the surface. This thermal compensation can be accomplished by blowing hot air or by thermal exchange from a hot plate. Blowing hot air is the most popular and inexpensive method.

By the way, from the research of S.C. Yang et al. [25], The experimental results could be identify the effect of the pulsed injection is carried out. The temperature of nine points, arranged on the surface of a glass substrate as a 3×3 matrix with a uniform 10 mm pitch, are measured after injection of snow dry-ice towards the center in a 45 °

incident angle at a cleaning distance of 80 mm. After spraying continuously for 2 s, the minimum temperature of the center point is -23.2 ˚C. After 2 s of pulsed spraying with a 100 ms timebase, the minimum temperature of the center point is -12.6 ˚C, with a gain of 10.6 ˚C difference in temperature. The temperatures of the other eight surrounding points are relatively higher in the pulsed spraying case. Thus, the pulsed snow dry-ice stream results in less to no hot air consumption and in addition consumes less CO_2.

2.7.2.3 Agglomeration process of dry-ice particles

Formation of dry-ice particles and their agglomeration process have been studied experimentally by Y.H. Liu et al. [37]. The dry-ice particles were produced by expanding liquid CO_2 at room temperature and pressure (25 ± 2 ˚C, 14.5 psi), and then introduced into a tube as an agglomeration chamber. In the experiments, the temperatures of the stream flow and the tube wall were measured by thermocouples, and dry-ice particles in the stream flow were observed by a high speed camera with a zoom lens.

That was found the dry-ice stream is able to be kept at a lower temperature by adding a glass tube to the outlet of the expansion nozzle. The temperature of snow dry-ice stream decreases and approaches a stable temperature in the early stage; then moves to a stable temperature in second step. The dry-ice particles agglomerated are observed visually after the second reduction of the temperature. Moreover, it was also found that the particle size of the agglomerates increased and the particle velocity decreased with increasing tube diameter.

Thus, tube size has great influence on the particle size and shape as well as velocity. Since the residence time is limited, a large number of collisions of primary particles can hardly be achieved; thus the agglomerates observed cannot be generated by the interparticle collisions in the flow. The agglomeration process of dry-ice particles can be explained by the particle deposition and reentrainment. Because some dry-ice particles of several micrometers are deposited on the tube wall and form a deposition layer. Then, agglomerates are reentrained from the layer into the stream flow.

Chapter 3

Research Methodology

This chapter describes a comprehensive research on hard disk drive assembly parts cleaning process by using snow dry-ice cleaning in three sections: section 1 describes how to generate the snow dry-ice stream and how to control the snow dry-ice generating process. In section 2 is the dry-ice particle and flow characterization. Then, the snow dry-ice blasting was applied for the HDD assembly parts cleaning. Moreover, the snow dry-ice generating system in laboratory scale was designed by using the results in section 1 and 2.

Chemicals and equipments

1) Carbon dioxide 99.5% in purity (CO_2)
2) CEM zero air (H_2O < 2 ppm)
3) AFMS-100 Deflex Power SNO™
4) Cooling unit (Cooling bath)
5) Ethylene glycol 99.5% in purity (EG)
6) Fujifilm® Prescale Film
7) Hard Disk Drive assembly part : used Head Gimbal Assembly (HGA)
8) CO_2 and zero air gas cylinders
9) High pressure regulator, CONCOA ®
10) CO_2 sample cylinder 300 ml, Swagelok ®
11) Thermocouple type K (Typical range -270 to 1,370°C)
12) Pressure transducer
13) Analog input module AI210 (Recording duration / Sampling time, 1s / 1 time)
14) High stability and precision gas balance (METTLER TOLEDO, XS32001L)
15) Optical microscope (with lenses 40X, 80X, and 100X)
16) Sample holder
17) Cleaning chamber
18) Positive pressure cupboard
19) Polymeric (acrylic) tube (OD 5 cm, ID 4.4 cm)

SECTION 1

THE SNOW DRY-ICE GENERATING AND PROCESSING CHARACTERIZATION

3.1.1 Snow dry-ice generating system

The snow dry-ice system model AFMS-100 Deflex Power SNO^{TM} (the commercial types) was used as the snow dry-ice generating process. Figure 3.1 shows the process flow diagram of the snow dry-ice generating system, which consist of supplying CO_2 unit with pressure controller (high-pressure regulator as shown in Figure 3.2), temperature controlling unit (cooling bath as shown in Figure 3.3), separator unit (CO_2 sample cylinder as shown in Figure 3.4), snow dry-ice controller box and the nozzle.

From the literature review [11], the changing of CO_2 conditions affect to the snow dry-ice stream characteristic. Thus, the changing of CO_2 conditions must be studied when the CO_2 fluid was supplied from the CO_2 cylinder into the snow dry-ice generating system. The CO_2 condition data was collected since the CO_2 moved into the snow dry-ice generating system. Then, the collection was finished when the CO_2 reached the atmospheric pressure condition at the nozzle tip. The pressure transducers and K-type thermocouples were installed on the various points for supplying CO_2 pressure and temperature measurements, respectively, as shown in Figure 3.1. The data of CO_2 conditions were monitored via analog input module (AI210) and acquired by a computer. From Figure 3.1, Pin and Tin were used to measure the inlet CO_2 conditions .The P1 and T1 were used as supplying CO_2 condition indicators. The point 3 was installed to collect the CO_2 data before expansion through the nozzle. Finally, the T4 was used to evaluate the CO_2 stream temperature at the atmosphere condition.

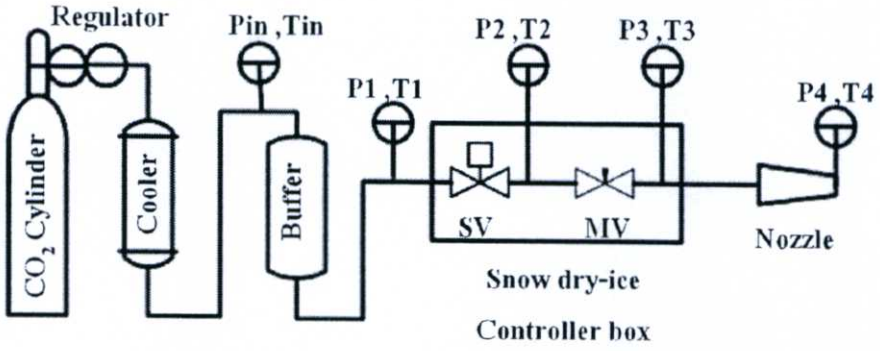

Figure 3.1 Process flow diagram of the snow dry-ice generating system that shows the various of pressure and temperature data collecting points.

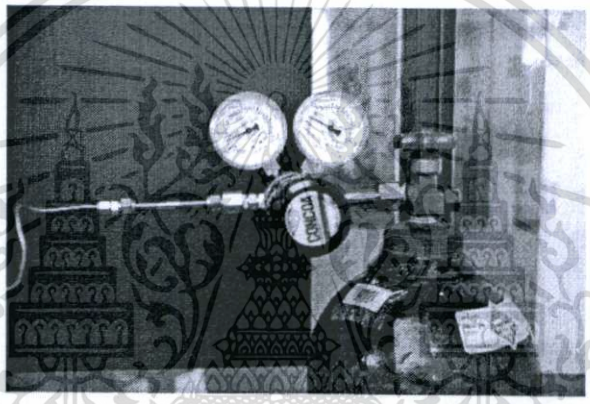

Figure 3.2 CO_2 gas cylinder with high pressure regulator

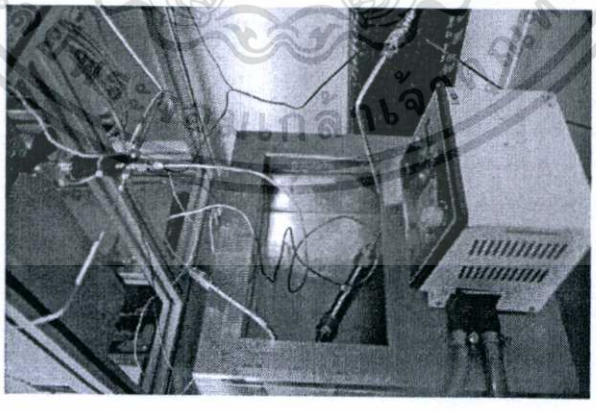

Figure 3.3 Cooling unit for controlling the supplying CO_2 temperature

3.1.1.1 Separator vessel

Then, the controlled conditions CO_2 passed through the separator vessel (as shown in Figure 3.4), which has two functions. The first function is working as a separator to separate between gaseous and liquid CO_2 phases, for increasing of the percentage of liquid phase in the supplying CO_2. Because the snow dry-ice generating would be prefer the supplying CO_2 in liquid phase more than gaseous CO_2 [11]. Then, the vessel is used to contain the controlled conditions supplying CO_2.

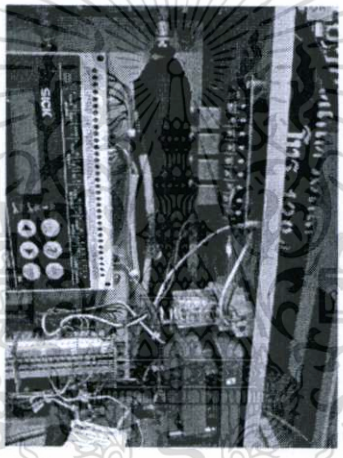

Figure 3.4 CO_2 sample cylinder 300 ml used as a buffer

3.1.1.2 Snow dry-ice controller box

The supplying CO_2 would flow through the snow dry-ice controller box (as shown in Figure 3.5) until the supplying CO_2 reached atmosphere pressure condition at the nozzle tip. Figure 3.6 shows the process flow diagram of the snow dry-ice controller box which is consist of stainless steel tube, fittings, and valves. All of these devices play an important role as the snow dry-ice generating device and affect the snow dry-ice stream characteristic. The effect of these devices would be discussed in Chapter 4.

Figure 3.5 Snow dry-ice controller box

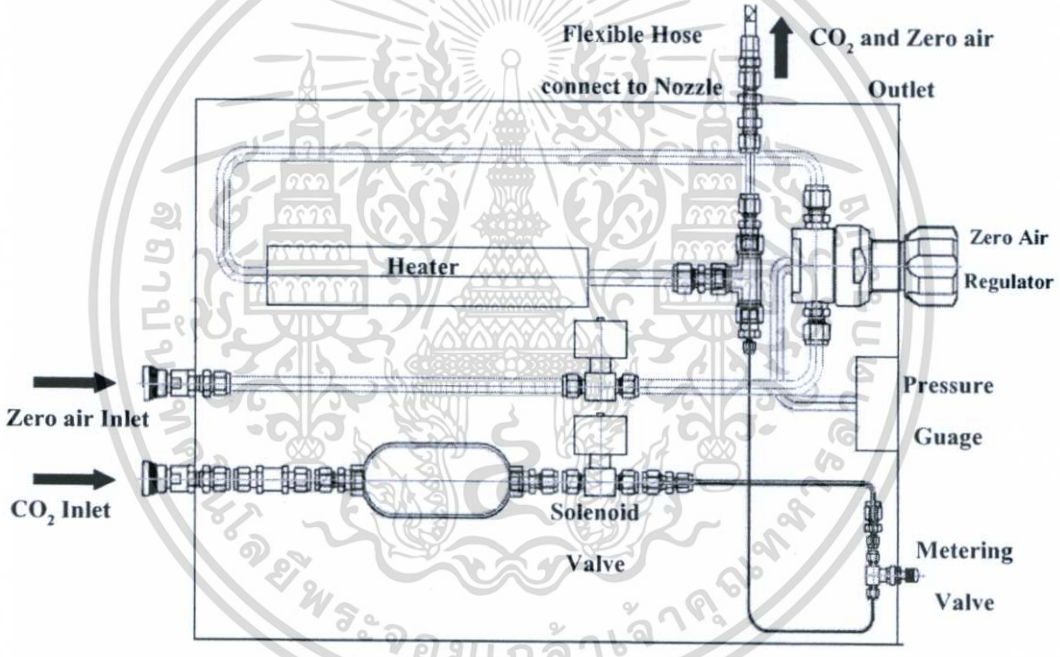

Figure 3.6 : PFD of the snow dry-ice controller box

The solenoid valve (SV) was used as on/off function for snow dry-ice generating system. The metering valve (MV) was used to control snow dry-ice flow rate. A reducer (from tube OD 1/18 in to tube OD 1/16 in) was used as a connector between the metering valve with a polymeric micro-tube that use as the nozzle and this reducer worked as an orifice of the snow dry-ice generating system. Finally, the snow dry-ice generating system was be end up with a polymeric (PEEK) micro-tube (OD 1/16 in, see in Figure 3.7) that connected with the reducer in

front of the metering valve and the designed nozzle at the end after the micro-tube filled through inside a flexible hose (as shown in Figure 3.8).

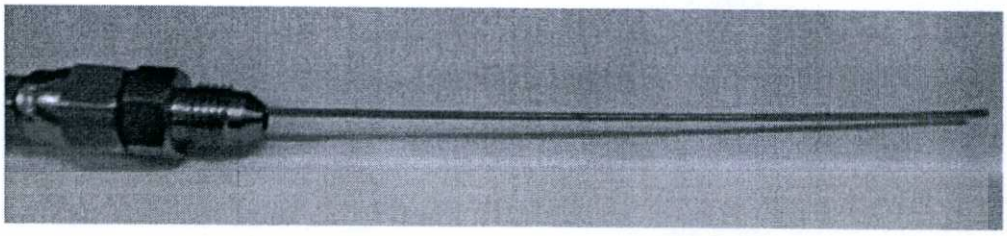

Figure 3.7 Polymeric micro-tube (OD 1/16)

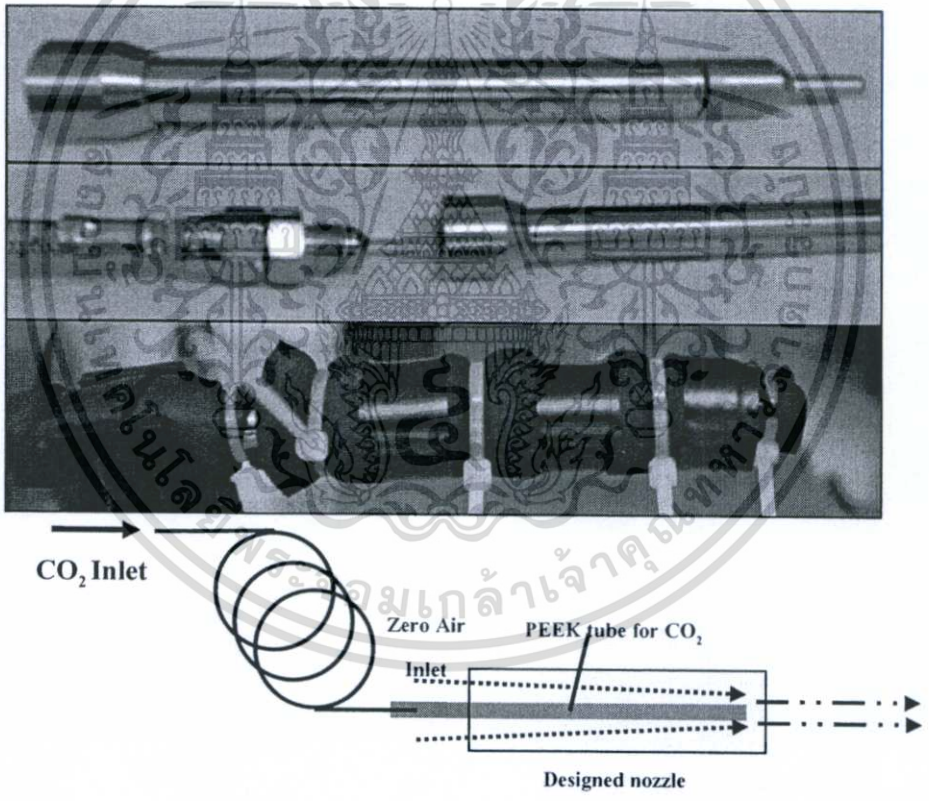

Figure 3.8 Designed nozzle with/without insulation

3.1.2 The processing characterization

3.1.2.1 Supplying CO_2 pressure

The supplying CO_2 pressure was varied from 900 psi until the pressure still around 350 psi. Thus, the high supplying CO_2 pressure was in the range of 700-900 psi. The medium supplying CO_2 pressure range were between 500 to 700 psi. The low supplying CO_2 pressure was used in below 500 psi.

3.1.2.2 Supplying CO_2 temperature

The experimental conditions were controlled by supplying CO_2 pressure as a major parameter. The supplying CO_2 temperature was changed in follow with the pressure range. When the thermodynamic theory of snow dry-ice formation was considered. The supplying CO_2 conditions could be control via its density. Thus, the supplying CO_2 density was controlled by varying of the supplying CO_2 temperature in the range as shown in Table 3.1.

Table 3.1 Supplying CO_2 conditions

Case of the experiment	Supplying CO_2 Conditions		
	Pressure Range (psi)	Temperature Range (°C)	Density Range (kg/m^3)
High pressure	700 - 900	17 - 25	140 - 220
Medium	500 - 700	6 - 15	90 - 140
Low	< 500	< 5	< 90

3.1.2.3 Effect of the supplying CO_2 conditions on the temperature profile of snow dry-ice stream

The temperature profile of the snow dry-ice stream when it was expanded through the nozzle into the acrylic tube (OD 5 cm, ID 4.4 cm), was observed by using the thermocouple type K that connected to a temperature recorder as shown in Figure 3.9. In the tube, temperature was controlled around 23-25°C at 14.5 psi (1 atm) and the relative humidity (%RH) was around 65-70 percentage. Finally, the measurement position x is the distance from the nozzle tip so the temperature of the snow dry-ice stream were measured at the x = 0, 2, 4, 6, and 8 cm.

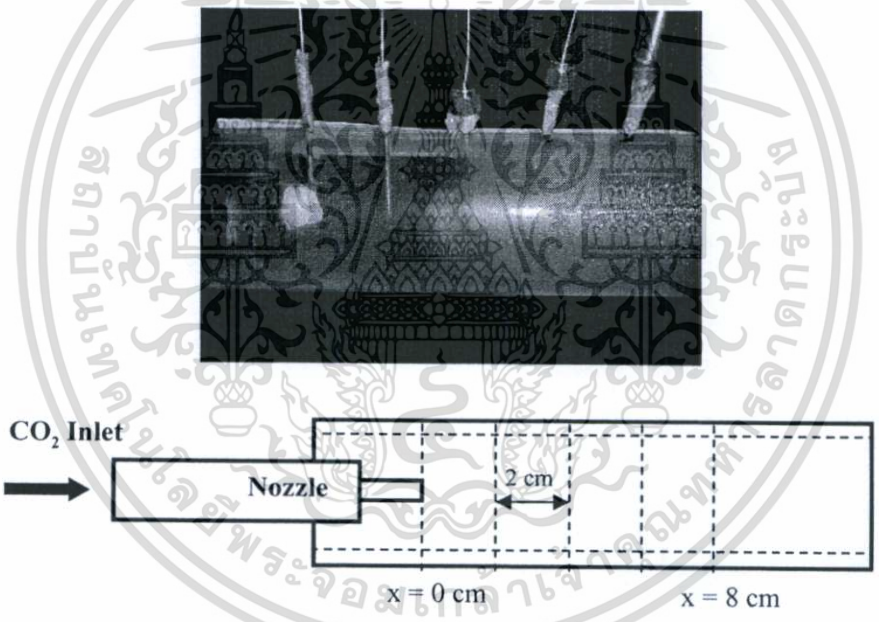

Figure 3.9 The test section for the snow dry-ice stream temperature profile

3.1.2.4 Effect of the supplying CO_2 condition on the CO_2 mass flow rate

When the snow dry-ice stream was generated by flowing the supplying CO_2 from the cylinder through the snow dry-ice generating system. The mass flow rate of the supplying CO_2 was obtained by using the high stability and precision level gas balance as shown the apparatus as in Figure 3.10. The CO_2 mass flow rate was evaluated through the lost rate of the CO_2 weight in cylinder.

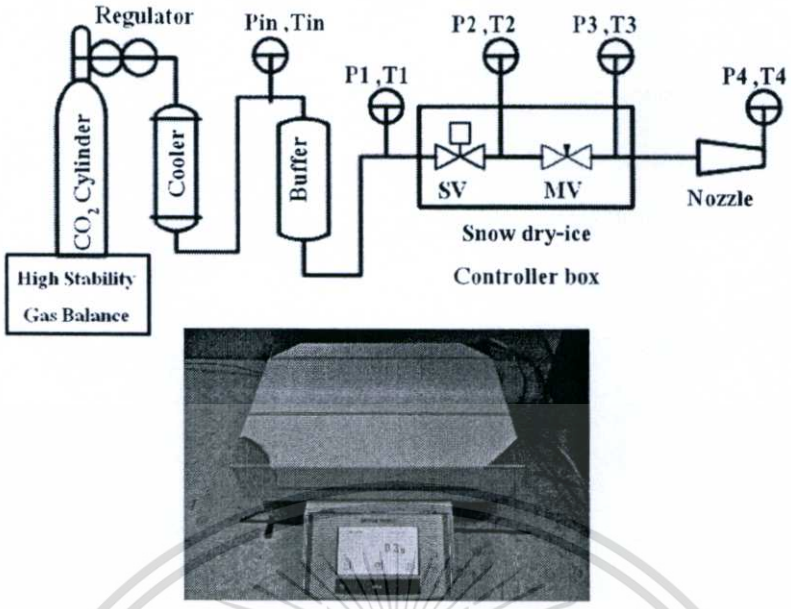

Figure 3.10 Process flow diagram of the snow dry-ice generating system with the high stability and precision level gas balance (Mettler Toledo, XS32001L)

SECTION 2

THE DRY-ICE PARTICLE AND FLOW CHARACTERIZATION

3.2 Dry-ice particle and flow characterization

3.2.1 Impact stress measurement

The impact stress of the snow dry-ice stream was measured by using the pressure measurement film (Prescale FUJIFILM ®). In addition, the mono-sheet type, which are available for the medium pressure range [10-55 MPa; (1,450-7977 psi)] is the most suitable for the experiment. Base on the recommended conditions in Table 3.1, the experiment apparatus for the snow dry-ice stream pressure measurement was set up as shown in Figure 3.11. The pressure measurement methodology was included the heater that used to contain the Prescale film temperature constant at around 30°C during the snow dry-ice injection times. The relative humidity during the experiments were between 65 up to 70 percentage relative humidity (%RH).

The distance between nozzle tip and the Prescale film was 10 mm. Finally, the injection time for all experiments was around or over 5 seconds. Note that the Prescale film should be covered the film sheet with the other sheets as a pressure distributor in case of the impact pressure measurement [29].

Table 3.2 Recommended conditions for the pressure measurement by using Prescale film [29]

Precision	±10% or less (measured by densitometer at 23°C, 65% RH)
Recommended temperature range	20°C ~ 35°C
Recommended humidity range	35% RH ~ 80% RH

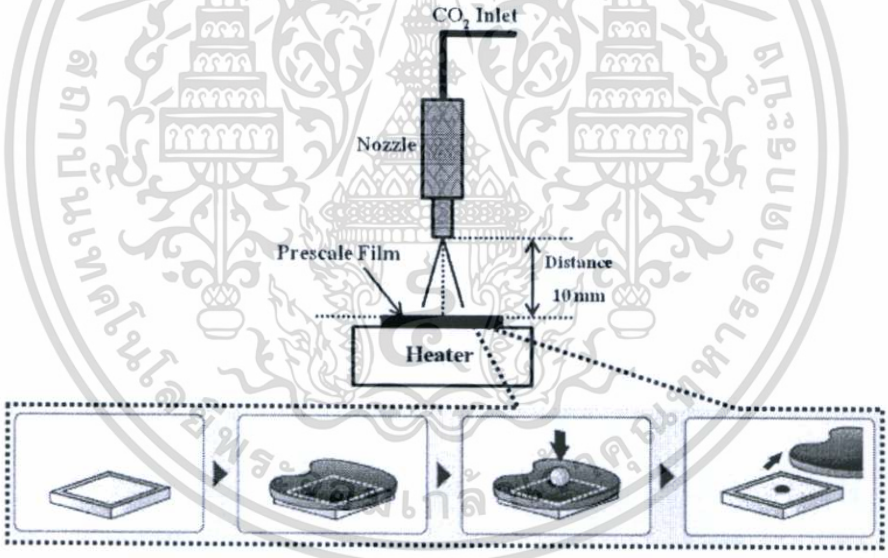

Figure 3.11 Schematic of the experimental set-ups for impact stress measurement

Then, the impacted Prescale films were used to estimate the impact stress of the dry-ice particles. The impacted films could be observed the changing of the film color into the red theme. The impact stress could be evaluated by using the pressure chart or standard momentary pressure chart [38] as a color density convertor (as shown in Figure 3.12).

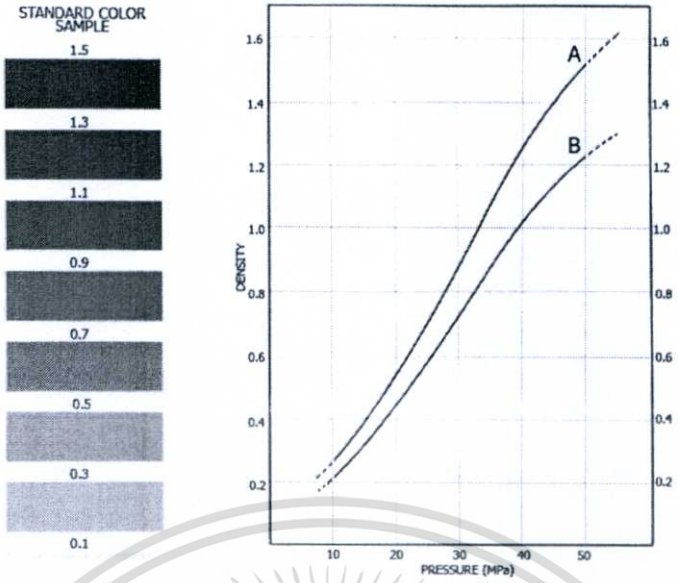

Figure 3.12 Standard momentary pressure chart for the mono-sheet type for medium pressure [39]

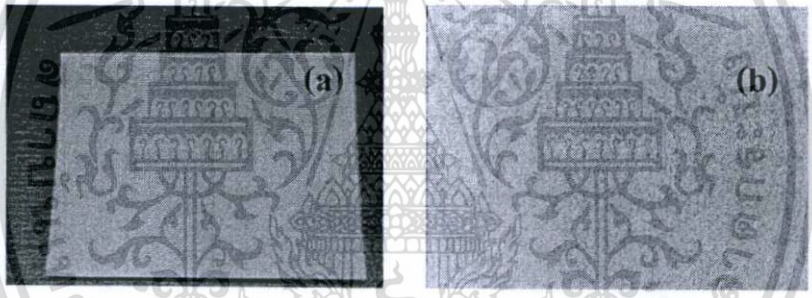

Figure 3.13 The Fujifilm Prescale film mono-sheet type for medium pressure (a) before and (b) after passed the snow dry-ice injection

3.2.2 Evaluate the diameter size of dry-ice particles

In this section, the experiment was set up as same as in the section 3.2.1. The injection time was 1 second, and the injection was a pulsed blasting. After the injection, the impacted Prescale film would be observed the dry-ice particles size distribution by using the optical microscope with 100X magnification (Olympus ®).

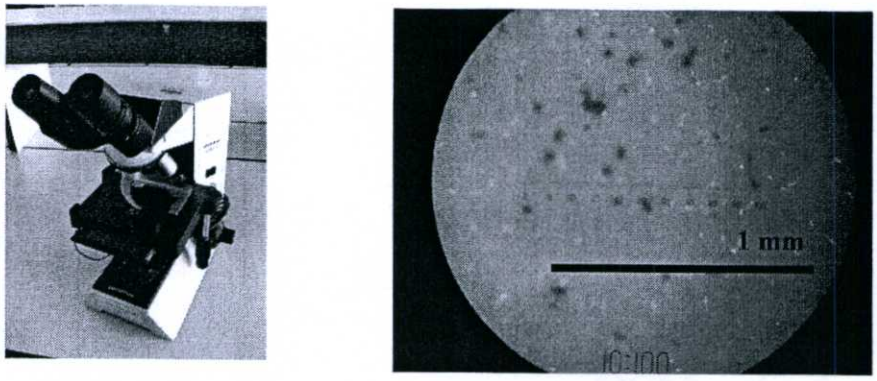

Figure 3.14 Optical microscope with lense 100X (a) and size of the dry-ice particles that appeared on the Prescale film (100X) as many red dots (b)

SECTION 3

CLEANING TEST

3.3 Hard disk drive assembly part cleaning

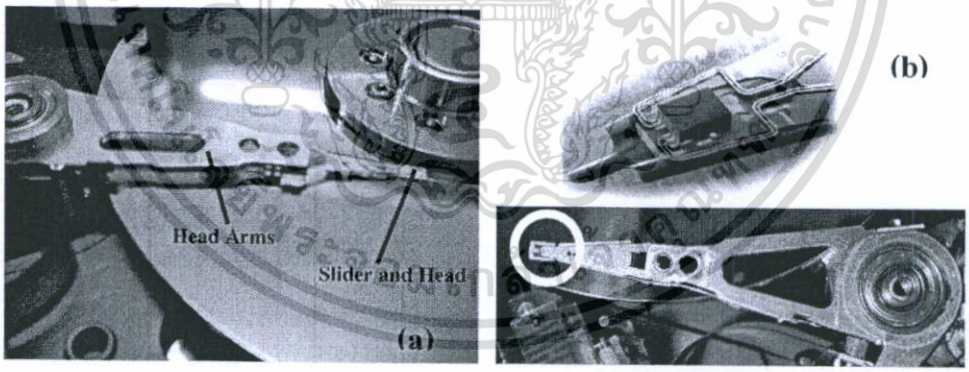

Figure 3.15 Hard disk drive components (a) and Head Gimbals Assembly (HGA) (b) that used as samples for cleaning test [16]

3.3.1 Preparation of the sample for cleaning test

The real HDD assembly part was used as the cleaning samples. The used head gimbals assembly (HGA) was selected as cleaning samples [see in Figure 3.15(b)]. From the

HDD components in Figure 3.15, HGA was stuck on head sliders, which were suspended at the ends of head arms. HGA is a one of very small and sensitive HDD assembly parts and HGA cannot have any residue on surface. HGA substrate made from a combination of materials, which may be ceramic or ferrite. Some of the HGA in the used HDDs might have some contaminants after the HDDs were used. The contaminant particle sizes were in the range of 14 to 200 nm [14]. In addition, the micro-sized particles that adhered to the slider were mainly composed of F, Fe, Cr, Al and Ni. Some of the micro-sized particles came from the lubricant on the disk surface, PFPE (perfluoropolyether) [14]. Moreover, the conventional cleaning method cannot eliminate the contaminants on the HGA part in any way, because the contaminants on the HGA surface have the size in the range of submicron or nano-sized [13,14].

The samples preparation method is consist of:

Step 1 To split the HGA parts from the HDDs

Step 2 To take before cleaning photo of the HGAs surface by using optical microscope with 80X lenses

Step 3 To store the HGA samples in the positive pressure cupboard at 25°C (under zero air atmospheres)

3.3.2 Cleaning method by using snow dry-ice blasting

The cleaning method was set up in the cleaning chamber that was controlled the environmental inside by using zero air. By using zero air feeding inside the chamber, it could be reduced chance of recontamination and condensation on the cleaned samples.

The cleaning procedure is consist of:

Step 1 To bring the HGA samples that passed the preparation in section 3.3.1 into the cleaning chamber and installed on the sample holder as shown in Figure 3.16.

Step 2 To set the cleaning distance at 10 mm.

Step 3 To set the supplying CO_2 pressure and temperature

Step 4 To turn on the solenoid vale (SV) to generate the snow dry-ice stream, then inject the stream strike to the HGA surface and keep the incident angle at 30°- 45° during the cleaning. In this step, the snow dry-ice injection was used in two types, that is consist of continuous and pulsed injection.

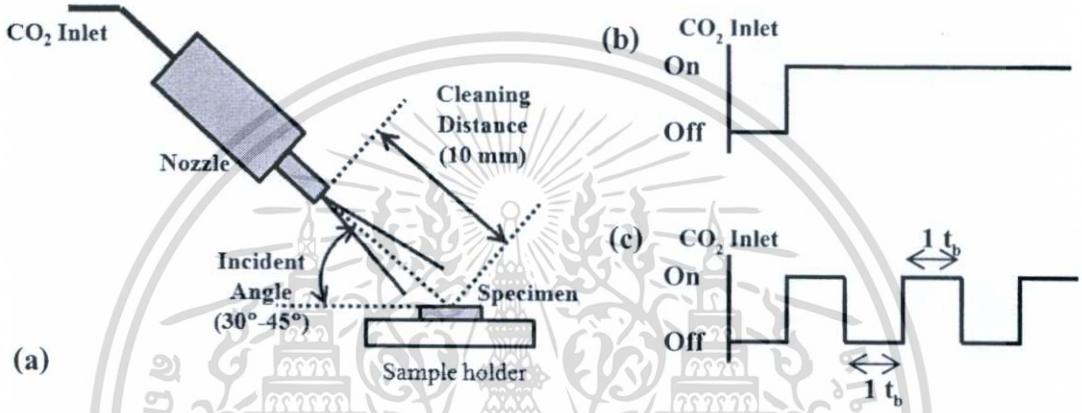

Figure 3.16 (a) Schematic representation of the experimental set-ups with cleaning factors: the incident angle, the cleaning distance and on/off cycles of the solenoid valve in case of (b) the continuous injection and (c) the pulse injection

Continuous injection

The continuous snow dry-ice injection, which keeps on/off cycles of the solenoid vale during the cleaning (5 seconds) as shown in Figure 3.16 (b).

Pulsed injection

To generate the pulsing stream mechanically, that used an on/off cycles of the solenoid valve as in Figure 3.16 (c). The time-base (t_b) interval for these experiments is 1 second. The spraying time of a snowing cycle for each experiment is 5 seconds.

Step 5 To turn off the SV

Step 6 To inject the zero air stream to wipe some of condensed droplets on the HGA surface

Step 7 To store the HGA samples in the positive pressure cupboard at 25°C (under zero air atmospheres)

Step 8 To Take the HGA surface photo after cleaning by using optical microscope with 80X lenses (operation in clean room)

3.3.3 Cleaning method by using snow dry-ice in combination of zero air stream

For this section, the experimental set-up and the cleaning environment were controlled as same as in section 3.3.2 In addition, the experimental steps were carried out same as in the section 3.3.2 procedure. However, the combination flow between the snow dry-ice aerosol and zero air stream was generated from a composite spray nozzle, this stream was used as a cleaning agent. Thus, the snow dry-ice generating system as indicated in Figure 3.17 was used in this section.

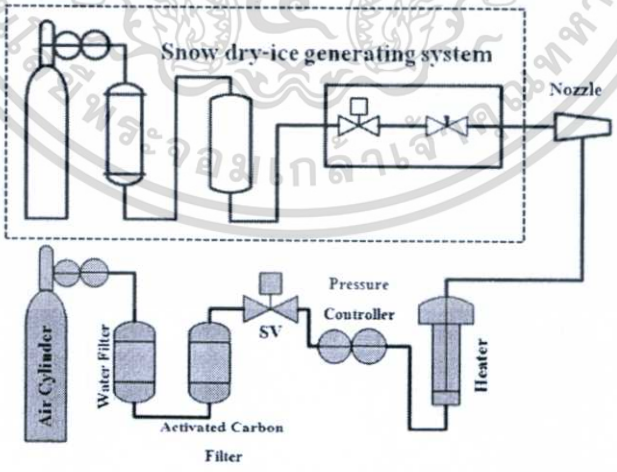

Figure 3.17 Snow dry-ice generating system that combined with the zero air line

Chapter 4

Results and Discussion

This chapter shows about the results and discussion in three sections. Section 1 describes the generating of snow dry-ice stream and the processing characterization of snow dry-ice generating process. Section 2 is the dry-ice particle and flow characterization. Then, the cleaning efficiency of the snow dry-ice blasting on the HDD assembly parts cleaning is shown in section 3.

SECTION 1

THE SNOW DRY-ICE GENERATING AND PROCESSING CHARACTERIZATION

4.1.1 Snow dry-ice generating system

The commercial used snow dry-ice system model AFMS-100 Deflex Power SNO™ was used to generate the snow dry-ice stream. From the experiment results, the snow dry-ice generating system have an excellent performance to generate the snow dry-ice stream, in the case of using the suitable supplying CO_2 conditions. Figure 4.1 shows the snow dry-ice stream that was generated by the snow dry-ice generating system. The milky stream in Figure 4.1 were the snow dry-ice stream, and it could be confirm by the experimental results in later section. Moreover, the snow dry-ice generating system has abilities in both to apply for pulse or continuous snow dry-ice generating. The various type of injection is one of the snow dry-ice system's flexibility for applying in various cleaning applications.

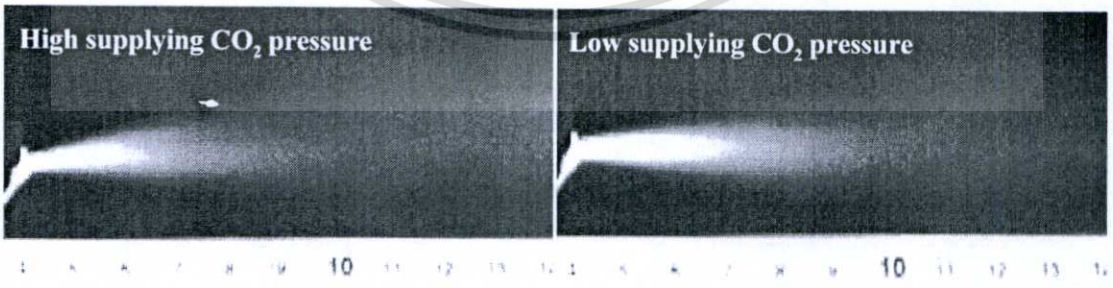

Figure 4.1 Snow dry-ice aerosol that were generated by the snow dry-ice system model AFMS-100 Deflex Power SNO™

4.1.2 The direction of supplying CO_2 phase changing

After let the controlled conditions supplying CO_2 into the snow dry-ice generating system, the supplying CO_2 conditions were found that the conditions changed in twice times significantly. At first, the thermodynamic phenomena were dropping in pressure that always was happened between points of P2 and P3 (pressure drop in the range of 5-20 psi), which were naturally dropped by moving through devices and fittings. However, there was not any changing in supplying CO_2 temperature at this area. Then, the supplying CO_2 enter to the snow dry-ice generating system until pass the metering valve, supplying CO_2 did not change its phase.

The other one changing was observed between the point P3 and the nozzle tip, which the pressure drop were extremely high. Because the high supplying pressure CO_2 fluid expanded through the orifice (reducer) and the polymeric micro-tube as a nozzle before moving into the atmospheric pressure. Thus, the pressure drop range varied by the range of supplying CO_2 that used in the experiments. For high supplying CO_2 pressure range, the pressure drop would be around 800 - 850 psi. When the supplying CO_2 pressure was in the low-pressure range, the pressure drop would be 400 to 600 psi. Therefore, at the second pressure drop, the pressure decreasing affected the reduction of supplying CO_2 temperature obviously. Especially, between the points T3 and T4, which the Joule-Thomson expansion was taken place. This expansion caused the CO_2 phase changing. Then, some of the CO_2 stream line were converted into the solid phase (dry-ice particles). Thus, the area between the orifice and the nozzle is one of the most significant areas that affect the snow dry-ice stream characteristic.

4.1.2.1 In case of high supplying CO_2 pressure range

The range of supplying CO_2 conditions for the high-pressure range (P1,T1) was in the range of 780 - 870 psi and 18 - 27 $^{\circ}$C. When the supplying CO_2 flew through the system, until the CO_2 changed into the milky stream at the nozzle tip. The data of CO_2 conditions were collected from the instruments. Thus, these data could confirm about the milky stream at the nozzle tip was an exactly snow dry-ice aerosol. For example, Figure 4.1 that shows the snow dry-ice stream generating by using supplying CO_2 pressure (P1) 850 psi and the supplying CO_2 temperature (T1) was 21 °C. The thermodynamic theory of snow dry-ice formation and CO_2 phase diagram were used to evaluate the direction of phase changing. Thus, the plotting of supplying CO_2 pressure (P1) and temperature (T1) data on the CO_2 phase diagram is shown in Figure 4.2. When the CO_2 expanded through the orifice and the polymeric micro-tube into

atmospheric pressure stage, and the temperature of the milky stream (T4) was -73.5 °C (point 3). From Figure 4.2, the CO_2 stream was a combination phase between the gaseous and solid. Thus, the snow dry-ice generating system could generate the snow dry-ice stream by using the suitable supplying CO_2 conditions in otherwise.

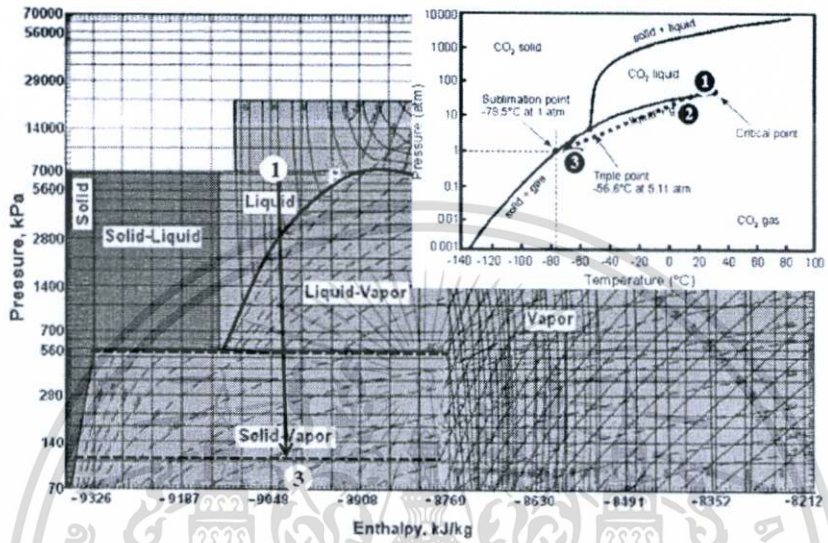

Figure 4.2 The *P-H* phase diagram for CO_2 [2] and *TP* phase diagram for CO_2 (small Figure) [2], which are shown about the supplying CO_2 phase changing in case of high supplying CO_2 pressure.

4.1.2.2 In case of low supplying CO_2 pressure range

From the results in the low supplying CO_2 pressure range, which used the supplying CO_2 pressure (P1) in the range of 400-600 psi and the supplying CO_2 temperature (T1) was in the range of 0-15 °C. For the example as same as in section 4.1.2.1, Figure 4.1 shows a generating of the snow dry-ice stream by using supplying CO_2 pressure (P1) 550 psi and supplying CO_2 temperature (T1) was 10 °C. When the CO_2 flew and expanded through the orifice and the nozzle into atmospheric pressure stage. From Figure 4.3, the temperature of the milky stream at nozzle tip (T4) was -55.6 °C (point 3). Thus, the CO_2 stream was a combination phase between the gaseous and solid.

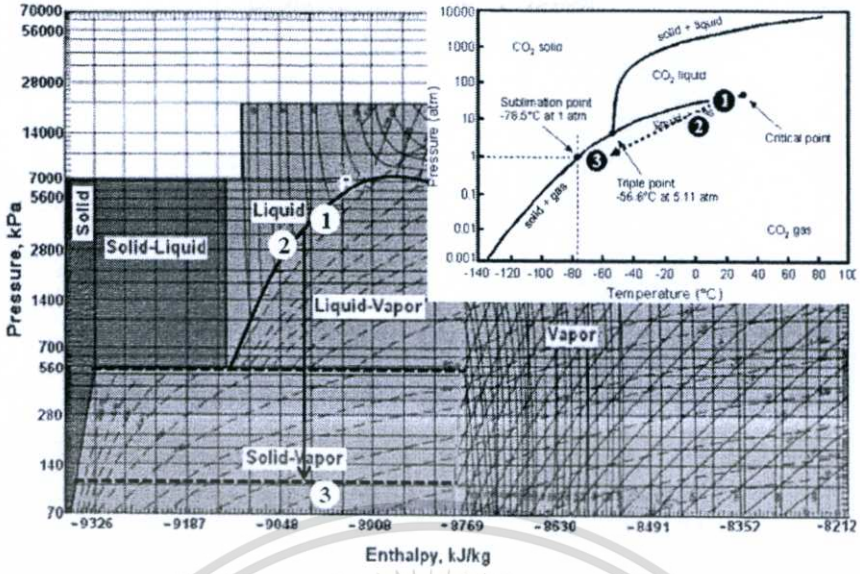

Figure 4.3 The *P-H* phase diagram for CO_2 [2] and *TP* phase diagram for CO_2 (small Figure) [2], which are shown about the supplying CO_2 phase changing in case of low supplying CO_2 pressure.

From the experimental results in section 4.1.2.1 and 4.1.2.2, it shows about the results when the supplying CO_2 conditions were changed. The supplying CO_2 conditions will directly affect the temperature of snow dry-ice stream (T4), even though the snow dry-ice generating system still could generate the snow dry-ice stream. The temperature of snow dry-ice stream (T4), which roughly illustrates the existence of dry-ice particles in the snow dry-ice stream. Thus, the difference in temperature of snow dry-ice stream represents for the difference in snow dry-ice stream characteristic. Then, the relationship between the supplying CO_2 conditions and the CO_2 stream temperature at the nozzle tip must be evaluated.

4.1.3 The relationship between the supplying CO_2 conditions and the snow dry-ice stream characteristic

From the experimental results in section 4.1.2, which are shown about the effect of the different supplying CO_2 conditions on the CO_2 stream temperature at the nozzle tip. When the snow dry-ice generating system was applied to use in various cleaning. The suitable supplying CO_2 conditions for using in the snow dry-ice generating system must be evaluated. Moreover, the characteristic of the snow dry-ice stream be able to study in many ways such as dry-ice particles size or amount, impact stress of the snow dry-ice stream etc. However, in this section, the percentage of the dry-ice particles or solid phase in the snow dry-ice stream was used as the simply way to study on the characteristic of the snow dry-ice stream.

4.1.3.1 In case of high supplying CO_2 pressure range

When the operating conditions were in the pressure range of 780 - 870 psi and 19 - 23°C for the temperature range. The snow dry-ice stream could be generated. However, the snow dry-ice stream or satisfied snow dry-ice stream cannot generate by using some of these supplying CO_2 conditions. Thus, the suitable operating conditions for snow dry-ice generating process must be considered. The criterions are the operating consistency and safety. When the snow dry-ice stream that was generated by using the high-pressure supplying CO_2 range. The snow dry-ice stream must contain as much as the dry-ice particles phase in the stream. Thus, from the CO_2 phase diagram and the snow dry-ice definition, the appropriate snow dry-ice stream should have the temperature around the triple point of CO_2 (-56 °C) with the upper and lower limit as 5 °C. However, the suitable conditions for snow dry-ice generating by using high-pressure range should give the temperature of the CO_2 stream at the nozzle tip under the lower horizontal dash line in Figure 4.4 or below -60°C. Thus, the range of processing window (shaded region as shown in Figure 4.4) in the case of high-pressure supplying CO_2 must be in the range of 800 - 850 psi and 20-22 °C for supplying CO_2 temperature.

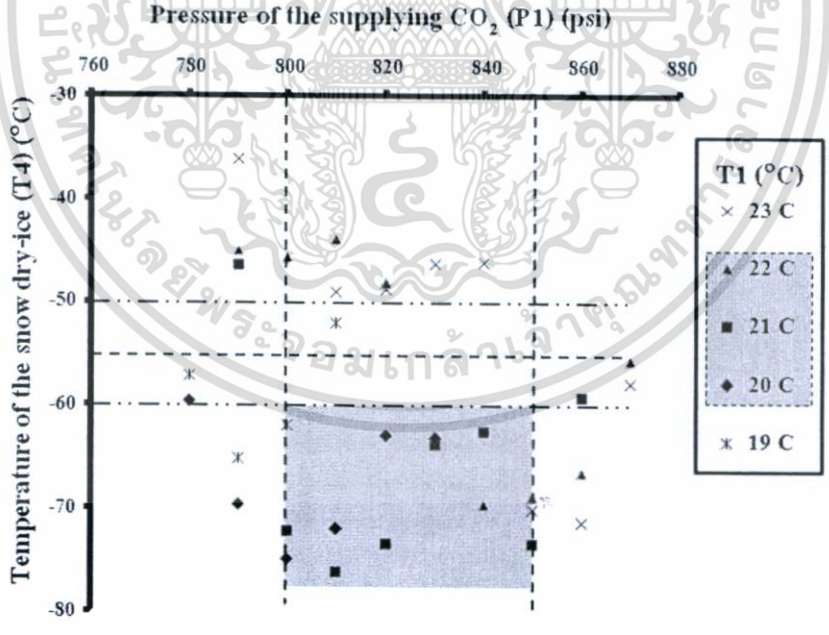

Figure 4.4 Relationship between the pressure of supplying CO_2 (P1) and the temperature of snow dry-ice at the nozzle tip (T4) in case of using high-pressure range

Effect of the CO_2 stream temperature on the dry-ice particles producing

From the data of the CO_2 conditions changing, the fraction between gas and solid particles in the snow dry-ice stream could be calculated by applying the lever arm rule with the CO_2 (*P-H*) phase diagram (see Figure 4.2). Thus, the roughly percentage of dry-ice particles in the snow dry-ice stream was estimated from the data of CO_2 pressure and enthalpy. The percentage of the CO_2 fluid that converted to solid particles in the snow dry-ice stream is shown in Figure 4.5. From the range of processing window in Figure 4.4, the high pressure CO_2 fluid would be converted to solid particles in the range of 38.9 - 43.4 percentages.

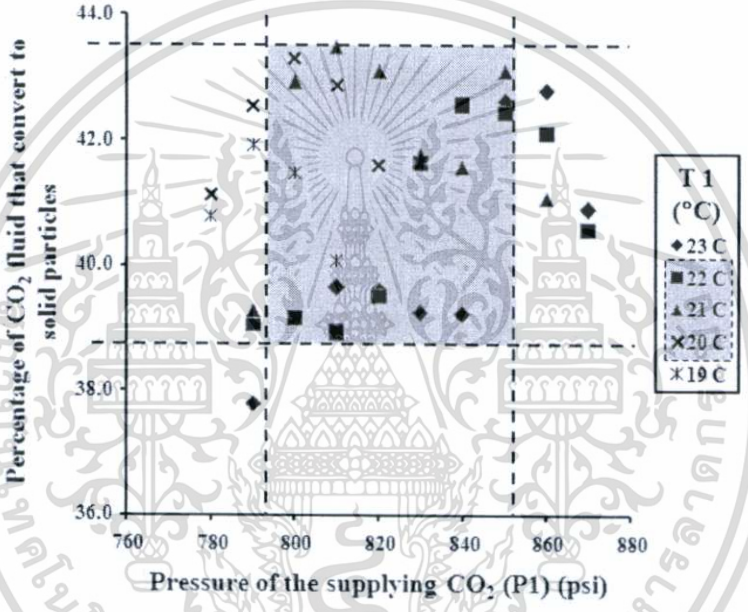

Figure 4.5 Relationship between pressure of the supplying CO_2 (P1) and amount of the CO_2 fluid that converted to solid particles when CO_2 is moving through the orifice into the atmosphere in case of high-pressure range.

The existence of dry-ice particle percentages is one of the snow dry-ice characteristic. This percentage can be told directly us about the cleaning efficiency, because the majority of particle removal by using snow dry-ice cleaning is the collision between the dry-ice particles and contaminant. Therefore, the increasing of solid particles phase in the stream is going to increase more opportunities to have the collisions in the other meaning. The tuning to optimize the snow dry-ice generating system must be discussed as one of the snow dry-ice generating issues. Thus, the discussion about the system tuning would appear in later section.

4.1.3.2 In case of low supplying CO_2 pressure range

By using low supplying CO_2 pressure range, the supplying CO_2 conditions in the same range as the case of using high supplying CO_2 pressure that were around 20-22 °C, the snow dry-ice generating system cannot generate the snow dry-ice stream. Thus, supplying CO_2 conditions must be inquired again. When the CO_2 density was calculated, then the density was used as a tuning target of the supplying CO_2 condition for the low-pressure supplying CO_2. For example of tuning, supplying CO_2 pressure must be around -3 to -4 °C or below -4 °C in the case of constant supplying CO_2 pressure at 450 psi, because at these conditions CO_2 will prefer liquid phase instead of vapor (from the calculation results in Table 4.1).

Table 4.1 Supplying CO_2 density at the various temperature when the supplying CO_2 pressure constant at 450 psi.

Supplying CO_2 temperature (°C)	Supplying CO_2 Density (kg/m^3)
25	68
20	70
5	80
- 3	84
- 4	952

Due to the equipment limitation, the supplying CO_2 temperature was in the range of 9 to 13 °C, when the supplying CO_2 pressure were in the range of 560 - 610 psi. Figure 4.6 is shown about the comparison between the experimental results by using low supplying CO_2 pressure and the results from high-pressure range in section 4.1.3.1. Nevertheless, the criteria for consideration of the suitable operating conditions in case of the low-pressure range must be changed in anyway. The snow dry-ice stream that generate from the low-pressure supplying CO_2 range will be applied for the precision cleaning with sensitive substrates. Thus, the snow dry-ice stream must have appropriate amount of dry-ice particles in snow dry-ice stream. Although, from Figure 4.6, the suitable operation conditions for low supplying CO_2 pressure should be in range of 570 to 590 psi (or below 600 psi) for the supplying CO_2 pressure and the supplying CO_2 temperature must below 12 °C or in the range of 9 - 11 °C. Thus, the processing window (in the

blocked area) for low-pressure range must let the system to generate the snow dry-ice stream that have the temperature between the upper and lower limit from the CO_2 triple point temperature.

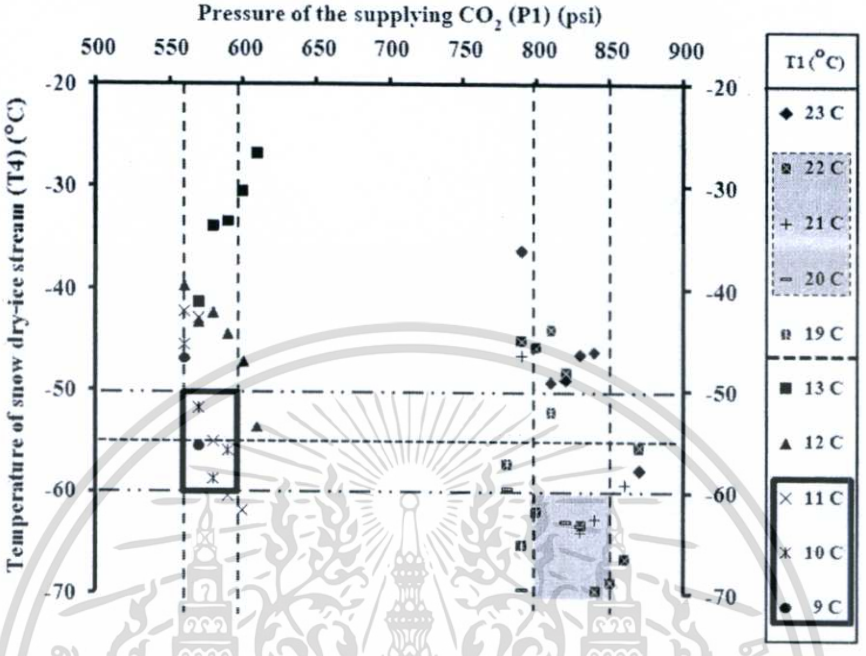

Figure 4.6 Comparison between the temperature of snow dry-ice stream at nozzle tip (T4) when using the pressure of supplying CO_2 (P1) in high-pressure and low-pressure range

Effect of the CO_2 stream temperature on the dry-ice particles producing

By the same procedure as in the section 4.1.3.1, Figure 4.7 shows the percentage of the CO_2 fluid that converted to solid particles in the snow dry-ice stream. Thus, the supplying CO_2 conditions were in the range of processing window (blocked area in Figure 4.6). The high pressure CO_2 fluid would be converted to dry-ice particles in the range of 38.3 to 41.5 percentages.

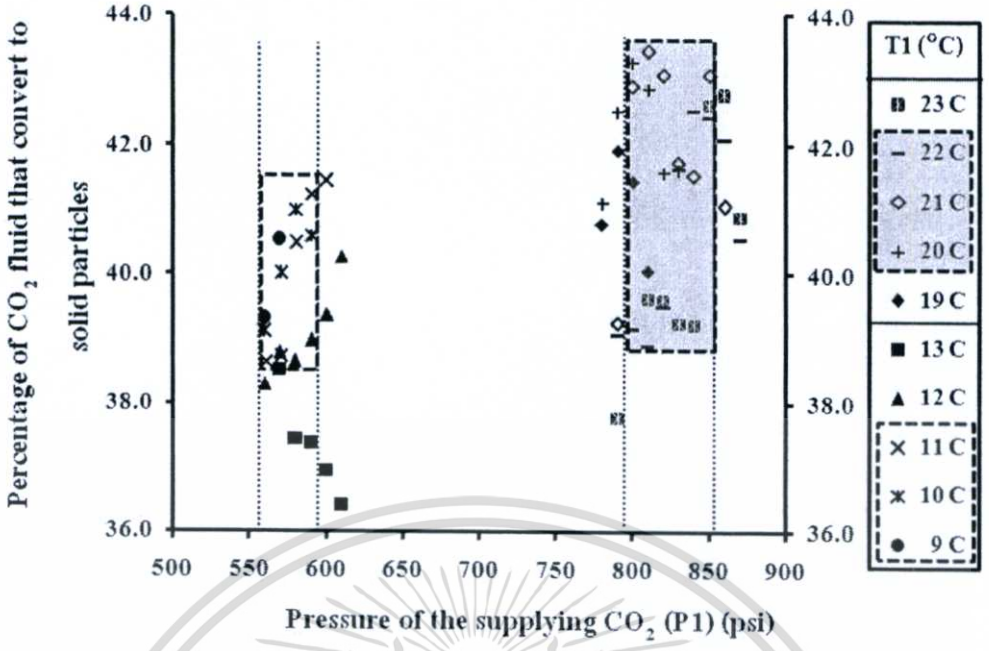

Figure 4.7 Comparison between the percentage of dry-ice particles in snow stream at the nozzle tip when using the pressure of supplying CO_2 (P1) in high-pressure and low-pressure range

From Figure 4.7, the minimum dry-ice particles percentages of snow stream that were generated from the different supplying conditions were noticed. These minimum percentage are quite different in the value. However, when these percentage value were considered in numerical viewpoint, these percentages were not different. Thus, the dry-ice particles percentage must be considered in the amount of micron or submicron particles. The quantity of the dry-ice particles in snow dry-ice stream will absolutely be different. Moreover, in the case of the snow dry-ice stream from the different supplying conditions, which have the same percentage of dry-ice particles. However, the snow dry-ice stream might differ in the other stream characteristic such as the impact stress, dry-ice particles size etc. Thus, the other snow dry-ice stream characteristic must be observed in later section.

4.1.4 The optimization in snow dry-ice generating systems

4.1.4.1 Using the Joule-Thomson expansion theory for the optimization in snow dry-ice generating systems

From the previous content, that concludes about the supplying CO_2 conditions and effect of the supplying condition on the snow dry-ice generating system. In addition, from the thermodynamic of snow dry-ice formation, the snow dry-ice generating system has the Joule-

Thomson expansion as the main mechanism, which affects the system efficiency. The efficiency refers to the amount of the dry-ice phase in the snow dry-ice stream.

Therefore, the μ_{JT} and Joule-Thomson inversion curve (JTIC) were used as a basis to consider the appropriate supplying CO_2 conditions. Figure 4.8 shows the Joule-Thomson inversion curve that was calculated by using the modified Peng-Robinson equation of state [31]. Figure 4.8 was plotted between the pressure reduced (Pr; Pr = (P/Pc)) and temperature reduced (Tr; Tr = (T/Tc)). Moreover, Figure 4.8 shows the plotting of the pressure and temperature data of CO_2 (EXP, P3 T3). These data are the conditions of the supplying CO_2, which contained before move into the Joule-Thomson expansion at the orifice (in this research refer as reducer, which is shown in Figure 4.9). From the plotting of data, the CO_2 fluid at points (EXP, P3 T3) are containing the μ_{JT} more than zero, because the points are in the inner region of Joule-Thomson inversion curve. In addition, the snow dry-ice generating system prefer to use the CO_2 that have the μ_{JT} more than zero as the supplier. Thus, the experimental supplying CO_2 conditions were suitable for the snow dry-ice generating. However, the plotting results must be ensured these are the exactly position on the Joule-Thomson inversion curve. Then, the Joule-Thomson coefficient (μ_{JT}) must be calculated to confirm the plotting results.

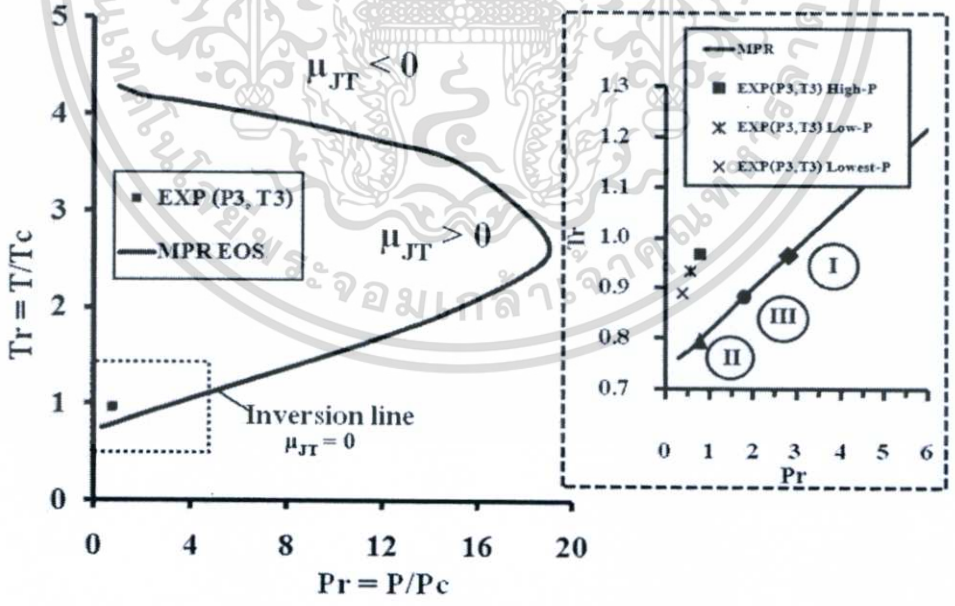

Figure 4.8 Joule-Thomson inversion curve that was predicted by using modified Peng-Robinson equation of state [32,36]

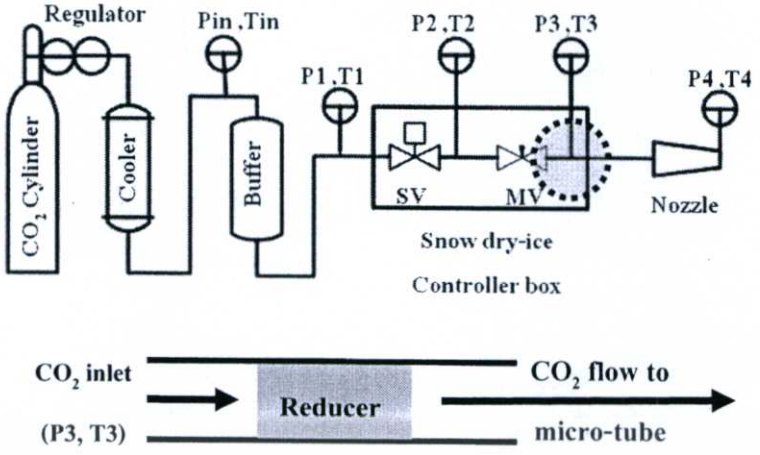

Figure 4.9 Schematic of Joule - Thomson expansion through a reducer in the snow dry-ice generating system

$$\mu_{JT} = \frac{\left[T\left(\frac{\partial v}{\partial T}\right)_P - v\right]}{c_P^{ideal\ gas} - \int_{P_{ideal\ gas}}^{P_{real}} \left[T\left(\frac{\partial^2 v}{\partial T^2}\right)_P\right] dP} \tag{4.1}$$

Then, the μ_{JT} calculation results are shown about the corresponding results between the plotting data and the μ_{JT} that were calculated by using Equation (4.1). The CO_2 fluid that has the conditions in the processing window range;

1) In case of the high supplying CO_2 pressure range in section 4.1.3.1 (800-850 psi and 20-22 $^{\circ}$C for supplying CO_2 pressure and temperature processing window range, respectively), the μ_{JT} is in the range of 0.0218 - 0.0380 K/psi.

2) In case of the low supplying CO_2 pressure range in section 4.1.3.2 (570-590 psi and 9-11 $^{\circ}$C for supplying CO_2 pressure and temperature processing window range, respectively), the μ_{JT} is in the range of 0.0546 - 0.0610 K/psi.

However, for the recommended supplying CO_2 conditions that can use as supplier for the snow dry-ice generating system, that is shown in Figure 4.10. The range of the supplying CO_2 pressure for the upper limitation equals as in case of the high supplying CO_2 pressure range in section 4.1.3.1 (around 800-870 psi), and the low-pressure region is low as around 400 psi. Thus, the supplying CO_2 will have the μ_{JT} in the range of 0.0203 - 0.0664 K/psi.

From the calculated μ_{JT} , the supplying CO_2 that has the conditions as mention above. When the supplying CO_2 moves through the Joule-Thomson expansion, the supplying CO_2 pressure and temperature will be reduced. Thus, the experimental results that are plotted in Figure 4.8, are in accordance with the calculation results by using the Joule-Thomson expansion theory.

From the accordance between experimental and calculation results, the Joule-Thomson inversion curve is also permitted to use for the optimization in the efficiency of the snow dry-ice generating systems. In addition, the Joule-Thomson inversion curve is one of the locus line that plots from the change of isenthalp curve. The point on the Joule-Thomson inversion curve (as μ_{JT} equal zero) these are the best point for the starting point of the snow dry-ice generating process. Thus, the optimization methodology was started from the applying of the Joule-Thomson inversion curve as a tuning target. When the Joule-Thomson inversion curve was used as the tuning parameters for the snow dry-ice generating system. The supplying CO_2 condition optimization could be done at least in three ways until the μ_{JT} of CO_2 (EXP, (P3,T3)) close to zero. Then, these conditions of supplying CO_2 after the tuning were plotted on the inversion curve, the points will approach on the Joule-Thomson inversion line. For example, the processing condition of the supplying CO_2 in high-pressure range was optimized. From Figure 4.8, the Case-I that available to optimize is done by increasing the supplying CO_2 pressure until the pressure nearby 3,000 psi. In Case-II is the decreasing of the supplying CO_2 temperature closely to -31 $^{\circ}$C. Then, Case-III is done by adjusting the supplying CO_2 temperature simultaneously with the pressure. The optimization of the processing condition was carried out and the results are shown in Table 4.2. However, the tuning process is preferable to decrease the temperature instead of the increasing of pressure. When the suitability of the generating and cleaning operations including the tube and fitting or any devices in the systems were considered.

Table 4.2 Data of the supplying CO_2 conditions and the percentage of the supplying CO_2 that convert to solid particles (the optimization of high-pressure range)

Case	Supplying CO_2 conditions		μ_{JT}	Percentage of high pressure
	Temperature ($^{\circ}$C)	Pressure (psi)	(K/psi)	CO_2 that convert to dry-ice
EXP	21.0	825	3.0×10^{-2}	42.4
I	21.0	3,000	5.2×10^{-5}	76.5
II	-31.1	825	1.6×10^{-6}	94.8
III	-4.5	1,900	2.6×10^{-6}	85.4

The tuning results to optimize the snow dry-ice generating in Table 4.2, the amount of the solid CO_2 particles in the snow stream that could be increased the percentage up to 94.8. The tuning to optimize systems is going to increase the cleaning efficiency in anyway,

because the cleaning mechanisms of snow dry-ice blasting in the literature review [11]. The prime mechanism that affect the cleaning efficiency is the collisions between the dry-ice particles and contaminants. Thus, the increasing of solid particles is going to increase more opportunities to have the collisions, in the other meaning.

4.1.5 Supplying CO_2 conditions for using in HDD assembly parts cleaning

When the snow dry-ice cleaning is used to apply for the HDD assembly parts cleaning. The supplying CO_2 conditions might be changed for the suitability between the blasting condition and the cleaning parts, because the HDD assembly parts are consist of many types or material sources. Then, the supplying CO_2 pressure is the majority concerning, because the damage from snow dry-ice stream pressure on parts or substrates must be avoided. Thus, Figure 4.10 shows the flexibility of the snow dry-ice blasting, when it is applied for the cleaning applications. Because of the supplying CO_2 conditions range that can use for HDD assembly parts cleaning are in the range of 380 - 870 psi for the pressure or in the range of 67-210 kg/m^3 for the density. However, the supplying CO_2 temperature must be changed together for the controlling of the dry-ice particles amount constant. When the supplying CO_2 have the conditions (P1,T1) same as one of recommended conditions (on the line in Figure 4.10). The snow dry-ice generating system could generate the appropriate snow dry-ice stream, which were the snow dry-ice stream that had the temperature around the CO_2 triple point temperature [-56 °C (± 7.61 °C)]. Thus, the high pressure CO_2 fluid will be converted to dry-ice particles in the range of 40 to 41 percentages. In addition, in case of the supplying CO_2 pressure and temperature reduction that relates with the decreasing of the supplying CO_2 density. The decreasing of the supplying CO_2 density might affect the dry-ice particle or flow characteristic as the results shown in Figure 4.10.

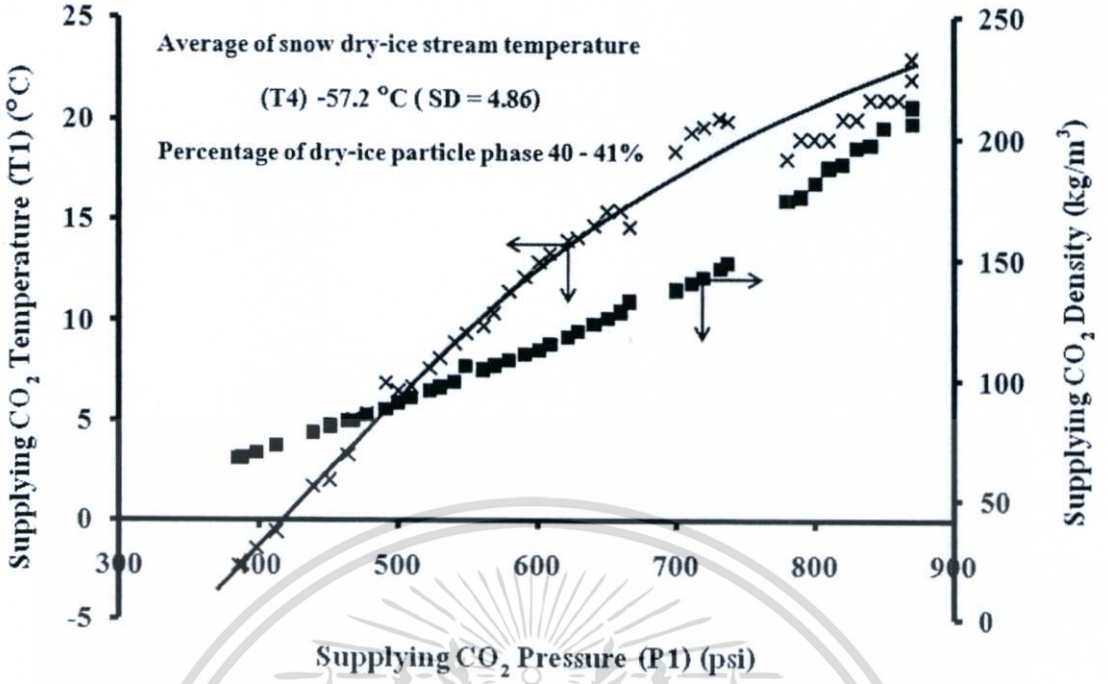

Figure 4.10 Supplying CO_2 conditions that can use for the snow dry-ice stream generating system and would be generated the appropriate snow dry-ice stream.

4.1.5.1 Effect of the supplying CO_2 density on the snow dry-ice stream temperature profile

During the snow dry-ice injection time, the characteristic of snow dry-ice stream was recorded by the video recorder with lenses 20X. Figure 4.11 shows the snow dry-ice stream characteristic at the various distances from the nozzle tip as the primary data. Moreover, Figure 4.11 shows the rate of dry-ice particles sublimation, when the particles moved far away from the nozzle tip. However, the photo of the snow dry-ice stream characteristic cannot tell the exactly rate of sublimation.

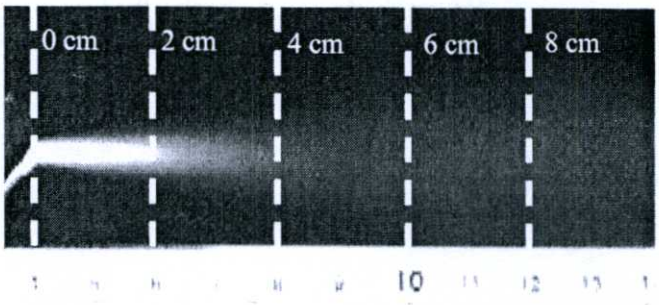

Figure 4.11 Snow dry-ice aerosol characteristic at the various distance from the nozzle tip, which were generated by the snow dry-ice system by using the condition of the supplying CO_2 as 500 psi and 7 °C.

The percentage of the dry-ice particles phase is enabled to estimate by using the CO_2 stream temperature data the and the CO_2 phase diagram. Thus, Figure 4.12 shows the temperature measured at the center of the stream line along with the flow axis. When the snow dry-ice stream were expanded into the polymeric tube (OD 5 cm and ID 4 cm) as shown in Figure 4.13. The measurement position x is the distance from the nozzle tip. The supplying CO_2 conditions in Figure 4.10 were used as the supplier conditions. These supplying CO_2 conditions controlled the temperature and dry-ice particles percentage at the nozzle tip (x = 0 cm) around – 56 °C and 40 percentage, respectively.

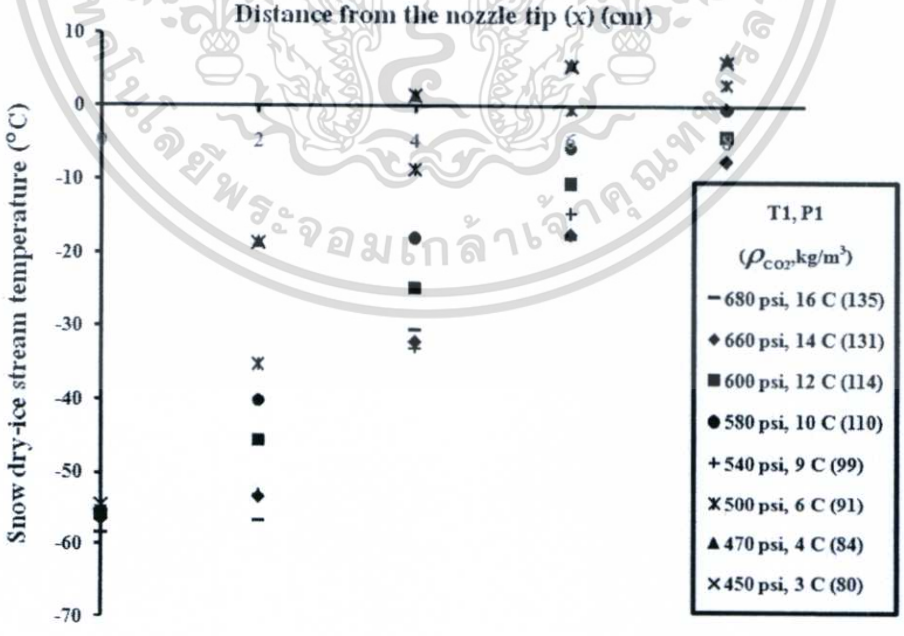

Figure 4.12 Snow dry-ice stream temperature variation with distance from the nozzle tip, which were generated by using the various supplying CO_2 conditions.

Figure 4.12 shows the increasing of the CO_2 stream temperature when the distance from the nozzle increased. For example, the temperature measured at x = 0 cm was about -56 °C; however, it increased to 0 °C at x = 8 cm and closed to room temperature at x > 8 cm. The temperature of the snow dry-ice stream increased sharply after injecting from the expansion nozzle. According to a phase diagram of CO_2, dry-ice can be formed at below -56 °C and 1 atm, which indicates that most of dry-ice produced from the nozzle sublimated to the atmosphere due to the temperature increase. Consequently, the decreasing of dry-ice particles in snow dry-ice stream were observed visually as shown by the decreasing of the milky stream in Figure 4.11.

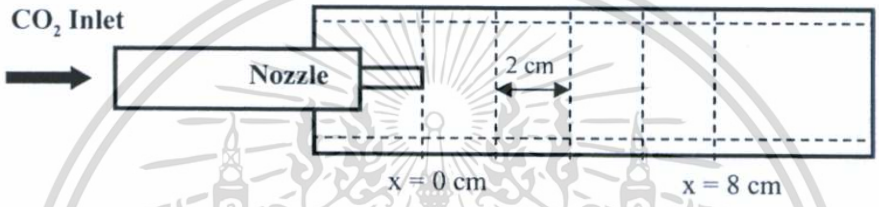

Figure 4.13 The test section for the snow dry-ice stream temperature profile

The dry-ice particles that was generated by using higher supplying density, the particle size might be larger than the dry-ice particle from the low supplying CO_2 density. Moreover, the dry-ice particles with the larger size must have the surface area for heat transfer with ambient in smaller than the particle in smaller size. Thus, when the snow dry-ice stream temperature at the nozzle tip was around the CO_2 triple point temperature (-56°C). The rate of dry-ice particles sublimation inversely increased as the decreasing of the supplying CO_2 density range. Thus, the dry-ice particles from the high density CO_2 might have the particles in larger size than the particles from low density CO_2.

4.1.5.2 Effect of supplying CO_2 density on the supplying CO_2 mass flow rate

From using the high stability gas mass balance, Figure 4.14 shows the relationship between the supplying CO_2 mass flow rate and density. Then, from the controlled volumetric flow (fixed cross sectional area of the nozzle), when the supplying CO_2 density was risen, the CO_2 mass flow rate in the system was increased too.

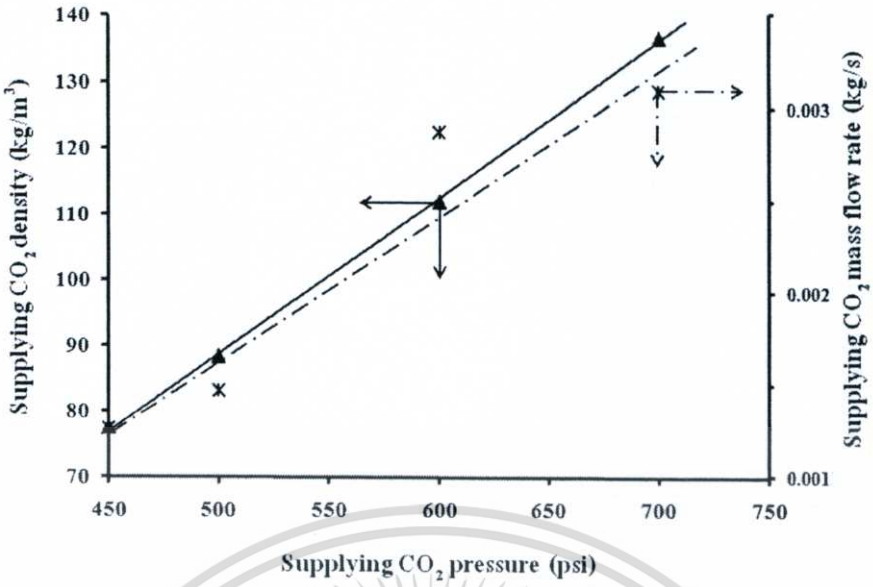

Figure 4.14 The relationship between the supplying CO_2 density and the mass flow rate of the CO_2 when it flew through the system

SECTION 2

THE DRY-ICE PARTICLE AND FLOW CHARACTERIZATION

4.2 The dry-ice particle and flow characterization

From this research objective, the snow dry-ice blasting was applied as a cleaning method for the HDD assembly part or any substrates. From the snow dry-ice cleaning mechanisms, the formation of snow dry-ice is based on the expansion of fluid CO_2 when being propelled through an orifice. The formation of snow dry-ice allows the snow dry-ice stream to be powerful and high pressure. Thus, the pressure effect on the cleaning substrate should be considered as a prime issue when the snow dry-ice cleaning be applied for the sensitive substrate. Moreover, the mechanisms responsible for the removal of particle residues from surfaces that occurs from the particle detachment involves an aerodynamic drag force of high-velocity gas flow and momentum transfer during the impact. Therefore, the impact stress, size and velocity of the dry-ice particles must be evaluated. The momentum transfer between the dry-ice and contaminant particles will directly affect the cleaning efficiency, especially for the contamination in submicron range. Thus, the velocity, impact stress, size, and momentum of the dry-ice particles would be observed.

4.2.1 Effect of supplying CO_2 density on the nozzle velocity

From the mass flow rate, the CO_2 flow velocity before it moved through the expansion at the nozzle were enabled to calculate by using Equation (2.19). The CO_2 fluid flow velocity in the micro polymeric tube (the nozzle) was assumed closely the CO_2 nozzle velocity. Then, the dry-ice particles velocity might equal the CO_2 nozzle velocity. From Figure 4.15, the CO_2 stream from the high supplying CO_2 density has the higher nozzle velocity more than the CO_2 stream from the low supplying CO_2 density. From Figure 4.15, the nozzle velocity of dry-ice particles were in range of 39-49 m/s when the supplying CO_2 density and pressure were in the range of 78-136 kg/m^3 and 450-700 psi, respectively.

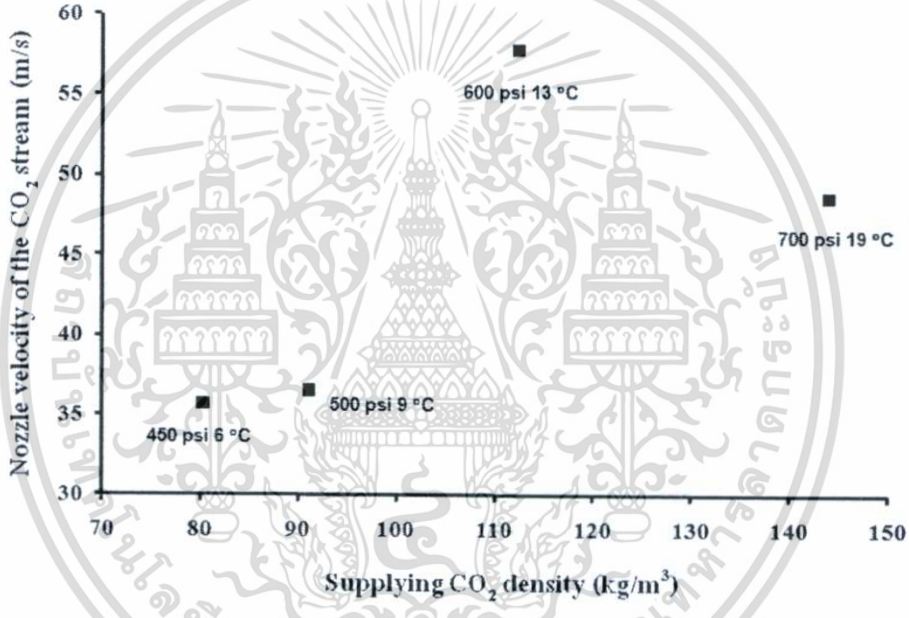

Figure 4.15 Relationship between the supplying CO_2 pressure and the CO_2 nozzle velocity

4.2.2 Measurement of the dry-ice particle and flow characteristic by using pressure measurement film

From the literature review [37], the dry-ice particle and flow characteristic can be observed by using the high-speed camera as a direct method. However, the indirect measurement was used for this research. Therefore, the dry-ice particle and flow characteristics were measured by using the pressure measurement film (Fuji® Prescale film), which can measure pressure and visualize pressure range. The Prescale film can measure pressure, pressure distribution and balance. The red patches will appear on Prescale sheets when pressure is applied

on the sheets as shown in Figure 4.16(a). The color density changes according to pressure level as shown in Figure 4.16(b). The entire Prescale functions as a sensor and can see at a glance the whole pressure distribution on it. Thus, when the snow dry-ice stream was applied on the Prescale mono-sheet, the impact stress of the dry-ice particle was obtained as a simply one.

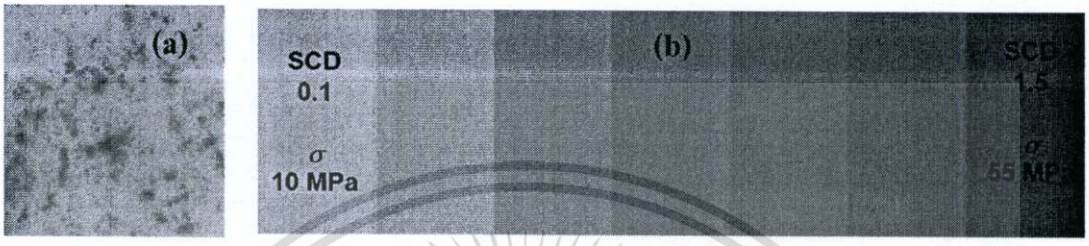

Figure 4.16 The red patches on Prescale sheets when pressure was applied (a) the standard momentary pressure chart (b)

4.2.2.1 Impact stress and momentum of dry-ice particle

From the appearance in red patches color on the impacted Prescale films, the impact stress of the dry-ice particles were evaluated by using the procedure as shown in section 3.2.1. Figure 4.17 shows the impact stress of the dry-ice particles from the various supplying CO_2 conditions. From Figure 4.17, when the dry-ice particles were generated by using the higher supplying CO_2 pressure and density, the dry-ice particles impact stress were going to rise. The dry-ice particles impact stress were in range of 48-54 MPa (6,962-7,832 psi) when the supplying CO_2 density and pressure were in the range of 88-136 kg/m^3 and 500-700 psi, respectively. However, for the supplying CO_2 density below 90 kg/m^3, the Prescale film did not show the red patch. Thus, the impact stress might be below 10 MPa (1,450 psi) for the case of low supplying CO_2 density. From Figure 4.12 that shows the high rate of dry-ice particle sublimation when the supplying CO_2 density below 90 kg/m^3. Therefore, the high of sublimation rate might be affect the impact stress of the dry-ice particles were not enough for the impact on Prescale film.

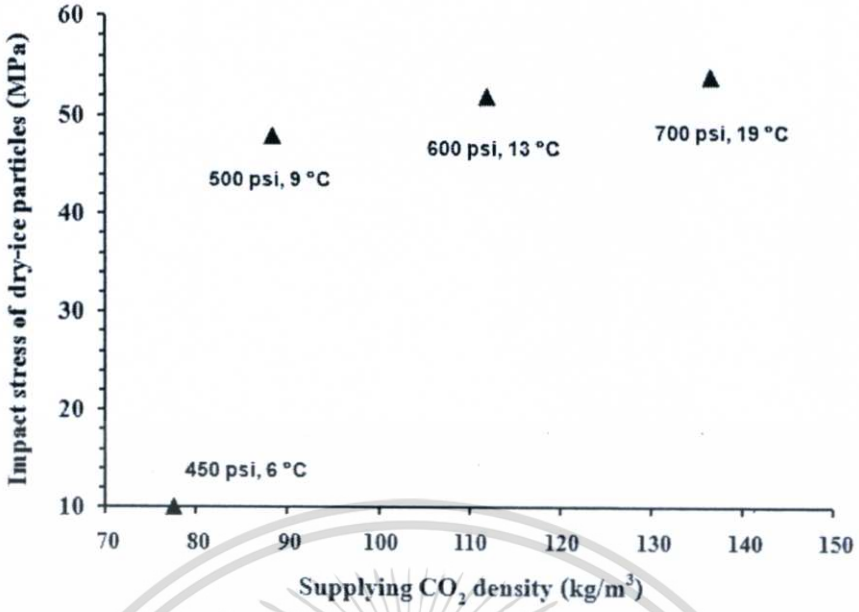

Figure 4.17 The effect of the supplying CO_2 density and pressure on the impact stress of the dry-ice particles in the snow dry-ice stream

When the theoretical calculation was used to compare with the impact stress from the experiments. The momentum of the dry-ice particle that will transfer when the collision occurs, which was calculated by using Equation (2.25). Then Figure 4.18 shows the comparison between the impact stress as the experimental results and the calculated momentum of the dry-ice particles. The momentum of dry-ice particles were decreased by the decreasing of the supplying CO_2 density as same as the impact stress results in Figure 4.17. Thus, the pressure measurement by using the Prescale film could be applied for the impact stress measurement in the snow dry-ice blasting or the other cryogenic aerosol injection. By the dry-ice particles momentum were in the range of 0.54×10^{-9} – 1.35×10^{-9} kg·m/s when the supplying CO_2 density and pressure were in the range of 78-136 kg/m^3 and 500-700 psi, respectively.

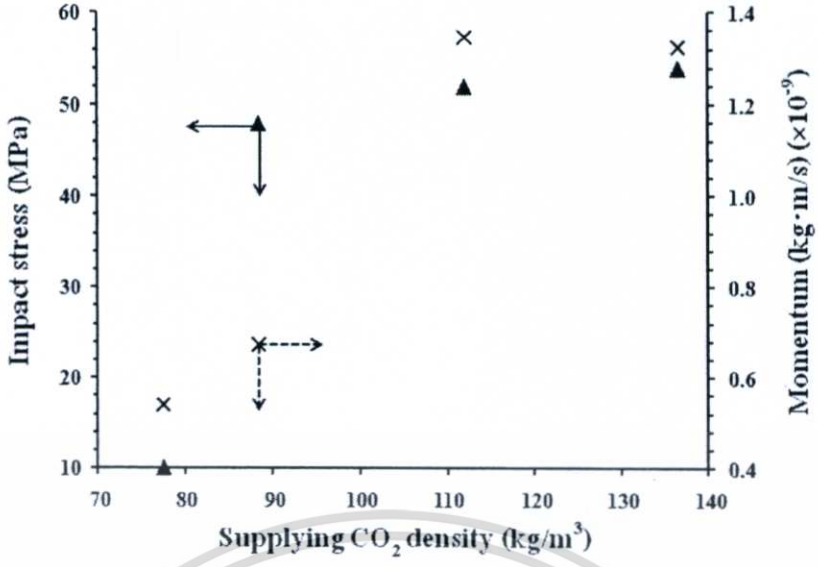

Figure 4.18 The comparison between the effect of supplying CO_2 density on the impact stress and the momentum of the dry-ice particles in the snow stream

4.2.2.2 Dry-ice particles size

By using the Prescale film, the size of the dry-ice particles were obtained from the same method as the impact stress measurement. The image analyzer program such as the ImageJ or the Photoshop is a necessary in the size measurement. Figure 4.19 shows the dry-ice particles size that were generated from the various supplying CO_2 conditions. Thus, from Figure 4.19 the red dots must be appeared from the impact stress that was in the range of 10 to 55 MPa (1,450-7,977 psi). Moreover, when the supplying CO_2 density and pressure were increased, the diameter size of dry-ice particles in the snow stream would be risen. Then, Figure 4.20 shows the average diameter dry-ice particles size that were in range of 27-33 μm. When the supplying CO_2 density and pressure were in the range of 78-136 kg/m^3 and 450-700 psi, respectively.

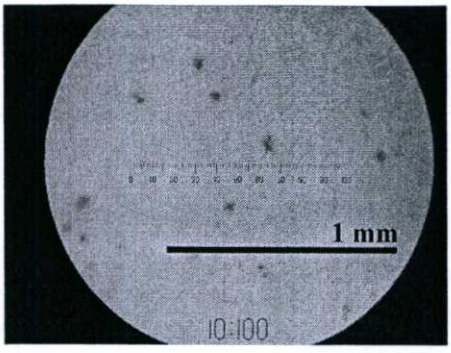

Figure 4.19 The impacted Prescale film by using the supplying CO_2 pressure as 700 psi and 19°C for the temperature with 100X optical microscope. The red patch dots is come from the impact of the dry-ice particles that might refer as the diameter size of the particles.

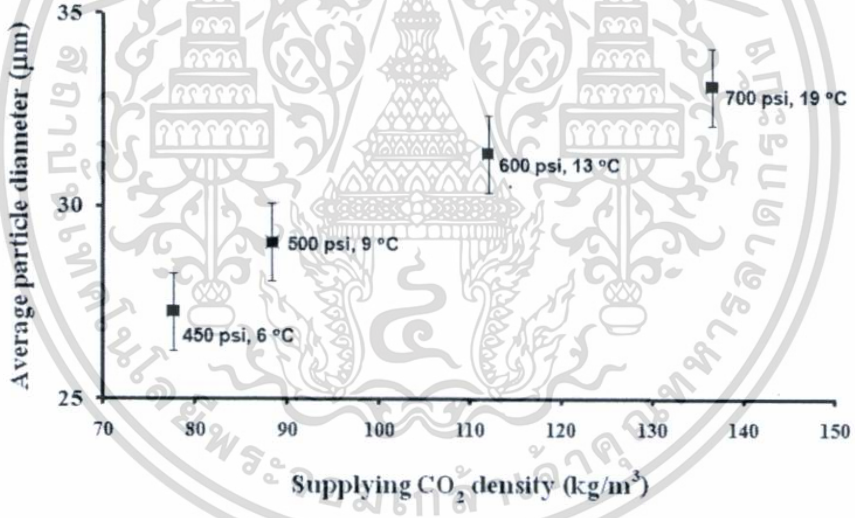

Figure 4.20 The relationship between the supplying CO_2 density and the average dry-ice particles size in the snow stream at distance 10 mm from the nozzle tip

SECTION 3

CLEANING TEST

4.3 The snow dry-ice cleaning efficiency

4.3.1 Contamination levels

The HGA samples from the used HDD were taken its surface characteristic by using 80X optical microscope. From all of its photographs, the contamination levels on HGA could be classified into 4 levels. These 4 levels are consist of;

1) Very low contamination level that cannot observe any contaminant on the surface area [as shown in Figure 4.21(a)]

2) Low contamination level that has the contamination area not over 5 percentage of all surface area [as shown in Figure 4.21(b)]

3) Medium contamination level that has the contamination area around 5 up to 20 percentage of the all HGA surface area [as shown in Figure 4.21(c)]

4) High contamination level that has the contamination area over 20 percentage of all HGA surface area [as shown in Figure 4.21(d)]

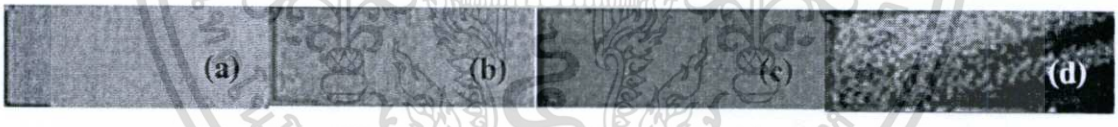

Figure 4.21 Classification of the contamination levels on the HGA surface at 80X optical microscope: (a) level very low, (b) level low, (c) level medium, and (d) level high

4.3.2 Cleaning efficiency

The snow dry-ice by using high supplying CO_2 pressure was applied for the cleaning test. Table 4.3 shows the possibility to apply the snow dry-ice stream for HGA cleaning, because the snow dry-ice stream could remove some of the contaminants on the HGA parts. However, Table 4.3 shows the cleaning results that some of the HGAs were damaged from the snow dry-ice stream. The high-pressure snow dry-ice cannot apply for the HGA part cleaning, because the HGAs were damaged from the pressure effect and impact stress of snow dry-ice stream. Table 4.3 shows the supplying CO_2 pressure that over 800 psi cannot absolutely use in the

HGA cleaning. The damage on samples would be disappeared when the supplying CO_2 pressure was reduced until below 500 psi. Thus, the low-pressure snow dry-ice stream was applied for the HGA parts cleaning. Moreover, the other problems including redeposition of contaminants, moisture condensation, and recontamination sources appeared in the cleaning results as shown in Figure 4.22 and 4.23. The cleaning operation did not operate in clean room or there were some of recontamination source in the system such as supplying CO_2 purity. Thus, from Table 4.3, the snow dry-ice generating system cannot eliminate the contaminants on the HGA parts until HGA cleanliness reaches the very low contamination level. Then, there was some reposition on the substrate in anyway because the system did not include the purge system.

Table 4.3 Supplying CO_2 conditions that used for snow dry-ice stream generating and the HGA cleaning results

Supplying CO_2 conditions		Contamination level		Cleaning results
Pressure (psi)	Temperature ($^{\circ}C$)	Before	After	
850	20	-	-	- Samples were damaged (100%)
800	20	-	-	- Samples were damaged (100%)
750	15	Low	-	- Most of samples were damaged (75%)
		Medium	Medium	
		High	-	
730	15	Low	Low	- Some of samples were damaged (50%)
		Medium	Medium	
		High	-	
700	15	Low	low	- Some of samples were damaged (40%)
		Medium	-	
		High	Medium	
650	12 - 13	Low	Low	- Some of samples were damaged (40%)
		Medium	Medium	
		High	Medium	

Table 4.3 Supplying CO_2 conditions that used for snow dry-ice stream generating and the HGA cleaning results (cont.)

Supplying CO_2 conditions		Contamination level		Cleaning results
Pressure (psi)	Temperature (°C)	Before	After	
630	10 - 12	Low	Low	- Some of samples were damaged (30%)
		Medium	Low	
		High	Medium	
600	10 - 12	Low	-	- Some of samples were damaged (30%)
		Medium	Low	
		High	Medium	
500	5	Low	Low	- Some of samples still were damaged (10%)
		Medium	Low	
		High	Medium	
450	1 - 3	Low	Low	- None of sample was damaged
		Medium	Low-Medium	
		High	Medium- High	

Figure 4.22 The HGA sample cleaning results by using snow dry-ice in case of redeposition and recontamination: (a) before cleaning and (b) after cleaning

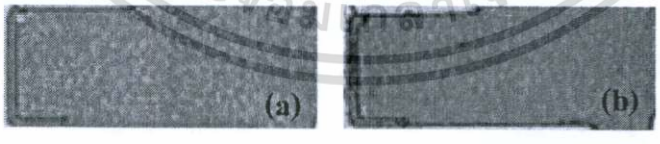

Figure 4.23 The HGA sample cleaning results by using snow dry-ice in case of recontamination: (a) before cleaning and (b) after cleaning

The most suitable supplying CO_2 conditions that could be applied for the HGA cleaning, the supplying CO_2 pressure range should be around 450 psi to avoid the possibility of the damage on substrates. The supplying CO_2 temperature should be in the range of 1-3 °C. From these CO_2 conditions, the HGA cleaning results were quite satisfying. The most of cleaned samples could reach the low contamination level.

However, the impact stress from the low-pressure range snow dry-ice stream were not enough to overcome the contaminant's adhesiveness. Thus, when the HGA has the high level in contamination, the low-pressure snow dry-ice cannot eliminate all of the contaminant until the cleaned sample reach the low contamination level.

The moisture condensation was generated by the snow dry-ice, which strikes to the surface and decreases the surface temperature. The moisture condensation froze and formed the condensed layer for long times. Then the frozen layer will change into liquid droplets, if the system does not have the condensed moisture removal method. Moreover, the moisture condensation must be avoided, which occur during the cleaning method. The layer of the ice or liquid droplet on substrate might be as a construction to reduce the chance of collisions between dry-ice particles and contaminants on substrate, which is directly cause to decrease the cleaning efficiency. From the literature review [11] that concludes the moisture condensation on the substrate might be one of the sources of the recontamination. In critical cleaning applications, such as submicron particles removal from substrate or precision cleaning, the moisture condensation must not occur. In otherwise, removal of these small particles will be more difficult happened, or submicron moisture particles can remain on the surface. Thus, the snow dry-ice cleaning procedure must have a method to control or reduce the moisture condensation. The easiest method is to use a hot plate as part of the sample support. For samples that cannot heat it directly, such as in case of our sample (HGA part), an external heat source such hot air gun or nitrogen purges are needed. Other choices for moisture control are dry boxes, enclosed hoods or environmental chambers that are purged or heated, or a combination of these.

In addition, the continuous snow dry-ice injection has the possibility of the moisture condensation on the substrate instead of using the pulse injection. Thus, the injection of the snow dry-ice stream should be done by the pulse injection. Then, the snow dry-ice generating system were changed by adding a purge line. The cleaning system that is shown in Figure 3.17 was used for experiments. The snow dry-ice particles were injected and vortically mixed into a heated propellant gas such as nitrogen or cleaned dry air, which flows coaxially with the capillary condenser assembly. Theoretically, the snow dry-ice cleaning system could be avoid or reduce the moisture condensation. However, this theory cannot be proven by using the experimental results, because the pressure of composite flow was too high. Thus, when used the combination flow, the pressure effect damaged the HGA parts. As results, this is one of the suggestions, which might be done more experiments.

Chapter 5

Conclusions and Suggestions

5.1 Conclusions

5.1.1 Snow dry-ice generating system

The snow dry-ice system model AFMS-100 Deflex Power SNO^{TM} was able to generate the snow dry-ice effectively. The snow dry-ice generating system has the abilities in both to apply for pulse or continuous snow dry-ice generating. The various type of injection is one of the snow dry-ice system's flexibility for applying in various cleaning applications. In additional, it could be confirmed the milky stream was the snow dry-ice stream that was generated from the system by using the procedure in section 4.2. Nevertheless, the snow dry-ice characteristic must be controlled by the supplying CO_2 conditions within the processing window range.

5.1.2 Processing characterization

The processing window range (suitable operating conditions) was contributed into two regions. The first processing window range that was used in the case of snow dry-ice stream generating from high-pressure range, the supplying CO_2 pressure should be in the range of 800 - 850 psi and 20 - 22 °C for the temperature range. From these conditions, the high pressure CO_2 fluid would convert to solid particles in the range of 38.9-43.4 %. When the Joule-Thomson expansion issue was considered, and from the given processing window range, the μ_{JT} of CO_2 (EXP) have the value in the range of 0.0218-0.0380 K/psi.

The second region of the processing window range, that used for the case of the low supplying CO_2 pressure range. The processing window for the supplying CO_2 should be changed into the range of 570 to 590 psi for the supplying CO_2 pressure and the supplying CO_2 temperature must be changed to the range of 9-11 °C. When the processing window range was changed from the high-pressure to low-pressure range, the solid particles conversion percentage were decreased. However, the supplying CO_2 fluid converted to solid particles in the range of 38.3 to 41.5 %, when the low supplying CO_2 pressure conditions were used. In addition, from the

μ_{JT} calculation, the μ_{JT} of CO_2 (EXP) have the value in the range of 0.0546 - 0.0610 K/psi for the given processing window range in the low-pressure CO_2 region.

5.1.3 System tuning for optimization

By adjusting the supplying CO_2 temperature simultaneously with the supplying CO_2 pressure for the evaluation of the zero μ_{JT} conditions. The optimizations of the processing conditions were carried out by applying the Joule-Thomson expansion theory. However, the tuning process is preferable to decrease the temperature of the supplying CO_2 instead of the increasing of the supplying CO_2 pressure. Finally, from the tuning examples of high-pressure supplying CO_2 conditions, the tuning will improve the percentage of the solid particles in the snow dry-ice stream line up to 94.8%.

5.1.4 Effect of the CO_2 density on the snow dry-ice stream characteristic

The supplying CO_2 conditions range that can use to generate the snow dry-ice stream is in the range of 380 - 870 psi for the pressure or in the range of 67-213 kg/m^3 for the supplying CO_2 density. However, the supplying CO_2 temperature must be changed together in case of the dry-ice particles phase was contained. The snow dry-ice generating system could generate the appropriate snow dry-ice stream, which had the temperature around CO_2 triple point temperature [-56 °C (± 4.86 °C)]. Thus, the high pressure CO_2 fluid would convert to dry-ice particles in range of 40 to 41 percentages. However, in case of the supplying CO_2 pressure and temperature reduction that relate with the decreasing of the supplying CO_2 density. The decreasing of the supplying CO_2 density might affect the dry-ice particle and flow characteristic. Moreover, when the snow dry-ice stream temperature at the nozzle tip was around the CO_2 triple point temperature. Then, the rate of dry-ice particle sublimation was consider from the snow dry-ice stream temperature profile at the various points far from the nozzle tip. Therefore, the rate of dry-ice particles sublimation inversely increased as the decreasing of the supplying CO_2 density.

5.1.5 The dry-ice particles and flow characterization

When the supplying CO_2 density and pressure were in the range of 78-136 kg/m^3 and 450-700 psi, respectively. The nozzle velocity of the dry-ice particles were in the range of 39-49 m/s. The calculated momentum of dry-ice particles were in the range of 0.54×10^{-9} to 1.35×10^{-9} kg·m/s. From the pressure measurement by using the Prescale film, the dry-ice particles impact

stress was obtained in range of 48-54 MPa (6,962-7,832 psi). The average diameter dry-ice particles size were evaluated by using the Prescale film and there were in the range of 27-33 μm. The pressure measurement by using the Prescale film could be applied for the impact stress measurement in the snow dry-ice blasting or the other cryogenic aerosol injection.

5.1.6 The cleaning test

From the results in cleaning section, the snow dry-ice stream has a possibility to apply as a cleaning agent for the HDD assembly parts, especially the parts which more sensitive and complicated for conventional cleaning. The HGA cleaning results, which were tending to be able eliminate the contamination from HGA surface by using the snow dry-ice blasting. Nevertheless, for the sensitive parts cleaning that must be concerned about the pressure effect as a prime issue. In addition, the moisture condensation, redeposition and recontamination resources cannot disregard when uses the snow dry-ice blasting as a cleaning method. Finally, the snow dry-ice cleaning might be taken from a laboratory niche cleaning method to use as an accepted solvent-free and dry cleaning process in industrial section.

5.2 Suggestions

1. More accurate method of measuring the dry-ice particle and flow characteristic should be developed and applied such as using the high-speed camera.
2. To resolve the problems in case of moisture condensation, contaminants redeposition and recontamination sources by using the purge system or the dry boxes [13]
3. The other parameter that relate with the nozzle such as cross sectional area or length should be varied.

References

[1] NECTEC. "**R&D.**" [Online]. Available : http://www.nectec.or.th/2008/r-d/hdd.html. 2010.

[2] G.W. Knoth, D.P. Jackson and N.W. Sorbo. "Automated CO_2 Composite Spray Cleaning System for HDD Rework Parts." **Journal of the IEST.**, vol. 52, no. 1, pp. 43-51, April 2009.

[3] S.A. Hoenig. "Cleaning surfaces with dry ice." **Compressed Air Magazine**. vol. 91, no. 8, pp. 22-25. 1986.

[4] R. Sherman and W. Whitlock. "The removal of hydrocarbons and silicone grease stains from silicon wafers." **Journal of Vacuum Science & Technology.**, B 8, pp. 563-567, 1990.

[5] L. Layden and D. Wadlow. "High velocity carbon dioxide snow for cleaning vacuum system surfaces." **Journal of Vacuum Science & Technology.**, A 8, pp. 3881-3883, 1990.

[6] R. Sherman, J. Grob and W. Whitlock. "Dry surface cleaning using CO_2 snow." **Journal of Vacuum Science & Technology.**, B 9, pp. 1970-1977, 1991.

[7] R. Sherman, D. Hirt and R. Vane. "Surface cleaning with the carbon dioxide snow jet." **Journal of Vacuum Science & Technology.**, A 12, pp. 1876-1881, 1994.

[8] M.M. Hills. "Carbon dioxide jet spray cleaning of molecular contaminants." **Journal of Vacuum Science & Technology.**, A 13, pp. 30-34, 1995.

[9] C. Toscano and G. Ahmadi. "Particle removal mechanisms in cryogenic surface cleaning." **The Journal of Adhesion.**, vol. 79, pp. 175-201, 2003.

[10] S. Banerjee and A. Campbell. "Principles and mechanisms of sub-micrometer particle removal by CO_2 cryogenic technique." **Journal of Adhesion Science and Technology.**, vol. 19, pp. 739-751, 2005.

[11] R. Sherman. "Carbon Dioxide Snow Cleaning." **Particulate Science and Technology.**, vol. 25, pp. 37–57, 2007.

[12] H. Yamaguchi, X. R. Zhang and K. Fujima. "Basic study on new cryogenic refrigeration using CO_2 solid–gas two phase flow." **International Journal of Refrigeration.**, vol. 31, pp. 404-410, 2008.

[13] R. Kohli and K.L. Mittal. **Developments in surface contamination and cleaning : fundamentals and applied aspects.** New York : William Andrew. 2008.

[14] D. Y. Lee, J. Hwang and G. N. Bae. "Effect of disk rotational speed on contamination particles generated in a hard disk drive." **Microsystem Technologies.**, vol. 10, pp. 103-108, 2004.

[15] T. Fujimoto, K. Takeda and T. Nonaka. "Airborne Molecular Contamination: Contamination on Substrates and the Environment in Semiconductors and Other Industries." 329-456. in R. Kohli and K.L. Mittal. **Developments in surface contamination and cleaning : fundamentals and applied aspects.** New York : William Andrew. 2008.

[16] School of Mechanical Engineering, Institute of Engineering Suranaree University of Technology. "**HDD Basic Technology**." [Online]. Available : http://eng.sut.ac.th/modules.php?name=Downloads. 2010.

[17] D. Y. Lee, J. Hwang and G. N. Bae. "Effect of disk rotational speed on contamination particles generated in a hard disk drive." **Microsystem Technologies.**, vol. 10, pp. 103-108, 2004.

[18] M. L. Free. 2008. "The Use of Surfactants to Enhance Particle Removal from Surfaces." 727-753. in R. Kohli and K.L. Mittal. **Developments in surface contamination and cleaning : fundamentals and applied aspects.** New York : William Andrew.

[19] J. B. Durkee. "Cleaning with Solvents." 759-868. in R. Kohli and K.L. Mittal. **Developments in surface contamination and cleaning : fundamentals and applied aspects.** New York : William Andrew. 2008.

[20] P. G. Clark and T. J. Wagener. "Removal of Particles by Chemical Cleaning." 873-887. in R. Kohli and K.L. Mittal. **Developments in surface contamination and cleaning : fundamentals and applied aspects.** New York : William Andrew. 2008.

[21] K. Gotoh. "Cleaning Using a High-speed Impinging Jet." 889-916. in R. Kohli and K.L. Mittal. **Developments in surface contamination and cleaning : fundamentals and applied aspects.** New York : William Andrew. 2008.

[22] R. Kohli. "Microabrasive Precision Cleaning and Processing Technology." 919-947. in R. Kohli and K.L. Mittal. **Developments in surface contamination and cleaning : fundamentals and applied aspects.** New York : William Andrew. 2008.

[23] W. T. McDermott and J. W. Butterbaugh. "Cleaning Using Argon/Nitrogen Cryogenic Aerosols." 951-984. in R. Kohli and K.L. Mittal. **Developments in surface contamination and cleaning : fundamentals and applied aspects.** New York : William Andrew. 2008.

[24] Real Science. **"The Freezing Point And The Dew Point – Part 2."** [Online]. Available : http://stevengoddard.wordpress.com/. 2010.

[25] S.C. Yang, K.S. Huanga and Y.C. Lin. "Optimization of a pulsed carbon dioxide snow jet for cleaning CMOS image sensors by using the Taguchi method." **Sensors and Actuators A.**, vol. 139, pp. 265-271, 2007.

[26] E.A. Hill. "Carbon Dioxide Snow Examination and Experimentation." **Precision Cleaning - The Magazine of Critical Cleaning Technology.**, February, pp. 36-39, 1994.

[27] R. Sherman. "Carbon Dioxide Snow Cleaning." 987-1011. in R. Kohli and K.L. Mittal. **Developments in surface contamination and cleaning : fundamentals and applied aspects.** New York : William Andrew. 2008.

[28] Wikipedia. **"Nozzle."** [Online]. Available : http://en.wikipedia.org/wiki/Nozzle. 2010.

[29] FUJIFILM Global. **"Prescale Measurement Film."** [Online]. Available : http://www.fujifilm.com/products/prescale/prescalefilm/. 2010.

[30] M. D. Koretsky. **Engineering and Chemical Thermodynamics.** USA : John Wiley & Sons. 2004.

[31] Wikipedia. **"Joule-Thomson effect."** [Online]. Available : http://en.wikipedia.org/wiki/Joule%E2%80%93Thomson_effect. 2010.

[32] S. Tengsuwan and S. Areerat. "Study on the Joule-Thomson expansion for the CO_2 cryogenic aerosol generating process." **Ladkrabang Engineering Journal.**, vol. 27, no. 4, pp. 55-60, 2010.

[33] B. Haghighi, M. R. Laee and N. S. Matin. "A comparison among five equations of state in predicting the inversion curve of some fluids." **Cryogenics.**, vol. 43, pp. 393–398, 2003.

[34] A. Maghari, Z. Safaei and S. Sarhangian. "Predictions of the Joule–Thomson inversion curves for polar and non-polar fluids from the SAFT-CP equation of state." **Cryogenics.**, vol. 48, pp. 48-55, 2008.

[35] R.H. Perry, D.W. Green, editors. **Perry's chemical engineers handbook**. 7th ed. New York, USA: McGraw-Hill. 1997.

[36] A. Danesh, D. H. Xu, D. H. Tehrani and A.C. Todd. "Improving predictions of equation of state by modifying its parameters for super critical components of hydrocarbon reservoir fluids." **Fluid Phase Equilibria**., vol. 112, pp. 45–61, 1995.

[37] Y. H. Liu, H. Maruyama and S. Matsusaka. "Agglomeration process of dry ice particles produced by expanding liquid carbon dioxide." **Advanced Powder Technology**., vol. 21, pp. 652-657, 2010.

[38] J. M. Smith, H. C. Van Ness and M. M. Abbott. **Introduction to chemical engineering thermodynamics**. 7th ed. New York, USA: McGraw-Hill. 2001.

[39] Pressure Metrics LLC.. **"Pressure Film."** [Online]. Available : http://www.pressuremetrics.com/catalog/index.php?cPath=32. 2011.

Appendices

Appendix A

Experimental data from the snow dry-ice generating by using snow dry-ice generating machine series AFMS-100 Deflex Power SNO™

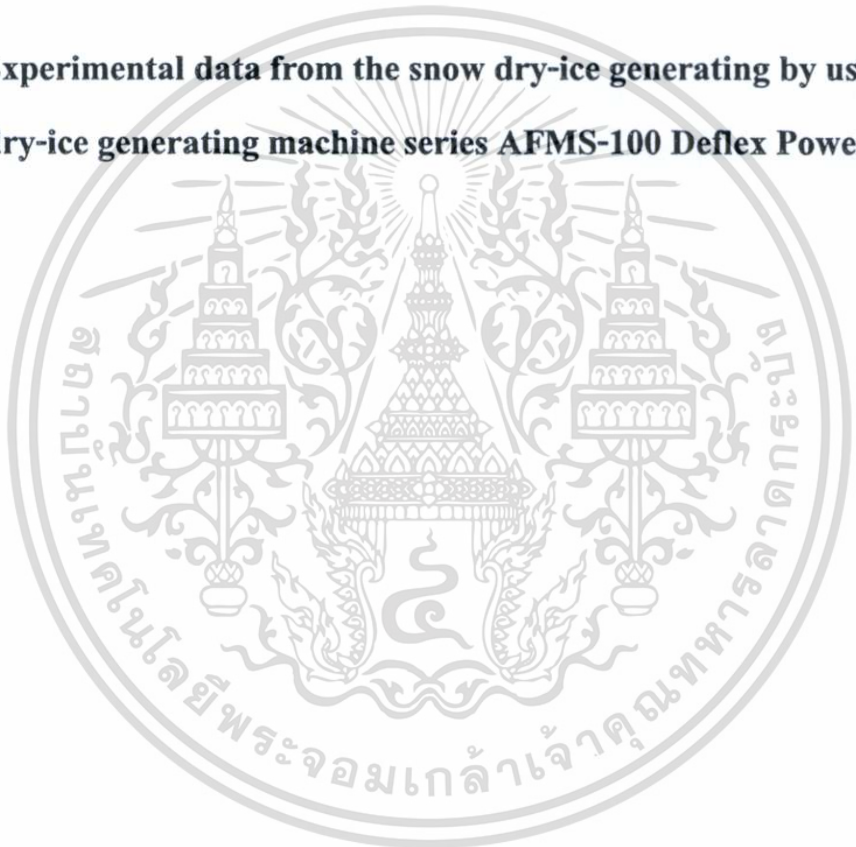

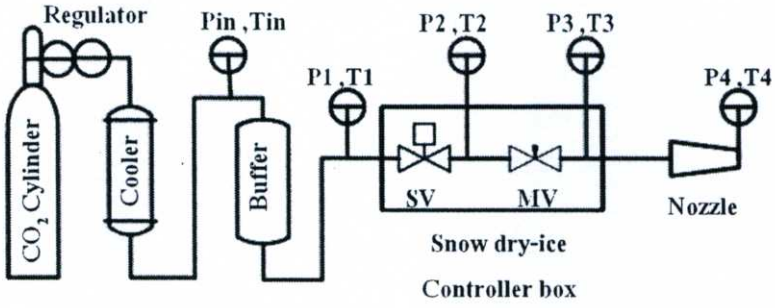

Figure A.1 PFD of the snow dry-ice generating system that shows the various of the pressure and temperature data collecting points.

Table A.1 Experimental data of CO_2 conditions at various points in the snow dry-ice generating system when used the supplying CO_2 temperature varied in range 26-27°C and high supplying CO_2 pressure range (780-870 psi)

EXP CASE	P inlet (psi)	T inlet (°C)	P1 (psi)	T1 (°C)	T2 (°C)	T3 (°C))	T4 (°C)
A01	883	24.5	872	27.3	27.0	26.8	-36.6
A02	873	24.4	863	27.2	27.2	26.8	-44.7
A03	862	24.3	852	27.0	27.2	26.7	-47.1
A04	849	24.3	841	26.7	27.4	26.9	-51.3
A05	838	24.3	830	26.7	27.4	27.1	-50.8
A06	827	24.0	819	26.9	27.5	27.3	-47.7
A07	820	24.0	813	27.1	27.7	27.5	-47.1
A08	859	24.4	851	26.4	27.3	26.7	-47.6
A09	847	24.4	839	26.2	27.3	26.8	-47.6
A10	838	24.4	830	26.3	27.3	26.8	-49.1
A11	829	23.8	821	26.4	27.1	26.6	-45.2
A12	830	18.6	808	25.9	25.6	25.2	-25.0

Table A.2 Experimental data of CO_2 conditions at various points in the snow dry-ice generating system when used the supplying CO_2 temperature varied in range 23-25°C and high supplying CO_2 pressure range (780-870 psi)

EXP CASE	P inlet (psi)	T inlet (°C)	P1 (psi)	T1 (°C)	T2 (°C)	T3 (°C))	T4 (°C)
A13	851	21.3	840	24.7	23.6	23.9	-44.4
A14	847	19.5	832	24.8	25.1	25.0	-22.0
A15	836	18.2	820	25.0	25.9	25.4	-27.6
A16	823	18.1	808	25.1	25.6	25.5	-23.9
A17	804	18.7	790	24.9	25.5	25.2	-24.7
A18	892	24.0	874	23.8	23.6	23.6	-48.4
A19	873	23.6	860	24.0	23.6	23.6	-42.8
A20	863	23.6	851	23.8	23.6	23.6	-43.5
A21	861	20.1	840	24.1	23.2	23.3	-19.1
A22	835	18.9	821	24.4	25.1	25.0	-27.1
A23	824	18.3	810	24.3	25.0	24.9	-29.3
A24	813	17.9	800	24.3	25.0	25.1	-29.4
A25	805	17.9	790	23.8	24.6	24.7	-29.7
A26	887	22.4	868	23.1	22.6	22.9	-57.9
A27	872	21.1	860	22.8	22.8	23.4	-71.4
A28	862	22.1	853	22.7	22.9	23.5	-70.2
A29	852	23.1	840	23.2	23.5	23.5	-46.2
A30	841	22.8	830	23.0	23.4	23.5	-46.4
A31	832	23.4	820	22.9	23.3	23.4	-48.9
A32	821	23.3	811	23.1	23.4	23.5	-49.1
A33	802	17.3	788	23.3	24.2	24.3	-36.2

Table A.3 Experimental data of CO_2 conditions at various points in the snow dry-ice generating system when used the supplying CO_2 temperature constant at 22°C and high supplying CO_2 pressure range

EXP CASE	P inlet (psi)	T inlet (°C)	P1 (psi)	T1 (°C)	T2 (°C)	T3 (°C))	T4 (°C)
A34	888	22.5	870	22.2	22.3	22.4	-55.6
A35	874	21.1	861	22.2	22.5	22.5	-66.5
A36	863	20.0	850	22.0	22.3	22.4	-68.8
A37	850	19.7	841	22.1	22.4	22.8	-69.6
A38	840	19.7	832	21.8	22.2	22.9	-63.2
A39	828	22.0	820	22.1	22.9	23.4	-48.2
A40	817	20.3	811	22.1	22.7	23.3	-44.0
A41	805	22.9	795	21.9	22.2	22.5	-45.7
A42	791	23.5	781	21.8	22.1	22.2	-45.1

Table A.4 Experimental data of CO_2 conditions at various points in the snow dry-ice generating system when used the supplying CO_2 temperature constant at 21°C and high supplying CO_2 pressure range

EXP CASE	P inlet (psi)	T inlet (°C)	P1 (psi)	T1 (°C)	T2 (°C)	T3 (°C))	T4 (°C)
A43	875	22.5	860	21.5	21.6	21.7	-59.2
A44	862	21.0	849	21.4	21.5	21.6	-73.5
A45	854	20.5	840	21.2	21.6	21.5	-62.6
A46	836	19.2	830	21.0	21.4	21.6	-63.9
A47	828	19.2	820	20.9	21.3	21.8	-73.5
A48	818	19.6	812	20.7	21.0	21.7	-76.2
A49	806	20.9	803	20.6	21.1	21.3	-72.3
A50	800	20.9	789	21.4	21.7	21.8	-46.5

Table A.5 Experimental data of CO_2 conditions at various points in the snow dry-ice generating system when used the supplying CO_2 temperature constant at 20°C and high supplying CO_2 pressure range

EXP CASE	P inlet (psi)	T inlet (°C)	P1 (psi)	T1 (°C)	T2 (°C)	T3 (°C))	T4 (°C)
A51	843	20.0	828	20.4	20.6	20.6	-63.2
A52	831	19.4	820	20.3	20.7	20.8	-62.9
A53	819	18.8	810	20.2	20.5	20.9	-72.0
A54	809	19.0	801	20.0	20.4	20.8	-74.9
A55	799	18.4	792	19.7	20.0	20.6	-69.6
A56	790	17.8	784	19.7	20.0	20.4	-59.6

Table A.6 Experimental data of CO_2 conditions at various points in the snow dry-ice generating system when used the supplying CO_2 temperature constant at 18-19°C and high supplying CO_2 pressure range (780-810 psi)

EXP CASE	P inlet (psi)	T inlet (°C)	P1 (psi)	T1 (°C)	T2 (°C)	T3 (°C))	T4 (°C)
A57	823	18.7	809	19.3	19.5	19.5	-52.1
A58	809	18.0	799	19.3	19.5	19.6	-61.9
A59	802	18.5	791	19.3	19.7	20.0	-65.2
A60	791	18.4	782	19.2	19.4	20.0	-57.2
A61	803	17.7	790	18.4	18.8	18.9	-46.0
A62	795	17.8	782	18.2	18.4	18.5	-49.6

Table A.7 Experimental data of CO_2 conditions at various points in the snow dry-ice generating system when used the supplying CO_2 temperature constant at 13°C and low supplying CO_2 pressure range

EXP CASE	P inlet (psi)	T inlet (°C)	P1 (psi)	T1 (°C)	T2 (°C)	T3 (°C))	T4 (°C)
A63	628	12.4	608	12.9	-	14.2	-26.8
A64	620	11.2	601	12.9	-	12.8	-30.5
A65	612	10.6	593	12.9	-	12.2	-33.4
A66	606	9.9	581	12.6	-	11.7	-33.9
A67	601	9.2	570	12.6	-	11.5	-41.3

Table A.8 Experimental data of CO_2 conditions at various points in the snow dry-ice generating system when used the supplying CO_2 temperature constant at 12°C and low supplying CO_2 pressure range.

EXP CASE	P inlet (psi)	T inlet (°C)	P1 (psi)	T1 (°C)	T2 (°C)	T3 (°C))	T4 (°C)
A68	625	11.5	608	11.8	-	13.3	-53.6
A69	622	11.3	600	11.8	-	12.9	-47.2
A70	624	10.1	591	11.9	-	12.3	-44.5
A71	608	9.6	580	12.2	-	11.7	-42.3
A72	606	9.3	574	12.3	-	11.2	-43.2
A73	599	8.6	561	11.7	-	10.2	-39.8

Table A.9 Experimental data of CO_2 conditions at various points in the snow dry-ice generating system when used the supplying CO_2 temperature constant at 11°C and low supplying CO_2 pressure range.

EXP CASE	P inlet (psi)	T inlet (°C)	P1 (psi)	T1 (°C)	T2 (°C)	T3 (°C))	T4 (°C)
A74	626	11.2	600	11.3	-	12.7	-61.9
A75	623	11.2	591	10.8	-	12.1	-60.5
A76	626	12.0	582	10.7	-	11.8	-55.1
A77	617	9.4	571	10.8	-	11.3	-42.8
A78	604	8.6	560	11.0	-	10.3	-42.3

Table A.10 Experimental data of CO_2 conditions at various points in the snow dry-ice generating system when used the supplying CO_2 temperature constant at 9-10°C and low supplying CO_2 pressure range.

EXP CASE	P inlet (psi)	T inlet (°C)	P1 (psi)	T1 (°C)	T2 (°C)	T3 (°C))	T4 (°C)
A79	620	10.8	587	10.4	-	11.9	-55.9
A80	617	9.8	580	10.3	-	11.6	-58.8
A81	613	9.3	570	9.9	-	11.2	-51.8
A82	606	8.8	562	9.8	-	10.6	-45.5
A83	610	9.1	569	9.4	-	11.0	-55.5
A84	605	8.6	560	9.2	-	10.4	-46.9

Table A.11 Experimental data of CO_2 conditions at various points in the snow dry-ice generating system when used the appropriated supplying CO_2 conditions in the available supplying CO_2 pressure range.

EXP CASE	P inlet (psi)	T inlet (°C)	P1 (psi)	T1 (°C)	T2 (°C)	T3 (°C))	T4 (°C)
AA01	892	24.0	874	23.8	23.6	23.6	-48.4
AA02	888	22.5	870	22.2	22.3	22.4	-55.6
AA03	887	22.4	868	23.1	22.6	22.9	-57.9
AA04	872	21.1	860	22.8	22.8	23.4	-71.4
AA05	874	21.1	861	22.2	22.5	22.5	-66.5
AA06	875	22.5	860	21.5	21.6	21.7	-59.2
AA07	863	20.0	850	22.0	22.3	22.4	-68.8
AA08	862	21.0	849	21.4	21.5	21.6	-73.5
AA09	850	19.7	841	22.1	22.4	22.8	-69.6
AA10	854	20.5	840	21.2	21.6	21.5	-62.6
AA11	841	22.8	830	23.0	23.4	23.5	-46.4

Table A.11 Experimental data of CO_2 conditions at various points in the snow dry-ice generating system when used the appropriated supplying CO_2 conditions in the available supplying CO_2 pressure range (cont.).

EXP CASE	P inlet (psi)	T inlet (°C)	P1 (psi)	T1 (°C)	T2 (°C)	T3 (°C))	T4 (°C)
AA12	840	19.7	832	21.8	22.2	22.9	-63.2
AA13	836	19.2	830	21.0	21.4	21.6	-63.9
AA14	843	20.0	828	20.4	20.6	20.6	-63.2
AA15	832	23.4	820	22.9	23.3	23.4	-48.9
AA16	828	22.0	820	22.1	22.9	23.4	-48.2
AA17	828	19.2	820	20.9	21.3	21.8	-73.5
AA18	831	19.4	820	20.3	20.7	20.8	-62.9
AA19	821	23.3	811	23.1	23.4	23.5	-49.1
AA20	817	20.3	811	22.1	22.7	23.3	-44.0
AA21	818	19.6	812	20.7	21.0	21.7	-76.2
AA22	819	18.8	810	20.2	20.5	20.9	-72.0
AA23	823	18.7	809	19.3	19.5	19.5	-52.1
AA24	805	22.9	795	21.9	22.2	22.5	-45.7
AA25	809	19.0	801	20.0	20.4	20.8	-74.9
AA26	809	18.0	799	19.3	19.5	19.6	-61.9
AA27	800	20.9	789	21.4	21.7	21.8	-46.5
AA28	799	18.4	792	19.7	20.0	20.6	-69.6
AA29	802	18.5	791	19.3	19.7	20.0	-65.2
AA30	803	17.7	790	18.4	18.8	18.9	-46.0
AA31	791	23.5	781	21.8	22.1	22.2	-45.1
AA32	790	17.8	784	19.7	20.0	20.4	-59.6
AA33	791	18.4	782	19.2	19.4	20.0	-57.2
AA34	795	17.8	782	18.2	18.4	18.5	-49.6
AA35	772	19.1	777	21.0	-	-	-66.4
AA36	770	19.0	775	20.8	-	-	-64.0

Table A.11 Experimental data of CO_2 conditions at various points in the snow dry-ice generating system when used the appropriated supplying CO_2 conditions in the available supplying CO_2 pressure range (cont.).

EXP CASE	P inlet (psi)	T inlet (°C)	P1 (psi)	T1 (°C)	T2 (°C)	T3 (°C))	T4 (°C)
AA37	746	17.4	749	19.6	-	-	-45.8
AA38	740	17.1	743	19.4	-	-	-48.8
AA39	731	16.7	733	19.0	-	-	-54.6
AA40	715	16.2	720	18.2	-	-	-56.5
AA41	705	15.8	710	17.8	-	-	-62.6
AA42	696	15.3	700	16.8	-	-	-65.2
AA43	687	14.4	692	16.4	-	-	-69.9
AA44	676	8.2	681	16.3	-	-	-70.0
AA45	567	8.2	559	9.6	-	-	-61.3
AA46	557	7.1	550	9.4	-	-	-62.5
AA47	549	6.4	541	8.9	-	-	-69.9
AA48	541	5.5	533	8.2	-	-	-68.1
AA49	529	3.4	522	7.3	-	-	-61.6
AA50	507	4.0	499	6.7	-	-	-48.1
AA51	498	3.5	491	5.9	-	-	-53.0
AA52	490	3.0	482	5.5	-	-	-49.3
AA53	471	1.9	469	4.0	-	-	-62.0
AA54	464	1.2	462	3.4	-	-	-63.6
AA55	454	0.0	453	2.4	-	-	-68.1
AA56	441	0.2	439	2.4	-	-	-44.8
AA57	413	-2.8	411	-0.1	-	-	-66.2
AA58	403	-3.5	402	-1.0	-	-	-65.9
AA59	388	-4.6	388	-1.9	-	-	-57.0

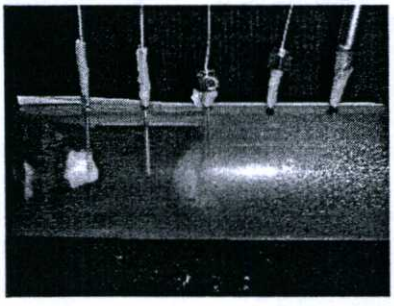

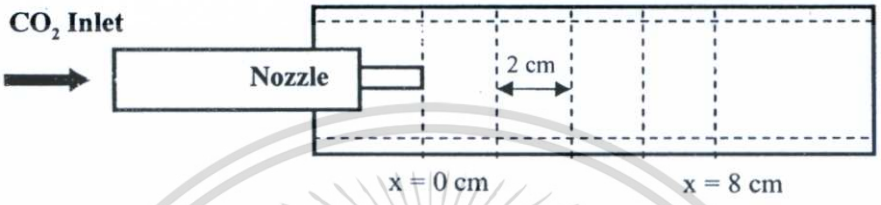

Figure A.2 The test section for the snow dry-ice stream temperature profile

Table A.12 Experimental data of the snow dry-ice stream temperature at various distance (x) from the nozzle tip

EXP CASE	P inlet (psi)	T inlet (°C)	x = 0 cm (°C)	x = 2 cm (°C)	x = 4 cm (°C)	x = 6 cm (°C))	x = 8 cm (°C)
AA60	680	16.1	-58.4	-56.6	-30.5	-18.0	-4.2
AA61	664	14.0	-56.4	-53.2	-32.1	-17.5	-7.5
AA62	623	13.5	-56.1	-43.2	-32.8	-15.0	-8.6
AA63	610	12.5	-57.4	-47.9	-17.8	-8.1	-3.2
AA64	600	12.2	-55.7	-45.5	-24.8	-10.5	-4.1
AA65	583	10.7	-56.4	-40.1	-18.0	-5.7	-0.4
AA66	577	9.8	-58.9	-56.8	-29.1	-16.0	-4.8
AA67	567	9.9	-56.0	-37.1	-18.0	-2.9	1.9
AA68	560	9.4	-56.1	-31.4	-7.3	0.6	3.4
AA69	554	9.1	-55.5	-27.4	-2.6	2.9	4.3
AA70	540	8.8	-55.8	-52.9	-32.9	-14.6	-0.1
AA71	533	8.3	-54.4	-51.6	-29.2	-10.7	1.7
AA72	520	7.3	-56.3	-41.6	-12.8	-2.7	1.5

Table A.12 Experimental data of the snow dry-ice stream temperature at various distance (x) from the nozzle tip (cont.)

EXP CASE	P inlet (psi)	T inlet (°C)	x = 0 cm (°C)	x = 2 cm (°C)	x = 4 cm (°C)	x = 6 cm (°C))	x = 8 cm (°C)
AA73	519	7.2	-55.7	-49.7	-28.1	-11.0	-0.1
AA74	510	6.6	-55.4	-35.2	-8.7	-0.4	3.0
AA75	502	6.2	-56.1	-31.8	-3.6	2.8	4.6
AA76	492	5.6	-56.0	-31.6	-3.2	2.4	5.2
AA77	469	4.0	-56.0	-18.4	1.6	5.8	6.6
AA78	462	3.6	-53.8	-20.8	0.1	4.9	6.1
AA79	453	2.7	-54.5	-18.7	1.4	5.4	6.1

Appendix B

Estimation of the dry-ice particles percentage in the snow dry-ice stream at the nozzle tip

B.1 Estimation of the dry-ice particles phase percentage

From the experimental data in Appendix A, these data of the CO_2 conditions can be converted into the enthalpy value. In this research, the enthalpy of the snow dry-ice stream at the nozzle tip could be calculated by using the Aspen HYSYS 2006 as a simulation program. In addition, the simulations were operated on the basis of the Peng-Robinson equation of state as a fluid package. Thus, from the CO_2 conditions data in Appendix A and the calculated enthalpy data, the CO_2 *PH* phase diagram would be used to estimate the dry-ice particles percentage in the snow dry-ice stream at the nozzle tip.

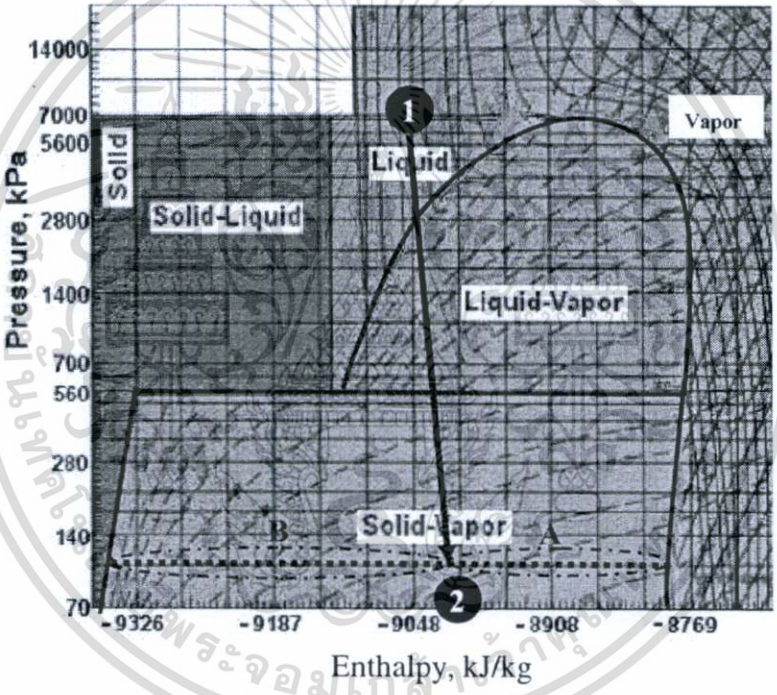

Figure B.1 The Pressure-Enthalpy *PH* phase diagram for CO_2 [11]

From Figure B.1, after the CO_2 pressure and enthalpy data were plotted on the CO_2 *PH* phase diagram, that the plotting shows about the direction of the CO_2 phase changing. Thus, from the second state in Figure B.1 that shows the CO_2 stream conditions at the nozzle tip. Then the second state point positions in the solid-vapor phase and on the atmospheric pressure line (dash line). Therefore, the percentage of the dry-ice particles phase in the stream could be estimated by using the lever arm rule in Equation B.1 and the CO_2 *PH* phase diagram (Figure B.1).

$$\%\text{solid phase} = \left(\frac{\text{Range A}}{\text{Range A+Range B}}\right) \times 100\% \qquad \text{(B.1)}$$

For example, the CO_2 has the conditions same as EXP CASE AA02 in Table B.1. By using Aspen HYSYS 2006, the CO_2 stream that has temperature at the atmospheric pressure condition around -55.6°C would have the enthalpy -9017 kJ/kg. Thus, the point 2 was plotted in Figure B.1. Then from the lever arm rule and Equation B.1, the percentage of dry-ice particles phase equal as;

$$\%\text{solid phase} = \left(\frac{\text{Range A}}{\text{Range A} + \text{Range B}}\right) \times 100\% = 40.6\%$$

Table B.2 Experimental data of CO_2 stream conditions and the percentage of dry-ice particles phase at the nozzle tip when used the supplying CO_2 temperature constant at 23°C and high supplying CO_2 pressure range (780-870 psi)

EXP CASE	P inlet (psi)	T inlet (°C)	P1 (psi)	T1 (°C)	T4 (°C)	Enthalpy (kJ/kg)	% dry-ice particles phase
A26	887	22.4	868	23.1	-57.9	-9018.9	40.9
A27	872	21.1	860	22.8	-71.4	-9029.9	42.8
A28	862	22.1	853	22.7	-70.2	-9028.9	42.6
A29	852	23.1	840	23.2	-46.2	-9009.3	39.2
A30	841	22.8	830	23.0	-46.4	-9009.5	39.2
A31	832	23.4	820	22.9	-48.9	-9011.5	39.6
A32	821	23.3	811	23.1	-49.1	-9011.7	39.6
A33	802	17.3	788	23.3	-36.2	-9001.0	37.8

Table B.2 Experimental data of CO_2 stream conditions and the percentage of dry-ice particles phase at the nozzle tip when used the supplying CO_2 temperature constant at 22°C and high supplying CO_2 pressure range (780-870 psi).

EXP CASE	P inlet (psi)	T inlet (°C)	P1 (psi)	T1 (°C)	T4 (°C)	Enthalpy (kJ/kg)	% dry-ice particles phase
A34	888	22.5	870	22.2	-55.6	-9017.0	40.6
A35	874	21.1	861	22.2	-66.5	-9025.9	42.1
A36	863	20.0	850	22.0	-68.8	-9027.8	42.4
A37	850	19.7	841	22.1	-69.6	-9028.4	42.5
A38	840	19.7	832	21.8	-63.2	-9023.2	41.6
A39	828	22.0	820	22.1	-48.2	-9010.9	39.5
A40	817	20.3	811	22.1	-44.0	-9007.5	38.9
A41	805	22.9	795	21.9	-45.7	-9008.9	39.1
A42	791	23.5	781	21.8	-45.1	-9008.4	39.1

Table B.3 Experimental data of CO_2 stream conditions and the percentage of dry-ice particles phase at the nozzle tip when used the supplying CO_2 temperature constant at 21°C and high supplying CO_2 pressure range (780-870 psi).

EXP CASE	P inlet (psi)	T inlet (°C)	P1 (psi)	T1 (°C)	T4 (°C)	Enthalpy (kJ/kg)	% dry-ice particles phase
A43	875	22.5	860	21.5	-59.2	-9020.0	41.1
A44	862	21.0	849	21.4	-73.5	-9031.6	43.1
A45	854	20.5	840	21.2	-62.6	-9022.7	41.6
A46	836	19.2	830	21.0	-63.9	-9023.8	41.7
A47	828	19.2	820	20.9	-73.5	-9031.6	43.1
A48	818	19.6	812	20.7	-76.2	-9033.8	43.5
A49	806	20.9	804	20.6	-72.3	-9030.6	42.9
A50	800	20.9	789	21.4	-46.5	-9009.5	39.3

Table B.4 Experimental data of CO_2 stream conditions and the percentage of dry-ice particles phase at the nozzle tip when used the supplying CO_2 temperature in range of 18 to 20°C and high supplying CO_2 pressure range (780-870 psi).

EXP CASE	P inlet (psi)	T inlet (°C)	P1 (psi)	T1 (°C)	T4 (°C)	Enthalpy (kJ/kg)	% dry-ice particles phase
A51	843	20.0	828	20.4	-63.2	-9023.2	41.6
A52	831	19.4	820	20.3	-62.9	-9023.0	41.6
A53	819	18.8	810	20.2	-72.0	-9030.4	42.9
A54	809	19.0	801	20.0	-74.9	-9032.7	43.3
A55	799	18.4	792	19.7	-69.6	-9028.4	42.5
A56	790	17.8	784	19.7	-59.6	-9020.3	41.1
A57	823	18.7	809	19.3	-52.1	-9014.1	40.1
A58	809	18.0	799	19.3	-61.9	-9022.2	41.5
A59	802	18.5	791	19.3	-65.2	-9024.9	41.9
A60	791	18.4	782	19.2	-57.2	-9018.3	40.8
A61	803	17.7	790	18.4	-46.0	-9009.1	39.2
A62	795	17.8	782	18.2	-49.6	-9012.42	39.8

Table B.5 Experimental data of CO_2 stream conditions and the percentage of dry-ice particles phase at the nozzle tip when used the supplying CO_2 temperature in range of 9 to 13°C and the supplying CO_2 pressure in low range (560-610 psi).

EXP CASE	P inlet (psi)	T inlet (°C)	P1 (psi)	T1 (°C)	T4 (°C)	Enthalpy (kJ/kg)	% dry-ice particles phase
A63	628	12.4	608	12.9	-26.8	-8993.1	36.4
A64	620	11.2	601	12.9	-30.5	-8996.2	37.0
A65	612	10.6	593	12.9	-33.4	-8998.7	37.4
A66	606	9.9	581	12.6	-33.9	-8999.1	37.4
A67	601	9.2	570	12.6	-41.3	-9005.2	38.5
A68	625	11.5	608	11.8	-53.6	-9015.4	40.3
A69	622	11.3	600	11.8	-47.2	-9010.1	39.4
A70	624	10.1	591	11.9	-44.5	-9007.9	39.0
A71	608	9.6	580	12.2	-42.3	-9006.1	38.7
A72	606	9.3	574	12.3	-43.2	-9006.8	38.8
A73	599	8.6	561	11.7	-39.8	-9004.0	38.3
A74	626	11.2	600	11.3	-61.9	-9022.2	41.5
A75	623	11.2	591	10.8	-60.5	-9021.0	41.3
A76	626	12.0	582	10.7	-55.1	-9016.6	40.5
A77	617	9.4	571	10.8	-42.8	-9006.5	38.7
A78	604	8.6	560	11.0	-42.3	-9006.1	38.7
A79	620	10.8	587	10.4	-55.9	-9017.3	40.6
A80	617	9.8	580	10.3	-58.8	-9019.6	41.0
A81	613	9.3	570	9.9	-51.8	-9013.9	40.0
A82	606	8.8	562	9.8	-45.5	-9008.7	39.1
A83	610	9.1	569	9.4	-55.5	-9016.9	40.5
A84	605	8.6	560	9.2	-46.9	-9009.9	39.3

Appendix C

Calculation of the Joule-Thomson coefficient and the Joule-Thomson inversion curve

C.1 Joule-Thomson coefficient (μ_{JT}) calculation

The definition of Joule-Thomson coefficient in section 2.5,

$$\mu_{JT} \equiv \left(\frac{\partial T}{\partial P}\right)_h \tag{C.1}$$

From the expression of μ_{JT} with using the Thermodynamic theory in section 2.5.1, the μ_{JT} can be calculated by using Equation (2.11) or (C.2).

$$\mu_{JT} = \frac{\left[T\left(\frac{\partial v}{\partial T}\right)_P - v\right]}{c_P^{ideal\ gas} - \int_{P_{ideal\ gas}}^{P_{real}} \left[T\left(\frac{\partial^2 v}{\partial T^2}\right)_P\right] dP} \tag{C.2}$$

Then, after set the $P_{ideal\ gas}$ equal to zero and integrating Equation (C.2), finally get Equation (C.3);

$$\mu_{JT} = \frac{\left[T\left(\frac{\partial v}{\partial T}\right)_P - v\right]}{c_P^{ideal\ gas} - \left[T\left(\frac{\partial^2 v}{\partial T^2}\right)_P\right] \times P_{real}} \tag{C.3}$$

In addition, when use Equation (C.3) to calculate the μ_{JT}, the other parameters in Equation must be known, which include $c_P^{ideal\ gas}$, v, $\left(\frac{\partial v}{\partial T}\right)_P$, $\left(\frac{\partial^2 v}{\partial T^2}\right)_P$, P_{real}, and temperature of CO_2 (T). Thus, in case of P_{real} and T can be obtained these CO_2 conditions from the experiments, however, the other parameters have to calculate or use another method.

Then, $c_P^{ideal\ gas}$ be able to calculate by Equation (C.4) [34],

$$C_P^{ideal\ gas} = \{5.457 + [(1.045 \times 10^{-3}) \times T(\mathrm{K})] - [(1.157 \times 10^{5}) \times T^2(\mathrm{K}^2)]\} \times R \tag{C.4}$$

by using R = 8.314 J mol^{-1} K^{-1}

Moreover, for the v, $\left(\frac{\partial v}{\partial T}\right)_P$, and $\left(\frac{\partial^2 v}{\partial T^2}\right)_P$ parameters, were evaluated by using the plotting of correlation data between CO_2 specific volume (v) and temperature (T in Kelvin).

In this research, the specific volume of CO_2 was calculated by using the modified Peng-Robinson in Equation (2.12) or (C.5) as equation of state [32,36]

$$P = \frac{RT}{V-b} - \frac{a_c \alpha(T_r)}{V^2 + 2Vb - b^2} \tag{C.5}$$

Moreover, it is more complicated when the specific volume from the MPR EOS was solved manually. Thus, the MATLAB R2010a program was used as a solver for the CO_2 specific volume calculation. The source code that was used for the MATLAB calculation shows in

following. Therefore, after input the CO_2 temperature and pressure, the CO_2 specific volume (v) was given for use in the substitution in Equation (C.3) and plotting diagram as a correlation between v and T.

MATLAB source code for CO2 specific volume calculation by using MPR EOS

```
%%MPR1 EOS
clear all
clc
%% Input&syms
syms V T P ac b m M af A
T=input('Input T (K):');  %%K
P = 36.9;    %%Bar
TC= 304.5; %%K
PC= 73.80; %%Bar
t = T/TC;
w = 0.224;
R = 83.14; %% cm3 bar / mol K
%% EOS
ac=((0.45724*(R^2)*(TC^2))/PC);
b =((0.0778*R*TC)/PC);
m =(0.3796+(1.485*w)-(0.1644*(w^2))+(0.01667*(w^3)));
M =1.21*m;
af=(1+(M*(1-(t^0.5))))^2;
A =(((R*T)/(V-b))-((ac*af*t)/((V^2)+(2*V*b)-(b^2)))-P);
%% Find V
V =solve(A,V);
V =V(1);
V =subs(V,{'R','T','V','b','P','ac','af','t'})
%% end MPR1 EOS
```

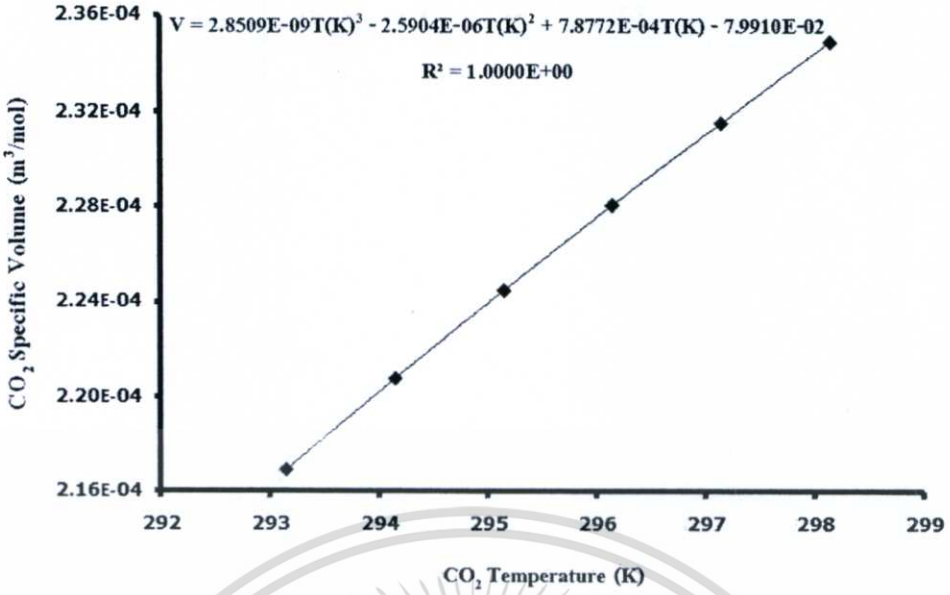

Figure C.1 The correlation between CO_2 specific volume and temperature at constant CO_2 pressure 850 psi

Finally, the data of v and T correlation was gotten, which the CO_2 vT diagram (see Figure C.1 as an example) will get from using MATLAB with the source code.

For example, to calculate the μ_{JT} of the CO_2 that has the pressure 850 psi and 22 °C (295.15 K) for temperature.

At first from the diagram in Figure C.1 the correlation between v and T as a function v(T) was gotten that is shown in Equation (C.6).

$$v(T) = 2.8509\text{E} - 09T^3(\text{K}) - 2.5904\text{E} - 06T^2(\text{K}) + 7.8772\text{E} - 04T(\text{K}) - 7.9910\text{E} - 02 \quad \text{(C.6)}$$

Then the differential form of Equation (C.6) or $\left(\frac{\partial v}{\partial T}\right)_P$ could be got, which is shown in Equation (C.7).

$$\left(\frac{\partial v}{\partial T}\right)_P = [8.5527\text{E} - 09 \times \text{T(K)}^2] - [5.1808\text{E} - 06 \times \text{T(K)}] + 7.8772\text{E} - 04 \quad \text{(C.7)}$$

The $\left(\frac{\partial^2 v}{\partial T^2}\right)_P$ form was got t as Equation (C.8);

$$\left(\frac{\partial^2 v}{\partial T^2}\right)_P = [1.7105\text{E} - 08 \times \text{T(K)}] - [5.1808\text{E} - 06] \quad \text{(C.8)}$$

Thus, the μ_{JT} could be calculated by substitute all of these parameters back into Equation (C.3) and get Equation (C.9),

$$\mu_{JT} = \frac{[[295.15 \times 3.6527E{-}06] - 2.245E{-}04]}{36.9 - [[295.15 \times (-1.2364E{-}07)] \times 5.8605E{+}06]}$$

Then get the μ_{JT} of the CO_2 that has temperature 22°C (295.15K) at constant pressure 850 psi equal to 0.3404 K/bar or 0.0235 K/psi.

Table C.3 Joule-Thomson coefficient calculation results of various CO_2 conditions when the supplying CO_2 pressure constant at 850 psi

EXP CASE	P3 (psi)	T3 (°C)	v (m^3/mol)	$\left(\frac{\partial v}{\partial T}\right)_P$	$\left(\frac{\partial^2 v}{\partial T^2}\right)_P$	μ_{JT} (K/bar)	μ_{JT} (K/psi)
C01	850	19	2.268.E-04	4.024E-06	-1.835E-07	0.270	0.019
C02	850	20	2.169.E-04	3.900E-06	-1.664E-07	0.287	0.020
C03	850	21	2.208.E-04	3.776E-06	-1.492E-07	0.303	0.021
C04	850	22	2.245.E-04	3.653E-06	-1.321E-07	0.322	0.022
C05	850	23	2.281.E-04	3.529E-06	-1.150E-07	0.345	0.024
C06	850	24	2.315.E-04	3.405E-06	-9.793E-08	0.376	0.026
C07	850	25	2.349.E-04	3.282E-06	-8.082E-08	0.417	0.029

Table C.2 Joule-Thomson coefficient calculation results of various CO_2 conditions when the supplying CO_2 pressure constant at 800 psi

EXP CASE	P3 (psi)	T3 (°C)	v (m^3/mol)	$\left(\frac{\partial v}{\partial T}\right)_P$	$\left(\frac{\partial^2 v}{\partial T^2}\right)_P$	μ_{JT} (K/bar)	μ_{JT} (K/psi)
C08	800	19	2.612.E-04	3.263E-06	-6.627E-08	0.483	0.033
C09	800	20	2.644.E-04	3.199E-06	-6.174E-08	0.493	0.034
C10	800	21	2.676.E-04	3.139E-06	-5.721E-08	0.506	0.035
C11	800	22	2.707.E-04	3.084E-06	-5.269E-08	0.521	0.036
C12	800	23	2.737.E-04	3.034E-06	-4.816E-08	0.540	0.037
C13	800	24	2.768.E-04	2.988E-06	-4.363E-08	0.563	0.039
C14	800	25	2.797.E-04	2.926E-06	-3.910E-08	0.584	0.040

Table C.3 Joule-Thomson coefficient calculation results of various CO_2 conditions when the supplying CO_2 pressure constant at 400 psi

EXP CASE	P3 (psi)	T3 (°C)	v (m^3/mol)	$\left(\frac{\partial v}{\partial T}\right)_P$	$\left(\frac{\partial^2 v}{\partial T^2}\right)_P$	μ_{JT} (K/bar)	μ_{JT} (K/psi)
C15	800	19	2.612.E-04	3.263E-06	-6.627E-08	0.483	0.033
C16	800	20	2.644.E-04	3.199E-06	-6.174E-08	0.493	0.034
C17	800	21	2.676.E-04	3.139E-06	-5.721E-08	0.506	0.035
C18	800	22	2.707.E-04	3.084E-06	-5.269E-08	0.521	0.036
C19	800	23	2.737.E-04	3.034E-06	-4.816E-08	0.540	0.037
C20	800	24	2.768.E-04	2.988E-06	-4.363E-08	0.563	0.039
C21	800	25	2.797.E-04	2.926E-06	-3.910E-08	0.584	0.040

C.2 Joule-Thomson Inversion Curve Estimation

Table C.4 Prediction of the Joule-Thomson inversion curve by using modified Peng-Robinson equation of state

Point	Pr	Tr	P		T	μ_{JT}	μ_{JT}
			(bar)	(psi)	(K)	(K/bar)	(K/psi)
CC01	0.300	0.761	22.1	321	231.7	2.071.E-04	1.428E-05
CC02	0.500	0.775	36.9	535	236.0	6.353.E-05	4.380E-06
CC03	0.771	0.795	56.9	825	242.1	2.306E-05	1.590E-06
CC04	1.775	0.882	131.0	1900	268.7	3.712.E-05	2.560.E-06
CC05	2.803	0.966	206.8	3000	294.2	7.491.E-04	5.166.E-05
CC06	4.000	1.062	295.2	4282	323.4	5.167.E-06	3.562E-07
CC07	5.000	1.141	369.0	5352	347.5	2.071.E-04	1.428E-05
CC08	6.000	1.218	442.8	6422	371.0	6.353.E-05	4.380E-06
CC09	9.000	1.455	664.2	9634	443.0	7.748.E-04	5.342E-05
CC10	12.000	1.701	885.6	12845	518.0	2.287.E-04	1.577E-05
CC11	15.000	1.993	1107.0	16056	607.0	6.550.E-04	4.516.E-05
CC12	18.000	2.365	1328.4	19267	720.0	5.057.E-06	3.487.E-07
CC13	19.000	2.627	1402.2	20338	800.0	1.826.E-04	1.259.E-05
CC14	18.000	2.989	1328.4	19267	910.0	3.492.E-04	2.408.E-05
CC15	15.000	3.530	1107.0	16056	1075.0	1.066.E-04	7.348.E-06
CC16	12.000	3.727	885.6	12845	1135.0	3.032.E-04	2.090.E-05
CC17	9.000	3.898	664.2	9634	1187.0	5.639.E-04	3.888E-05
CC18	6.000	4.039	442.8	6422	1230.0	7.223.E-05	4.980E-06
CC19	4.000	4.122	295.2	4282	1255.0	1.201.E-04	8.281E-06
CC20	3.000	4.158	221.4	3211	1266.0	8.715.E-04	6.009E-05
CC21	2.000	4.194	147.6	2141	1277.0	5.475.E-04	3.774E-05
CC22	1.000	4.286	73.8	1070	1305.0	2.669.E-04	1.840E-05

Appendix D

Evaluation of the snow dry-ice stream characteristic and the pressure measurement of the dry-ice particles

D.1 Supplying CO_2 mass flow rate

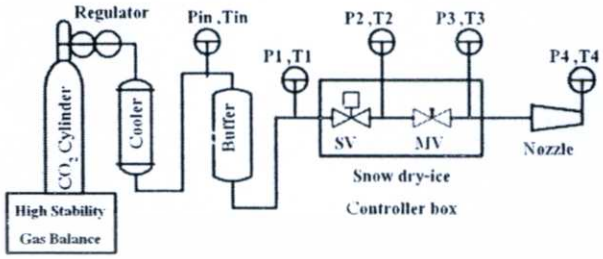

Figure D.1 Process flow diagram of the snow dry-ice generating system with the high stability and precision level gas balance (Mettler Toledo XS32001L)

When the snow dry-ice stream was generated by flowing the supplying CO_2 from the cylinder through the snow dry-ice generating system. The mass flow rate of the supplying CO_2 were obtained by using the high stability and precision level gas balance. Which were evaluated through the lost rate of the CO_2 weight in cylinder.

Table D.4 The mass flow rate data of the supplying CO_2

EXP CASE	P1 (psi)	T1 (°C)	Injection Time (second)	Weight lost (g)	Mass flow rate (g/s)	Mass flow rate (kg/s)
D01	716	19.0	20	57.7	2.885	0.00289
D02	731	19.5	20	64.1	3.205	0.00321
D03	723	19.0	20	66.7	3.335	0.00334
D04	714	18.5	20	58.9	2.945	0.00295
D05	607	13.5	20	44.5	2.225	0.00223
D06	594	13.3	20	59.5	2.975	0.00298
D07	603	13.8	20	51.2	2.560	0.00256
D08	601	13.1	20	72.5	3.625	0.00363

Table D.5 The mass flow rate data of the supplying CO_2 (cont.)

EXP CASE	P1 (psi)	T1 (°C)	Injection Time (second)	Weight lost (g)	Mass flow rate (g/s)	Mass flow rate (kg/s)
D09	609	13.4	20	59.6	2.980	0.00298
D10	532	9.0	60	90.0	1.500	0.00150
D11	505	9.1	60	92.0	1.533	0.00153
D12	506	8.5	60	88.3	1.472	0.00147
D13	513	9.2	60	83.8	1.397	0.00140
D14	504	8.2	60	87.6	1.460	0.00146
D15	462	6.5	60	73.3	1.222	0.00122
D16	465	6.2	60	77.8	1.297	0.00130
D17	465	6.6	60	77.0	1.283	0.00128

D.2 Nozzle Velocity of the CO_2 stream

From the CO_2 mass flow rate that flew through the snow dry-ice generating system were obtained as the data is shown in Table D.1. The CO_2 flow velocity before the CO_2 moved through the expansion at the nozzle that can be calculated by using Equation (D.1). When the CO_2 fluid flow velocity in the micro polymeric tube (the nozzle) were assumed closely the CO_2 gas flow velocity in the combination stream flow at the nozzle tip. The dry-ice particles in the snow stream should equal the CO_2 gas flow velocity. Then, the nozzle velocity of snow dry-ice stream could be calculated by using Equation D.1.

$$U_0 = \frac{\dot{m}}{\rho_{CO_2} \cdot \emptyset} \tag{D.1}$$

by U_0 is the CO_2 nozzle velocity (m/s).

$\dot{m}$ is the supplying CO_2 mass flow rate (kg/s) from data in Table D.1..

ρ_{CO_2} is the supplying CO_2 density (kg/m^3) that calculated from HYSYS 2006.

$\emptyset$ is the nozzle cross sectional area constant at 4.42×10^{-7} m^2.

For example, from EXP case 01 data, and substitute into Equation D.1,

Thus, the nozzle velocity,

$$U_0 = \frac{0.0029}{142.5\times4.42\times10^{-7}} = 46.04\ \frac{m}{s}$$

Table D.2 The nozzle velocity of the snow dry-ice stream

EXP CASE	P1 (psi)	T1 (°C)	Mass flow rate (kg/s)	ρ_{CO_2} (kg/m^3)	$\emptyset$ (m^2)	U_0 (m/s)
D01	716	19.0	0.00289	144.0	4.42×10^{-7}	48.59
D08	601	13.0	0.00363	112.5	4.42×10^{-7}	57.78
D14	505	9.1	0.00146	91.1	4.42×10^{-7}	36.55
D16	465	6.2	0.00130	80.3	4.42×10^{-7}	35.70

D.3 Impact stress and diameter size of the dry-ice particle

D.3.1 The impact stress measurement

From the pressure measurement method by using the Fuji ® Prescale film (mono-sheet type for medium pressure range), the impacted Prescale films would be taken the color photo. Then the photo would be analyzed by using the Photoshop CS3 program. Which was used to evaluate the RGB (Red Green Blue) value of the red theme on the impacted Prescale films. From this RGB value, the standard color density (SCD) was converted into the impact stress (σ) of the dry-ice particles in the snow dry-ice stream.

Figure D.2 The standard color density (SCD) scale that uses to convert the color from the particle impact to the impact stress value (σ) (a). The impacted Prescale film by the snow dry-ice stream that generated from supplying pressure 700 psi and 19°C for temperature (b)

Table D.3 The impact stress of the dry-ice particles

EXP CASE	P1 (psi)	T1 (°C)	ρ_{CO_2} (kg/m^3)	Impact stress, σ (Mpa)
D01	716	19.0	144.0	54
D08	601	13.0	112.5	52
D14	505	9.1	91.1	48
D16	465	6.2	80.3	10

D 3.2 The diameter size of the dry-ice particle measurement

From the pressure measurement method by using the Fuji ® Prescale film (mono-sheet type for medium pressure range), the impacted Prescale films could be measured the diameter size of dry-ice particles by using its optical micrograph. Then the photo would be analyzed by using the ImageJ program. Which was used to measure the diameter size of the red dots on the impacted Prescale films.

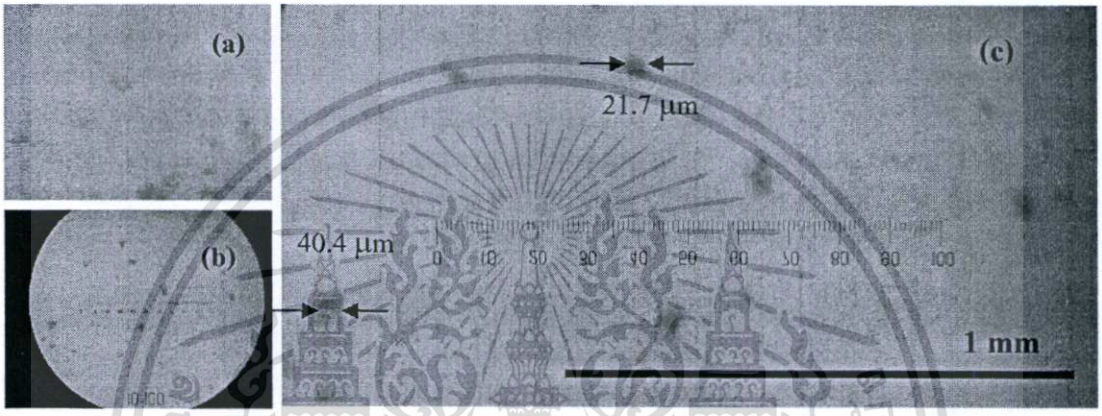

Figure D.3 The impacted Prescale film (mono-sheet type for medium pressure) that used to measure the snow dry-ice stream that generated from supplying CO_2 pressure 700 psi and 19°C, which is observed by optical microscope 20X (a) and 100X (b). In addition, the ImageJ program was used to measure the diameter size of dry-ice particles in the optical micrograph 100X (c).

Table D.4 The diameter size of the dry-ice particles

EXP CASE	P1 (psi)	T1 (°C)	ρ_{CO_2} (kg/m^3)	Maximum d (µm)	Minimum d (µm)	Mean d (µm)
D01	716	19.0	144.0	63.38	19.05	33.10
D08	601	13.0	112.5	47.96	21.18	31.37
D14	505	9.1	91.1	40.24	21.16	29.07
D16	465	6.2	80.3	46.23	17.92	27.28

D.4 Momentum of the dry-ice particle

D.4.1 To calculate the impact velocity (U) [10]

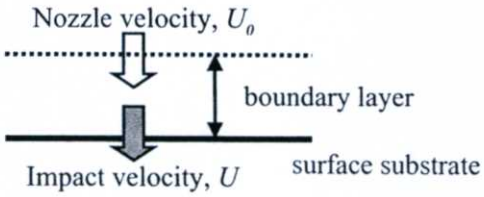

Figure D.4 The dry-ice particle velocity when it moved through the boundary layer

The particle impact velocity could be estimated by using Equation (D.2).

$$U = U_0\left(1 - \frac{\delta}{U_0\tau}\right) \tag{D.2}$$

When U is the impact velocity (m/s).

U_0 is the nozzle velocity (m/s) from Table D.2.

τ is the velocity relaxation time (μs) by using Equation (D.3).

Step 1 To evaluate the Cunningham correction factor, C_c

$$C_c = 1 + \frac{2}{Pd}[6.32 + 2.01exp(-0.1095Pd)] \tag{D.3}$$

where:

P is the absolute pressure (kPa) from Table D.4.

d is the dry-ice particle diameter (μm) from Table D.4.

Example, from data of EXP case D01,

$$C_c = 1 + \frac{2}{4{,}925\times 33}[6.32 + 2.01exp(-0.1095 \times [4{,}925 \times 33])]$$
$$= 1.000078$$

Step 2 To evaluate the velocity relaxation time, τ

$$\tau = \frac{2r^2\rho_P C_c}{9\eta} \tag{D.4}$$

by r is the dry-ice particle radius (m) from Table D.4.

ρ_p is the dry-ice particle density (kg/m^3) constant at 1,500 kg/m^3.

η is the CO_2 gas viscosity (Pa·s) that be calculated from HYSYS.

C_c is the Cunningham correction factor that obtains from Equation (D.3).

$$\tau = \frac{2\times\left(\frac{33\times10^{-6}}{2}\right)^2\times1{,}500\times1.000078)}{9\times(1.015\times10^{-5})} = 0.008997\mu s$$

Step 3 To evaluate the boundary layer thickness, δ

$$\delta = 0.16 \times \frac{x}{(Re)^{1/7}} \quad \text{(D.5)}$$

Then *Re* is the Reynolds number given as follows:

$$\text{Re} = \frac{U_0 x}{v} \quad \text{(D.6)}$$

where

v is the kinematic viscosity of the CO_2 gas calculated at plume temperature of –73 °C so it constant at 3.48×10^{-6} m^2/s.

U_o is the nozzle velocity (m/s) from Table D.2.

x is the distance between nozzle and substrate that constant at 0.01 m.

For the calculation example,

$$\text{Re} = \frac{46.6\times0.01}{3.48\times10^{-6}} = 1.34\times10^5$$

Then, $$\delta = 0.16 \times \frac{0.01}{(1.34\times10^5)^{1/7}} = 296\ \mu m$$

Step 4 To calculate the impact velocity (U) in finally

From Equation (D.2), (D.4) and (D.5);

$$U = 46.6 \times \left(1 - \frac{2.96\times10^{-4}}{46.6\times(9\times10^{-3})}\right) = 46.5 \text{ m/s}$$

D.4.2 Momentum of the dry-ice particle

The dry-ice particle shape is assumed as a spherical particle. Thus, the dry-ice particle diameter could be obtained. The mass of the dry-ice particle will be evaluated by using Equation (D.7). Then Equation (D.8) can be used to estimate the momentum of the dry-ice particle before the impact with surface.

$$m = \frac{4\rho_P\pi r^3}{3} \quad \text{(D.7)}$$

where

ρ_p is the dry-ice particle density that constant at 1,500 kg/m^3.

r is the dry-ice particle radius from Table D.4 (m).

and

$$\bar{P} = m \cdot U \tag{D.8}$$

where

m is the dry-ice particle mass(kg) from Equation (D.7).

U is the impact velocity (m/s) from Equation (D.2).

Example in momentum calculation,

$$m = \frac{4\times(1{,}500)\times\pi\times\left(\frac{33\times10^{-6}}{2}\right)^3}{3} = 2.85\times10^{-11}kg$$

Thus,

$$\bar{P} = (2.85\times10^{-11})\times 46.5 = 1.3256\times10^{-9}kg\cdot m/s$$

Table D.5 The momentum of the dry-ice particles

EXP CASE	P1 (psi)	T1 (°C)	ρ_{CO_2} (kg/m^3)	τ (μs)	δ (μm)	U (m/s)	$\bar{P}$ (kg·m/s)
D01	716	19.0	144.0	0.008997	296	46.57	1.33E-09
D08	601	13.0	112.5	0.008097	289	55.36	1.35E-09
D14	505	9.1	91.1	0.006955	309	34.86	6.74E-10
D16	465	6.2	80.3	0.006121	310	33.85	5.41E-10

Author Biography

Siwach Tengsuwan was born on 9 January 1986 in Uttaradit province, Thailand. In March 2009, he was received his degree in Bachelor of Engineering in Chemical Engineering at King Mongkut's Institute of Technology Ladkrabang, Bangkok, Thailand. He had successfully completed a training period from April to May 2008, as a student trainee in Rayong Olefins Co.,Ltd., Olefins Department, Siam Cement Group (SCG).

During these two years for Master of Engineering program in Chemical Engineering at KMITL, his work at Polymer Processing and Supercritical Fluid Technology Research Group involved snow dry-ice, polymeric foam processing, and supercritical fluid technology.

Publications:

1. **S. Tengsuwan** and S. Areerat. "Study on the Joule-Thomson expansion for the CO_2 cryogenic aerosol generating process." **Ladkrabang Engineering Journal**, vol. 27, no. 4, pp. 55-60, 2010.

Presentations:

1. **S. Tengsuwan** and S. Areerat. (2010, November 22-23) Preparation of Study on the Joule-Thomson expansion for the optimization in snow dry-ice generating systems. Oral presented at 17th Regional Symposium on Chemical Engineering 2010 (RSCE2010), Bangkok, Thailand.
2. **S. Tengsuwan,** A. Phueknapo and S. Areerat. (2009, October 26-27) Preparation of Snow dry-ice blasting device for cryogenic cleaning. Oral presented at 19th Conference of The Thai Institute of Chemical Engineering and Applied Chemistry 2009 (TICHE 2009), Thailand.